THE ROLE OF RNA-BINDING PROTEINS IN ASTROCYTE-TO-NEURON REPROGRAMMING

Giuliana Ciccopiedi

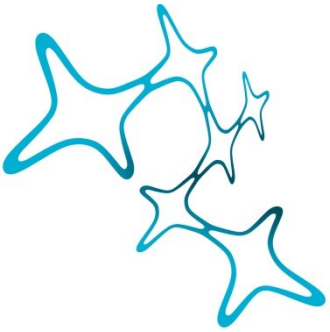

Graduate School of
Systemic Neurosciences

LMU Munich

Dissertation
der Graduate School of Systemic Neurosciences
der Ludwig-Maximilians-Universität München

October, 2023

Supervisor
Prof. Dr. Michael A. Kiebler
Biomedical Center Munich/Cell Biology
Ludwig-Maximilians-Universität München

First Reviewer: Prof. Dr. Michael A. Kiebler
Second Reviewer: Dr. Giacomo Masserdotti
External Reviewer: Prof. Dr. Marisa Karow

Date of Submission: 16.10.2023
Date of Defense: 04.03.2024

Table of contents

ABSTRACT

RNA-binding proteins (RBPs) regulate gene expression through a variety of post-transcriptional mechanisms, contributing to many important brain functions including proper neuronal development. The brain-specific RBPs Pumilio2 (Pum2) and Staufen2 (Stau2) have emerged as key regulators of RNA transport and translational control with significant impact in the nervous system. Their action is not only important in mature neurons, where they regulate synaptic plasticity and learning and memory formation, but also in embryonic neurogenesis as important cell fate regulators. The involvement of Pum2 and Stau2 in cell fate commitment during neurogenesis prompted the question whether they are also involved in establishing neuronal fate in the context of direct neuronal reprogramming. In contrast to the key role(s) of transcription factors (TFs) to instruct direct lineage conversion, the contribution of post-transcriptional mechanisms to cell fate conversion remains largely unexplored. In this thesis, I investigated the role of Pum2 and Stau2 in neuronal reprogramming using direct astrocyte-to-neuron conversion as experimental paradigm. I found that depletion of Pum2 or Stau2 impairs the efficiency of Neurogenin2 (Neurog2)-driven neuronal reprogramming, with Pum2 having a greater impact on the successful cell fate conversion than Stau2. Notably, the effects of Pum2 on cell fate conversion manifested only after 5 days of the conversion process. Interfering with Pum2 expression 2 days after Neurog2 overexpression, the time point corresponding to the early fate establishment, reduced reprogramming efficiency similarly to the continuous loss of Pum2 function. These findings suggest that Pum2 exerts its functions at a later stage of the process, rather than in the initial phase of establishing neuronal identity. Interestingly, the reduced generation of neurons in the absence of Pum2 is accompanied by an increased presence of non-reprogrammed cells with an aberrant morphological phenotype that clearly differs from the appearance of typical wildtype astrocytes undergoing reprogramming. Taken together, my findings support a working hypothesis of a late-stage role for Pum2 to ensure the irreversible commitment of reprogrammed cells towards a neuronal fate. My experiments therefore yield new insight into the reprogramming process by adding a functional contribution of RBP-mediated post-transcriptional regulation for neuronal fate establishment.

ABBREVIATIONS

Ascl1	Achaete-scute homolog1
Ago	Argonaute
Anks1	Ankyrin repeat and SAM domain-containing 1
BBS	BES-buffered saline
BES	N,N-bis(2-hydroxyethyl)-2-aminoethanesulfonic acid
bFGF	basic fibroblast growth factor
bHLH	basic helix-loop-helix
BSA	bovine serum albumin
Cadm3	Cell adhesion molecule 3
Calm3	Calmodulin 3
CamKII	Calcium/Calmodulin-dependent protein kinase II
Cbfa2t3	Core-binding factor, runt domain, alpha subunit 2, translocated to, 3
CBP80	cap-binding protein 80
CNS	central nervous system
CTCF	corrected total cell fluorescence
DAPI	4′,6-diamidino-2-phenylindole
Dcx	Doublecortin
DDX	DEAD-box helicase (DDX1, DDX6)
DIV	days *in vitro*
DMEM	Dulbecco’s modified eagle medium
DNA	deoxyribonucleic acid
DPBS	Dulbecco’s phosphate buffered saline
DPI	days post-infection
DPT	days post-transfection
Dscaml1	Down syndrome cell adhesion molecule-like 1
dsRBP	double-stranded RNA-binding protein
E	embryonic day
EDTA	ethylenediaminetetraacetic acid
eEF1A	eukaryotic translation elongation factor 1A

EGF	epidermal growth factor
EGFP	enhanced green fluorescent protein
eIF4E	eukaryotic translation initiation factor 4E
FBS	fetal bovine serum
FCS	fetal calf serum
FMRP	Fragile X Mental Retardation Protein
$GABA_A$	γ-aminobutyric acid type A
GFAP	Glial Fibrillary Acidic Protein
GFP	green fluorescent protein
Gng4	Guanine nucleotide-binding protein (G protein), Gamma 4
HBSS	Hank's balanced salt solution
HEK293T	human embryonic kidney 293T
HEPES	4-(2-Hydroxyethyl)piperazine-1-ethanesulfonic acid
Hes	Hairy and enhancer of split (Hes5, Hes6)
HI	heat-inactivated
Homer2	Homer homolog 2
IPC	intermediate progenitor cell
iPSCs	induced pluripotent stem cells
IRES	internal ribosome entry site
LB	Luria-Bertani broth
MEM	minimal essential medium
miRNA (or miR)	microRNA
mRNA	messenger RNA
Myt1l	Myelin transcription factor 1 like
NeuroD	Neuronal Differentiation (NeuroD1, NeuroD2, NeuroD4)
Neurog	Neurogenin (Neurog1, Neurog2)
NLS	nuclear localisation signal
NMEM	neuronal minimal essential medium
NPC	neural progenitor cell
NSC	neural stem cell
ns	not significant

NTC	non-targeting control
P	postnatal day
p	probability
PABPN1	Poly(A) binding protein nuclear 1
PAX2	Paired box 2
Pax6	Paired box 6
PBS	phosphate buffered saline
PDL	poly-D-lysine
PFA	paraformaldehyde
Pou3f3	POU Class 3 Homeobox 3
Prox1	Prospero-related homeobox 1
Ptbp1	Polypyrimidine tract-binding protein 1
PUF	Pum and FBF
Pum	Pumilio (Pum1, Pum2)
PVDF	polyvinylidene fluoride
RBP	RNA-binding protein
RFP	red fluorescent protein
RGC	radial glial cell
Rgs4	Regulator of G-protein signaling 4
RNA	ribonucleic acid
RNP	ribonucleoprotein particle
ROI	region of interest
Sema5a	Semaphorin-5A
Shf	Src homology 2 domain containing F
shNTC	short hairpin RNA with no known targets in the mammalian genome
shPum2/shStau2	short hairpin RNA targeting *Pumilio2* or *Staufen2* mRNA
shRNA	short hairpin RNA
Slit1	Slit homolog 1
Snca	Alpha-synuclein
St3gal5	ST3 beta-galactoside alpha-2,3-sialyltransferase 5
Stau	Staufen (Stau1, Stau2)

TF	transcription factor
Tle4	Transducin-Like Enhancer of Split 4
Trim32	Tripartite motif containing 32
Trnp1	TMF-regulated nuclear protein 1
UTR	untranslated region
min	minute
h	hour
nm	nanometer
µm	micrometer
mm	millimeter
cm	centimeter
µg	microgram
mg	milligram
µl	microliter
ml	milliliter
mM	millimolar
M	molar
v/v	volume/volume
w/v	weight/volume
g	gravitational force
rpm	revolutions per minute
RT	room temperature

1 INTRODUCTION

1.1 The key roles of RNA-binding proteins in the central nervous system

In a highly complex system such as the brain, a tightly coordinated regulation of gene expression is an essential prerequisite to ensure proper development and functionality (Schieweck et al., 2021a). In particular, due to the complex shape and cell type diversity, neurons rely on numerous post-transcriptional mechanisms to ensure a spatiotemporally controlled protein expression. RNA-binding proteins (RBPs) play a crucial role in the post-transcriptional regulation of gene expression by interacting with messenger RNAs (mRNAs) and regulating their metabolism and function (Hentze et al., 2018; Schieweck et al., 2021a). Interestingly, dysfunctions of these post-transcriptional regulators are directly correlated with several neurological, neurodevelopmental, or neurodegenerative diseases demonstrating their importance in the nervous system (Boczonadi et al., 2014; De Conti et al., 2017; Sartor et al., 2015; Wan et al., 2012). RBPs recognise *cis*-acting elements within the transcripts and assemble with their target mRNAs to form so called ribonucleoprotein (RNPs) particles or RNA granules, which can be of heterogenous size and composition (Doyle and Kiebler, 2011; Fritzsche et al., 2013; Kiebler and Bassell, 2006). It is now generally believed that these RNPs determine the fate of their associated RNA molecules by influencing many aspects of the RNA metabolism (Doyle and Kiebler, 2011; Dreyfuss et al., 2002). RBPs interact with transcripts already in the nucleus, where they regulate key steps of pre-mRNA processing such as 5'-capping, splicing and 3'-polyadenylation, as well as nuclear export events (Doyle and Kiebler, 2011; Dreyfuss et al., 2002; Macchi et al., 2004). The nuclear events enable a complex "RNA signature" for a given transcript, consisting of regulatory elements at both the primary sequence and structure levels. This RNA signature, unique for each transcript, is recognised by a specific set of RBPs and determines the future cytoplasmic fate of the mRNAs (Doyle and Kiebler, 2011). Once exported to the cytoplasm, the RNPs are further remodelled in order to regulate other aspects of the RNA metabolism such as mRNA stability, localisation, translation control and eventually local protein synthesis at the site of demand (**Figure 1**) (Doyle and Kiebler, 2011).

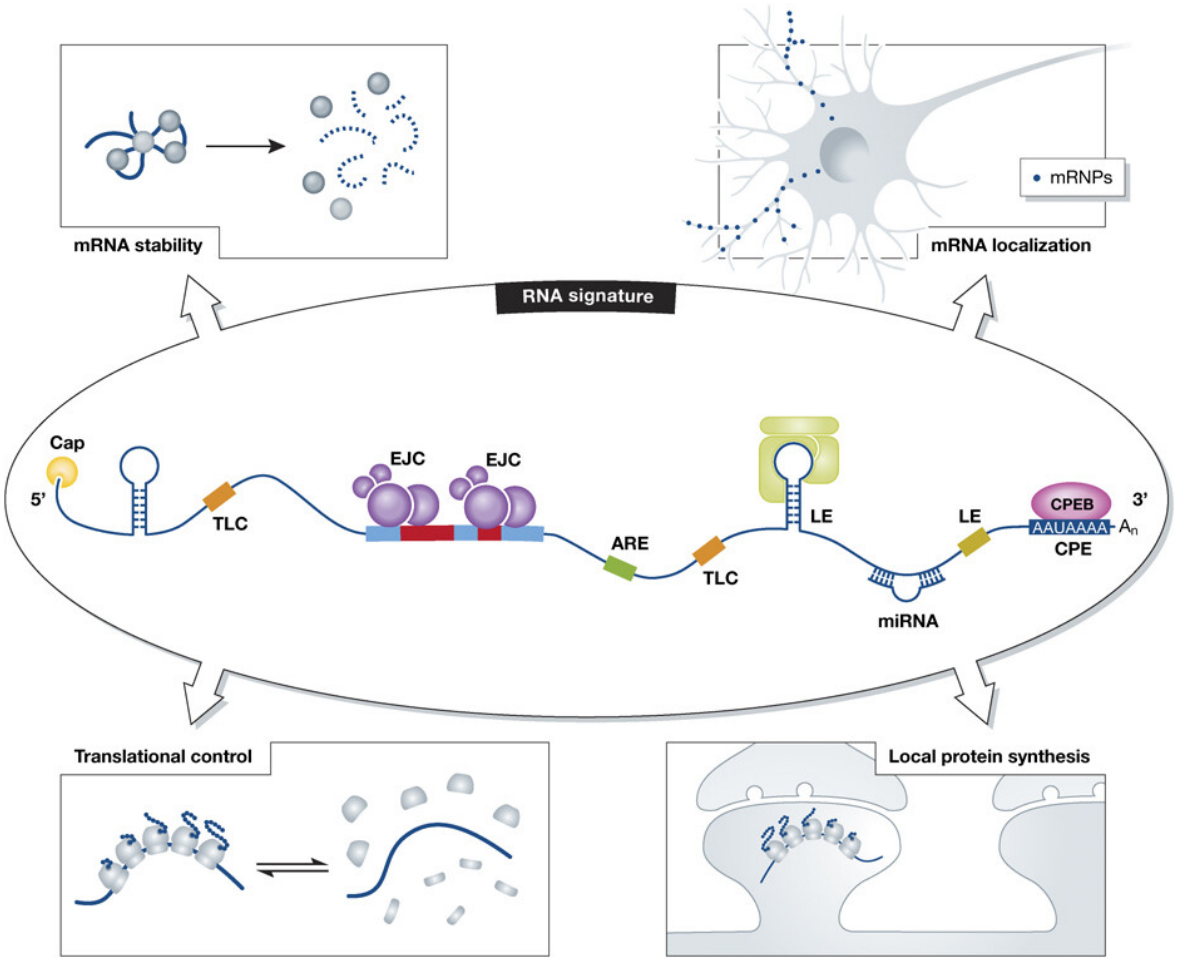

Figure 1: RNA signature as a mechanism to define mRNA fate in the cytoplasm
The RNA signature, defined by pre-mRNA processing events in the nucleus, provides a transcript-specific label that determines how the mRNA is further processed in the cytoplasm. By recognising unique combinations of these *cis*-acting elements, a set of RBPs will regulate different aspects of the metabolism of a given transcript (listed in the four displayed panels) (Doyle and Kiebler, 2011; Dreyfuss et al., 2002). RNA signature is made of multiple regulatory elements: ARE, AU-rich element; Cap, 7-methylguanosine; CPE, cytoplasmic polyadenylation element; CPEB, cytoplasmic polyadenylation element-binding protein; EJC, exon junction complex; LE, localisation element; TLC, translation control element. Taken from (Doyle and Kiebler, 2011). Licence Number: 5627120618719

In the central nervous system, mRNA localisation and local translation are essential mechanisms for the spatial and temporal regulation of gene expression (Holt and Schuman, 2013). Indeed, due to their highly polarised structure with processes extending far from the cell body, neurons must respond to external stimuli by rapidly adjusting protein expression in different compartments. Localisation of mRNAs enable (local) protein synthesis not only in the soma, but also in distal neuronal compartments such as synapses close to dendrites or axonal growth cones (Holt and Schuman, 2013). Such processes underlie fundamental cellular mechanisms in both dendrites and axons including dendritic arborization, long-term

synaptic plasticity as well as axon outgrowth (Doyle and Kiebler, 2011; Holt and Schuman, 2013). It's generally accepted that mRNAs are transported, as part of RNPs, along the neuronal cytoskeleton of axons and dendrites with the help of molecular motors such as kinesins, dyneins and myosins (Buxbaum et al., 2015; Gumy et al., 2014; Kiebler and Bassell, 2006). RBPs are thought to interact with the motor proteins either directly through physical interaction or indirectly through an adapter protein (Mofatteh and Bullock, 2017). In the case of dendritic mRNA trafficking, the presence of several RPBs in transport RNPs, which act as translation repressors, led to the hypothesis that mRNAs transported within the RNPs travel to their synaptic destination in a translationally repressed state (Dahm and Kiebler, 2005; Fritzsche et al., 2013). The recruitment of RNPs to selected synapses can occur in an activity-dependent manner (Doyle and Kiebler, 2011). To explain the dendritic mRNA trafficking, the so-called "*sushi belt model*" has been postulated. According to this model, RNPs are constantly transported bidirectionally in dendrites to provide specific mRNAs only to previously activated synapses. This process could be combined with an activity-dependent tagging of synapses, which could recruit dynamic microtubule extending into dendritic spines, allowing the recruitment of individual RNPs (Doyle and Kiebler, 2011). Once at its final destination, the mRNA is thought to be anchored at specific postsynaptic sites and the RNP is disassembled. This, in turn, would allow local translation of mRNAs into proteins contributing to the structural and functional rearrangement of synapses (Bauer et al., 2019; Buxbaum et al., 2014; Doyle and Kiebler, 2011; Park et al., 2014). In many cases, synaptic proteins are multi-subunit complexes in which only one of the subunits is translated locally, while the other(s) are translated in the soma and conventionally transported to the synaptic target. One notable example is the active enzyme Calcium/Calmodulin-dependent protein kinase II (CamKII), which has two subunits, CamKIIα and CamKIIβ. The α-subunit is translated locally when the synapse is activated and associates there with the β-subunit, which is translated in the cell body and only then transported to the synapse. Thus, the enzyme is only active when the synapse has been previously activated (Doyle and Kiebler, 2011). Experimental support of the "*sushi belt model*" was provided by a study on the 3'-untranslated region (UTR) dependent dendritic transport of the *regulator of G-protein signaling 4* (*Rgs4*) mRNA (Bauer et al., 2019). Once the process is complete at the synapses, the mRNA can either be degraded or, alternatively, reassembled into RNPs to resume transport and another round of translation (Bauer et al., 2019).

1.1.1 Staufen2 and its role in RNA transport regulation

Staufen2 (Stau2) belongs to the family of double-stranded RBPs (dsRBPs), which bind specifically to double-stranded RNA via dsRNA-binding domains (Heraud-Farlow and Kiebler, 2014). The Staufen (Stau) family of dsRBPs play a conserved role in RNA localisation in different organisms, including *Drosophila*, *Xenopus*, *Aplysia*, zebrafish and mouse (Heraud-Farlow and Kiebler, 2014). Stau was originally described for the localisation of maternal and neurogenic RNA in *Drosophila* oocytes and neuroblasts, respectively (Li et al., 1997; St Johnston et al., 1991). Mammalian Stau exists as two orthologues, Stau1 and Stau2, and both can be expressed as multiple isoforms resulting from alternative splicing events (Duchaine et al., 2002; Heraud-Farlow and Kiebler, 2014; Monshausen et al., 2001). Unlike Stau1, which is ubiquitously expressed and found in most cell types, Stau2 is expressed specifically in the brain and gonads, and only at low levels in other tissues (Duchaine et al., 2002). Both Stau1 and Stau2 localise as particles in the soma and dendrites of primary rodent hippocampal neurons, suggesting a common role in the delivery of RNA to dendrites. However, as they have been reported to be components of distinct particles, they are likely to have non-redundant functions in neurons (Duchaine et al., 2002). Stau2 has been implicated in the regulation of dendritic transport of mRNAs encoding proteins relevant at synapses, thus contributing to dendritic spine morphogenesis, synaptic plasticity and memory formation in mammalian neurons (Heraud-Farlow and Kiebler, 2014). Indeed, Stau2-containing RNPs have been reported to traffic bidirectionally along microtubules into dendrites of hippocampal neurons (Bauer et al., 2019; Kiebler et al., 1999; Kohrmann et al., 1999). In support of its role in RNA localisation is the finding that expression of a dominant-negative form of Stau2 in neurons leads to a reduction in a large proportion of dendritic RNAs with a concomitant increase in somatic RNA levels (Goetze et al., 2006; Tang et al., 2001). Stau2-containing RNPs show a distinct protein and mRNA composition (Fritzsche et al., 2013; Heraud-Farlow et al., 2013). Stau2 binds complex, long-ranged RNA hairpins in the 3'-UTR of its mRNA targets (Fernandez-Moya et al., 2021). Several studies have identified a repertoire of mRNAs associated with Stau2 in the brain and cell lines but not all of them are directly regulated by Stau2 (Furic et al., 2008; Heraud-Farlow et al., 2013; Kusek et al., 2012; Maher-Laporte and DesGroseillers, 2010). For example, of the approximately 1200 mRNAs found to be associated with Stau2 in the embryonic rat brain, only 38 were directly affected by Stau2 (Heraud-Farlow et al., 2013). Most of the identified Stau2 targets encode synaptic proteins including signalling molecules such as G protein-coupled receptor (GPCR) involved in learning and memory (Heraud-Farlow et al., 2013). Another study of

Stau2-RNA complexes in the embryonic mouse brain identified significant Stau2 binding in the 3'-UTR of 356 neuronal mRNAs (Sharangdhar et al., 2017). One of the identified Stau2 targets of interest is *Calmodulin 3* (*Calm3*), encoding an essential calcium-binding protein required for kinase activation at the synapse (Sharangdhar et al., 2017; Wayman et al., 2008). Stau2 was shown to mediate the dendritic localisation of *Calm3* mRNA in hippocampal neurons via a retained intron within the 3'-UTR. In addition, the dendritic *Calm3* mRNA localisation was shown to be promoted by synaptic activity (Sharangdhar et al., 2017). Consistent with this is the study reporting the activity-dependent recruitment of *Rgs4* mRNA to dendritic synapses, which is directly modulated by Stau2 (Bauer et al., 2019). These findings establish Stau2 as an important regulator of the dendritic localisation of mRNA targets in an activity-dependent manner. It's worth mentioning that *Calm3* mRNA was shown to accumulate in the nucleus of neurons in the absence of Stau2 (Sharangdhar et al., 2017). This mislocalisation event of a Stau2 target is consistent with the role of Stau2 in the nucleus previously proposed by (Macchi et al., 2004). In addition to the predominant cytoplasmic localisation of Stau2, the authors showed that Stau2 can enter the nucleus through an intrinsic nuclear localisation signal (NLS), allowing a nucleus-cytoplasmic shuttling activity. One can therefore speculate that when Stau2 is not binding any RNAs, the NLS is unmasked, leading to the import of Stau2 into the nucleus to bind other mRNA targets (Macchi et al., 2004). Furthermore, a series of Stau2 protein interactors have been identified in the Kiebler lab (Fritzsche et al., 2013). Interestingly, the authors revealed that several known translational repressors are enriched in Stau2-containing RNPs, including Pumilio2 (Pum2), Fragile X Mental Retardation Protein (FMRP), Dead box helicase 6 (DDX6/Rck), Purα, as well as several components of the RNA-induced silencing complex (RISC). In addition, this study revealed the absence of the eukaryotic translation initiation factor 4E (eIF4E) in Stau2-RNP and the presence of the nuclear cap-binding protein 80 (CBP80) and the nuclear polyadenylate binding protein 1 (PABPN1), the presence of which prevents translation initiation (di Penta et al., 2009; Fritzsche et al., 2013; Kim et al., 2009). Furthermore, ribosomes were not found to be present in Stau2-RNPs (Fritzsche et al., 2013; Heraud-Farlow et al., 2013). Taken together, these findings provide experimental support for the theory that localised mRNAs are translationally silenced during transport (Dahm and Kiebler, 2005; Fritzsche et al., 2013). Notably, evidence for a role of Stau2 in the stabilisation of synaptic target mRNAs was also reported, thus suggesting that mammalian Stau2 may act as a multifunctional post-transcriptional regulator (Heraud-Farlow et al., 2013).

1.1.2 Pumilio2 and its role in translational regulation

The mammalian Pumilio2 (Pum2) is a member of the Pum and FBF (PUF) protein family comprising highly conserved RBPs (Goldstrohm et al., 2018; Wang et al., 2018). Mammals express two Pum genes, *Pum1* and *Pum2*, both with high homology to *Drosophila* Pum (Spassov and Jurecic, 2002). Pum2 binds a short nucleotide sequence (UGUANAUA) in the 3'-UTR of its target mRNAs (White et al., 2001; Zhang et al., 2017). There is evidence revealing several possible mechanisms of how Pum2 regulates protein expression, including translation, stability and transport (Goldstrohm et al., 2018; Hotz and Nelson, 2017; Martinez et al., 2019; Van Etten et al., 2012). Pum has been shown to act as a repressor of RNA translation in many organisms including yeast, *Drosophila* and *Xenopus* (Nakahata et al., 2003; Parisi and Lin, 2000; Wickens et al., 2002). Several lines of evidence suggest that Pum can repress translation in multiple ways, including a deadenylation-dependent mechanism. Different members of the PUF proteins, including yeast Puf5p or human Pum1 and Pum2 have been reported to recruit the CCR4-NOT (CNOT) deadenylase complex to mRNA targets, resulting in the shortening of the polyA tail at the 3'-end of mRNAs. Consequently, this PUF-mediated deadenylation leads to mRNA instability and translational inhibition (Goldstrohm et al., 2007; Van Etten et al., 2012). Also in *Drosophila*, one of the Pum targets, the RNA *hunchback* (*hb*), essential for embryonic segmentation, was reported to be subject to polyA-dependent translational regulation mediated by Pum (Wreden et al., 1997). Pum2 can also repress translation by blocking the assembly of the initiation complex on the mRNA 5'-cap structure. Indeed, Pum2 has been reported to repress translation of *RINGO/SPY* mRNA by directly binding to the 5'-cap structure in *Xenopus* oocytes. In this way, Pum2 prevents eIF4E from binding to the cap. It has been suggested that Pum2 blocks thereby translation initiation (Cao et al., 2010). Additionally, a Pum2-mediated mechanism affecting translation elongation was also reported. Here, human Pum2 was shown to form an inhibitory complex by interacting with Argonaute (Ago) proteins and the elongation factor 1A (eEF1A), a GTPase required for translation elongation. In doing so, Pum2 represses translation in the elongation phase (Friend et al., 2012). Similar to the deadenylation-dependent repression mechanism, the corresponding mammalian PUM2/Ago/eEF1A complex was also found in *C.elegans*, suggesting that such Pum-mediated repression mechanisms are evolutionarily conserved (Friend et al., 2012). In addition to its direct role in protein expression control, it has been reported that Pum2 regulates RNA transport. A pioneer study has shown that the Pumilio homolog Puf118 is required for the localisation of mRNAs at the front of migrating cells during chemotaxis in the amoeba *Dictyostelium*

discoideum (Hotz and Nelson, 2017). It has also been reported that Pum2 prevents the transport of transcripts into axons by retaining them in the cell body, thereby controlling axonal protein synthesis in developing neurons (Martinez et al., 2019). The crucial impact of Pum2 on translation and its numerous RNA interactors suggest an important role in regulating cellular physiology. Despite extensive research on Pum proteins in different organisms as well as *in vitro* experiments, their role and contribution to neuronal function is still not really understood. Studies in *Drosophila* have provided the first evidence for a crucial role of Pum in the nervous system. Here, Pum was shown to (i) modulate dendrite morphogenesis in peripheral neurons via translational control, (ii) influence synaptic growth and function by regulating eIF4E mRNA expression and (iii) control neuronal excitability by repressing the translation of a voltage-gated sodium channel (Mee et al., 2004; Menon et al., 2009; Menon et al., 2004; Schweers et al., 2002; Ye et al., 2004). These findings point towards a role of Pum2 in neuronal functioning. Supporting for this notion is the finding that the Stau/Pum pathway is needed for synaptic plasticity and long-term memory (Dubnau et al., 2003). Pum2 forms RNA granules that localise to the somatodendritic compartment of hippocampal neurons (Vessey et al., 2006). Thereby, it also interacts with other RBPs such as FMRP and possibly with Stau2 (Fritzsche et al., 2013; Zhang et al., 2017). In addition, Pum2 and Stau2 were found to share a significant proportion of their mRNA targets, supporting the idea that Pum2 also contributes to the activity-dependent regulation of localised mRNA targets (Heraud-Farlow and Kiebler, 2014; Schieweck et al., 2021b; Zahr et al., 2018; Zhang et al., 2017). However, whether and how Pum2 regulates localised translation is still unclear. In general, Pum2 has been reported to affect dendritic spine morphogenesis, synaptic transmission and thus function in mammalian neurons (Vessey et al., 2010). Specifically, loss of Pum2 in immature neurons was associated with increased dendrite outgrowth, making Pum2 a negative regulator of dendrite development. In mature neurons, Pum2 knockdown resulted in reduced dendritic spines and increased elongated dendritic filopodia. An increase in the number of excitatory synapses and the frequency of excitatory currents was also observed. Further support for the role of Pum2 in synaptic transmission comes from evidence that it negatively regulates, like *Drosophila* Pum, the translation of transcripts encoding sodium channels, such as *Sodium voltage-gated channel alpha subunit 1* and *8* (*Scn1a*, *Scn8a*) and the AMPA receptor subunit *Glutamate ionotropic receptor AMPA type subunit 2* (*Gria2*) in the hippocampus, thus attenuating neuronal excitation (Dong et al., 2018; Driscoll et al., 2013; Vessey et al., 2010). Notably, in addition to the most commonly reported role in translational repression, an essential role of Pum2 in

translational activation has recently been reported (Schieweck et al., 2021b). Indeed, the authors showed that Pum2 activates the expression of key GABAergic synaptic components, such as the $GABA_A$ receptor scaffold protein Gephyrin (Schieweck et al., 2021b). Taken together, these findings support the idea that Pum2 may exert its functions in the nervous system through different regulatory roles, making this RBP, like Stau2, a potential multifunctional post-transcriptional regulator.

1.1.3 Stau2 and Pum2 critically contribute to embryonic neurogenesis

Post-transcriptional regulation of gene expression has emerged as a key player not only in synaptic physiology and functionality in mature neurons, but also in critical aspects of neurogenesis. By regulating different stages of the RNA life cycle, *e.g.* splicing, stability, transport/localisation and translation of key fate determinants, RBPs contribute significantly to embryonic corticogenesis (Parra and Johnston, 2022; Pilaz and Silver, 2015). Research over the past decade has shown that, in addition to their roles in mature brain, Stau2 and Pum2 play a crucial role in cell fate specification during mammalian cortical development (Chowdhury et al., 2021; Kusek et al., 2012; Vessey et al., 2012; Zahr et al., 2018). The role of Stau in neurogenesis was first uncovered in *Drosophila* (Li et al., 1997). In neural progenitors (or neuroblasts), Stau binds RNA targets coding for cell fate determinants *e.g. prospero* (*Pros*) forming a RNA complex that also contains the translational repressor Brain tumor (Brat) and the adaptor protein Miranda (Chia et al., 2008). During the asymmetric division of neuroblasts, the Stau-containing RNA complex is asymmetrically segregated in the differentiating cell progeny, which is committed to become the ganglion mother cell (GMC) (Broadus et al., 1998; Li et al., 1997). Once segregated in the GMC, the RNA complex releases the mRNA cargo from translational repression. The proneurogenic transcription factor (TF) Pros can then promote GMC differentiation into neurons by activating genes involved in differentiation and repressing genes involved in proliferation (Chia et al., 2008). The asymmetric cell division is a conserved feature of neural development, occurring also during mammalian corticogenesis (Gotz and Huttner, 2005). During cortical development, radial glial cells (RGCs), which are the major progenitors of cortical neurons and glia, undergo asymmetric division leading to direct or indirect neurogenesis (Huilgol et al., 2023; Noctor et al., 2004). In direct neurogenesis, RGCs divide asymmetrically and give rise to another RGC and a neuron. In indirect neurogenesis, RGCs divide asymmetrically to self-renew and give rise to an intermediate progenitor cell (IPC), which then divides symmetrically to produce two neurons (Noctor et al., 2004; Sessa et al.,

2008). As an additional function, RGCs act as scaffolding platform guiding the migration of newborn neurons to the cortical plate (Rakic, 1972; Tan and Shi, 2013). The organisation of neurons into different layers then depends on the time of their generation, with the earliest-born neurons organised into the deepest layers and later-born neurons organised into more superficial cortical layers (Hevner et al., 2003). Similar to *Drosophila* Stau, mammalian Stau2 has been shown to be asymmetrically enriched in RGCs in the developing mouse cortex (Kusek et al., 2012; Vessey et al., 2012). Here, Stau2 assembles with mRNA targets encoding cell fate determinants, like *Prospero-related homeobox 1* (*Prox1*) and *tripartite motif containing 32* (*Trim32*) to form RNPs that also contain the translational repressor Pum2 and the DEAD-box helicase 1 (DDX1) (Vessey et al., 2012). Stau2-containing RNPs are asymmetrically segregated during progenitor cell division in one of the two daughter cells likely to become the IPC (Kusek et al., 2012; Vessey et al., 2012). Stau2-associated targets are thought to be translationally repressed during RGC division and are only translated upon segregation to promote differentiation and to suppress stem cell status (Vessey et al., 2012). The identity of the RNA cargo delivered by Stau2 during mouse corticogenesis has been identified (Chowdhury et al., 2021; Kusek et al., 2012). Interestingly, the recent characterisation of Stau2-associated mRNA targets along different time points of corticogenesis (Chowdhury et al., 2021) revealed several previously validated Stau2 targets in mature brain, *e.g. CamKIIa, Sacm1l, Calm3, Rgs2, Stx1a, Nnat, Actg1* (Fritzsche et al., 2013; Heraud-Farlow et al., 2013). Furthermore, Pum2 and DDX1, both found in the RNA complex with Stau2 in RGCs, were also previously found to be part of Stau2-containing RNPs in post-mitotic neurons (Elvira et al., 2006; Fritzsche et al., 2013). Taken together, this evidence strongly suggests that Stau2-containing RNPs in RGCs and mature brain share many similarities (Vessey et al., 2012). Notably, *Prox1* mRNA, previously shown by (Vessey et al., 2012) as Stau2 target asymmetrically localised in RGCs, was not further validated by the more recent characterisation of Stau2-associated targets in mouse cortex by (Chowdhury et al., 2021). However, *Prox1* as Stau2 target during development is still an important option, as the authors acknowledged that this lack of validation may be due to experimental reasons (Chowdhury et al., 2021). The complexity of the Stau2 RNA cargo was revealed by the evidence that some targets are permanently present, while others change dynamically over time during corticogenesis (Chowdhury et al., 2021). The subset of genes permanently present in the Stau2-delivered RNA cargo were associated with fundamental cellular processes, such as chromosome organisation, macromolecule localisation, translation, mRNA splicing and DNA repair. On the other hand, temporal

changes over time affected targets mostly associated with processes that vary during neurogenesis, such as cell projection organisation, synaptic transmission and neurite outgrowth (Chowdhury et al., 2021). Genes encoding extracellular matrix (ECM) proteins, which are important for cell growth, differentiation and migration in neuronal development were also enriched in the dynamic target set (Chowdhury et al., 2021; Maeda, 2015; Schwartz and Domowicz, 2018). Such dynamic changes in targets over time are thought to provide a sophisticated mechanism for ensuring the orderly generation of neurons (Chowdhury et al., 2021). In support of the idea that Stau2 localises mRNA targets that can promote the IPC fate, there is evidence that during the peak of IPC generation, there is a highly enriched set of genes encoding IPC determinants, that are unbound at later stages, when the neurogenic IPC production has been terminated (Chowdhury et al., 2021). Interestingly, the absence of one of the three main components of the asymmetrically segregated RNA complex (Stau2, Pum2 or DDX1) leads to misregulation of neurogenesis with increased generation of neurons and a reduction in the progenitor pool (Vessey et al., 2012). Therefore, it is hypothesised that by binding, localising and repressing mRNA targets that promote neurogenesis, this Stau2- and Pum2-dependent RNA complex maintains the pool of progenitors in an undifferentiated state until the RGC is ready to differentiate into a neuron (Vessey et al., 2012) (**Figure 2**).

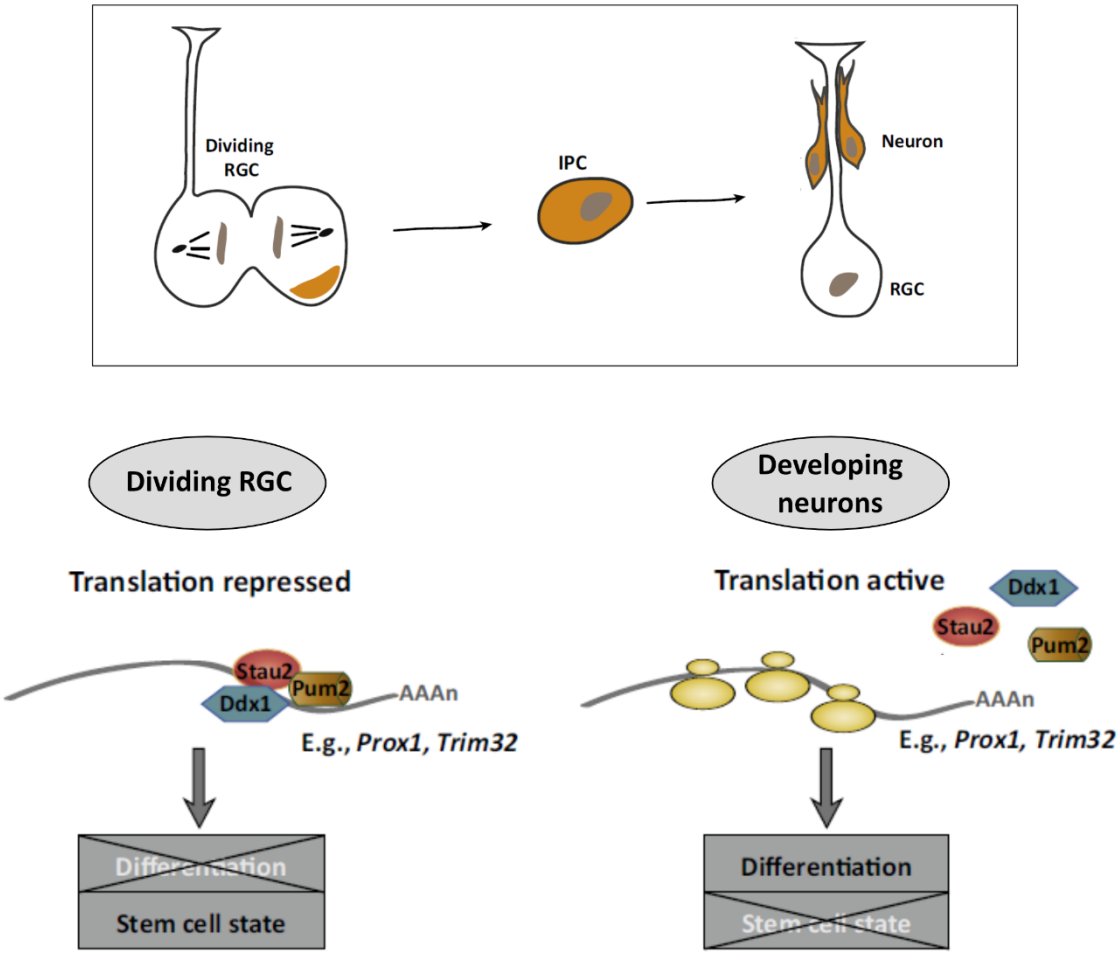

Figure 2: Possible roles of the Stau2 and Pum2-containing RNA complex in the embryonic developing cortex

During RGC division, Stau2 affects the asymmetric distribution of targets encoding cell fate determinants such as *Prox1* and *Trim32* in one of the two daughter cells that are likely to become first IPCs and then neurons. Due to the presence of Pum2 in the Stau2-containing RNA complex, the localised targets are thought to be translationally repressed ensuring the maintenance of stem cell status. Upon RGC division, the repression of the targets is lifted, promoting neuronal differentiation (Vessey et al., 2012). Modified from (Heraud-Farlow and Kiebler, 2014), distributed under Creative Commons Attribution 3.0 Unported Licence, https://creativecommons.org/licenses/by/3.0/

Notably, a similar role for Pum2 has also been observed in human germ cell development, where this RBP acts as a translational repressor in order to maintain germ line stem cells (Moore et al., 2003). In support of Pum2 role in embryonic neurogenesis, there is further evidence that in mouse cortical RGCs, Pum2 is a major post-transcriptional contributor ensuring the correct and temporal generation of different neuronal subtypes. In particular, it has been shown that RGCs are predisposed to generate all neuronal subtypes, by co-expressing mRNAs encoding different neuronal specification proteins. In this context, Pum2

forms a complex with 4E-T that translationally represses neuronal specification mRNAs, ensuring the temporal and specific protein expression of different neuronal phenotypes (Zahr et al., 2018). Translational repression control by the eIF4E/4E-T complex has previously been shown to mediate appropriate neurogenesis by controlling the expression of mRNAs encoding proneurogenic proteins (Yang et al., 2014). Disruption of either Pum2 or 4E-T leads to abnormal protein expression generating a deep layer neuron phenotype in committed superficial layer neurons (Zahr et al., 2018). In this work, the authors also identified Pum2-associated mRNA targets, a subset of which were also 4E-T targets. Interestingly, the Pum2/4E-T shared targets mainly encode proteins associated with transcriptional regulation and neuronal development. Indeed, many Pum2/4E-T shared targets encode TFs such as POU Class 3 Homeobox 3 (Pou3f3/Brn1), Transducin-Like Enhancer of Split 4 (Tle4) and the members of proneurogenic basic helix-loop-helix (bHLH) Neurogenin1 (Neurog1), Neurogenin2 (Neurog2) and Achaete-scute homolog1 (Ascl1) (also known as Mash1) (Zahr et al., 2018). An important role of Pum2 in hippocampal development has also been reported. Depletion of Pum2 was shown to reduce the self-renewal of neural stem cells and their differentiation into neurons. In addition, Pum2 depletion resulted in increased protein expression of its mRNA targets, further supporting its role as a translational repressor important in neurogenesis (Zhang et al., 2017). The authors also reported that Pum2 interacts with FMRP, another important translational repressor, previously shown to be involved both in mature neurons and neurogenesis (Chen et al., 2014; Luo et al., 2010; Saffary and Xie, 2011). These findings support the idea that, similar to mature neurons, both Stau2 and Pum2 may act in a complex interactome of different RBPs to control gene expression and contribute to cell fate specification during neurogenesis (Schieweck et al., 2021a; Zahr et al., 2018).

1.2 Direct reprogramming as innovative strategy for neuronal cell replacement

A major challenge in the field of regenerative medicine has always been the limited capacity of the adult mammalian central nervous system (CNS) to innately regenerate after significant neuronal loss due to traumatic brain injury or neurodegenerative disease (Barker et al., 2018). In fact, even with confirmed adult neurogenesis, the limited number and activity of neural stem cells (NSCs) in the adult brain, makes them insufficient to replace significant neuronal loss (Kase et al., 2020). Potential neuronal replacement strategies that have been investigated include: rescue of dysfunctional but not lost cells by the use of neurotrophic factors, replacement of lost cells (i) by transplantation of exogenously derived and *in vitro*

cultured cells, *e.g.* human fetal tissue cells, human embryonic stem cells (hESCs), and induced pluripotent stem cells (iPSCs), (ii) by recruitment of endogenous neuronal precursors, (iii) by directly reprogramming of local non-neuronal cells within the brain (Barker et al., 2018). The direct conversion of local reactive glia, such as scar-forming or neurotoxic glial cells, into neurons has emerged as an innovative and viable option to replace functional neurons. This technology offers many advantages, including the direct generation of neurons bypassing the intermediate pluripotent state, and the potential enhancement of the activated environment around the neuronal loss to support the regenerative process. In addition, neuronal reprogramming eliminates the challenges associated with the exogenous cell transplantation such as ethical issues, immune reactions and tumorgenicity (Barker et al., 2018; Wan and Ding, 2023). Since almost all our cells have identical DNA, it is the differential expression of distinct subsets of genes that defines the identity of a cell type (Breschi et al., 2020; Regev et al., 2017). Direct reprogramming has overturned the old concept that the cell identity is fixed and irreversible after development, demonstrating that conversion between cells derived from the same or different lineages, even across germ layers is possible (Masserdotti et al., 2016). A key example is the proven direct conversion of astrocytes, fibroblasts and hepatocytes into functional neurons *in vitro* by defined factors (Heins et al., 2002; Marro et al., 2011; Vierbuchen et al., 2010). In contrast to other somatic cell reprogramming approaches, where the cells are first induced to become iPSCs or NSCs which can then differentiate into neurons, in direct reprogramming the cells are converted into neurons without undergoing the intermediate step of pluripotent stem cells or neural stem cells (Chen et al., 2023) (**Figure 3**).

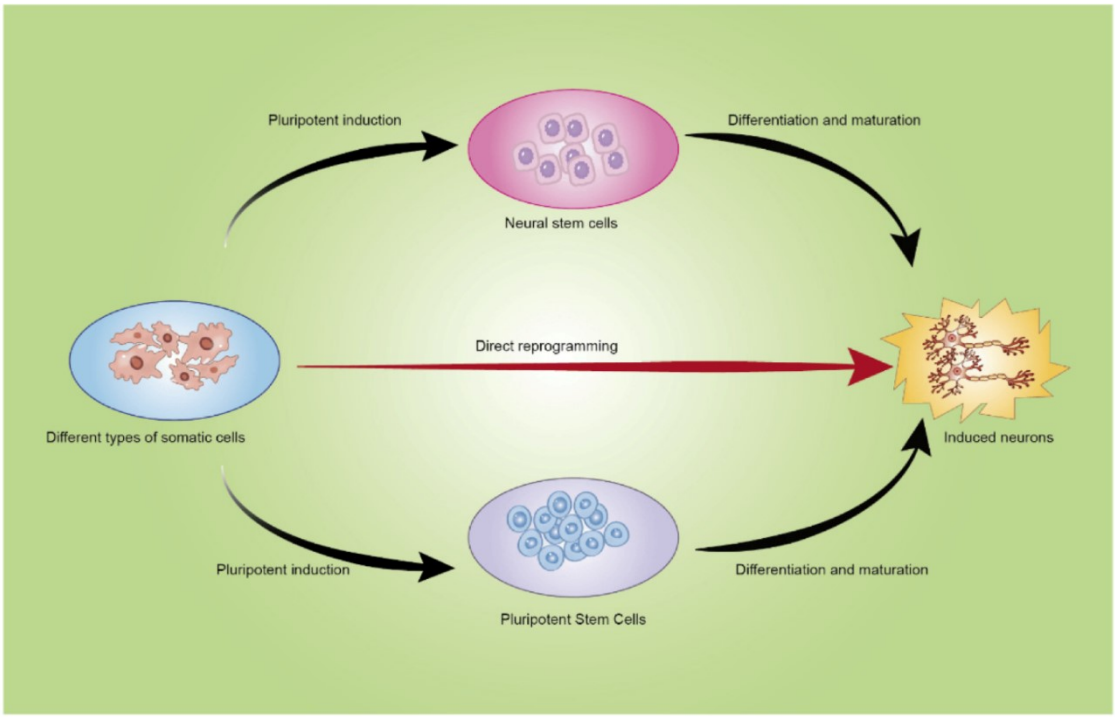

Figure 3: Different pathways of somatic cell reprogramming into neurons
Somatic cells can be forced to become iPSCs or NSCs. These stem cells can then be induced to differentiate into neurons. In direct reprogramming, somatic cells are directly induced to become neurons without the need for a stem cell state. Taken from (Chen et al., 2023), distributed under Creative Commons Attribution 4.0 International (CC BY) licence, https://creativecommons.org/licenses/by/4.0/

1.2.1 The role of TFs in direct neuronal reprogramming

The principle of direct reprogramming is based on crossing the lineage boundaries established during cell specification by re-expressing one or a combination of key TFs that are essential during development and can direct the conversion of one differentiated cell into another (Masserdotti et al., 2016). In this case, TFs are primarily responsible for the changes in gene expression that lead to the activation of neuron-specific genes and the silencing of the starter cell-specific genes (Bocchi et al., 2022). Differentiated glial cells, such as astrocytes, have been shown to be a good source for reprogramming-based neuron replacement. Since astrocytes and neurons share a common developmental origin, the re-expression of a single neurogenic TF, which plays an essential role in embryonic neurogenesis, is sufficient to direct their conversion into neurons *in vitro* (Bertrand et al., 2002; Heins et al., 2002). Heins and colleagues were the first to report that postnatal glial cells isolated from the mouse cerebral cortex can be converted into neurons *in vitro* by the forced expression of the single TF Paired Box 6 (Pax6) (Heins et al., 2002). During

neurogenesis, Pax6 is expressed in the NSCs and neural progenitor cells (NPCs) in the dorsal telencephalon and modulates the dorsoventral patterning of the embryonic mammalian telencephalon (Hebert and Fishell, 2008; Stoykova et al., 2000). The two proneural bHLH TFs, Neurog2 and Ascl1, were also shown to be master regulators of neuronal reprogramming *in vitro*, inducing the conversion of astrocytes into functional synapse-forming neurons capable of firing action potentials (Berninger et al., 2007; Heinrich et al., 2010; Heinrich et al., 2011). The potency of these TFs in cell conversion is explained by their key role in embryonic neurogenesis. *Neurog2* and *Ascl1* are proneural genes whose expression is induced at high levels in neural progenitors, leading to the activation of neuronal differentiation pathways (Bertrand et al., 2002). During development, Neurog2 and Ascl1 are expressed in progenitors of different regions, giving rise to different neuronal subtypes. Neurog2 is a downstream target of Pax6 and is upregulated in NSCs in the dorsal telencephalon. Here, Neurog2 regulates the specification of glutamatergic projection neurons through the induction of downstream factors such as Neuronal differentiation (NeuroD*)* and T-box brain transcription factor 1 and 2 (Tbr1, Tbr2*)* (Fode et al., 2000; Schuurmans and Guillemot, 2002). In the ventral telencephalon, progenitor cells express different TFs, including Ascl1, GS Homeobox 1/2 (Gsx1/2) and Distal-Less Homeobox (Dlx1/2), which regulate the specification of GABAergic neurons and interneurons (Imayoshi and Kageyama, 2014). Reflecting their role in development, Neurog2 and Ascl1 induce direct conversion of cortical astrocytes into neurons with glutamatergic and GABAergic identity, respectively (Heinrich et al., 2010; Heinrich et al., 2011; Masserdotti et al., 2015). In contrast to cortical astrocytes, spinal cord (SC)-derived astrocytes are instructed by Neurog2 and Ascl1 to become neurons close to a ventral SC GABAergic V2b interneuron type (Kempf et al., 2021). This is consistent with the role of Neurog2 and Ascl1 in generating specific interneuron subtypes during SC development (Lu et al., 2015; Misra et al., 2014). Similarly, cerebellum-derived astrocytes were directly induced by Neurog2 or Ascl1 to become neurons with predominantly GABAergic identity (Chouchane et al., 2017). Taken together, this evidence supports the important aspect that not only the TF used for reprogramming, but also the regional identity of the starter cell is crucial for the generation of different neuronal subtypes (Chouchane et al., 2017; Hu et al., 2019). Transcriptomic studies of postnatal cortical astrocyte-to-neuron conversion induced by Neurog2 or Ascl1 revealed very dynamic and rapid changes in gene expression occurring during the first 48h of reprogramming. In addition, Neurog2 and Ascl1 were shown to induce largely distinct transcriptional programmes during reprogramming, with only a few genes commonly

regulated by both TFs. These include genes encoding the transcriptional regulators Prox1, Hairy and enhancer of split 6 (Hes6), TMF-regulated nuclear protein 1 (Trnp1), Insulinoma-associated 1 (Insm1), SRY-box containing gene 11 (Sox11) and NeuroD4 (Masserdotti et al., 2015). Of these, NeuroD4 alone was sufficient to induce the generation of functional neurons (Masserdotti et al., 2015). Noteworthy, despite some evidence for similarities in ordered gene activation in reprogramming and *in vivo* development, it appears that embryonic neurogenesis is not fully recapitulated in direct neuronal reprogramming and that different transcriptional events may be triggered to achieve neuronal identity (Masserdotti et al., 2016). In fact, only a few of the Neurog2-regulated genes during reprogramming are Neurog2 downstream effectors in progenitor cells during mouse telencephalon development (Gohlke et al., 2008; Masserdotti et al., 2016; Masserdotti et al., 2015). Another bHLH family member, NeuroD1, has also been identified as a key TF in neuronal reprogramming, as it is sufficient to reprogramme astrocytes into functional glutamatergic neurons *in vitro* and *in vivo* (Guo et al., 2014). During development, NeuroD1 is a downstream target of Neurog2 and is important for the production of glutamatergic neurons in the developing and adult cerebral cortex and hippocampus, and is required for the survival and maturation of newborn neurons during adult neurogenesis (Fode et al., 2000; Gao et al., 2009; Hevner et al., 2006). Neurog2, Ascl1 and NeuroD1 are often referred as pioneer factors because of their ability to bind DNA in a closed conformation, thereby enabling the expression of inactivated genes and cell fate switching (Bocchi et al., 2022; Morris, 2016). In addition to the activation of neuronal genes, another important step in direct neuronal reprogramming is the silencing of genes that define the starter cell identity and all potential alternative fates. Although still under investigation, the existence of pan-repressors of alternative fates has been suggested (Bocchi et al., 2022). For example, in the context of fibroblast-to-neuron reprogramming, induced by the expression of three TFs, Ascl1, Brn2 (also known as Pou3f2) and Myelin transcription factor 1 like (Myt1l), Myt1l, acts as a transcriptional repressor of non-neuronal lineages (Mall et al., 2017; Wapinski et al., 2013). Indeed, when co-expressed with Myogenic Differentiation 1 (Myod1), Myt1l induces fibroblasts-to-neuron conversion by repressing the activation of skeletal muscle genes (Lee et al., 2020). The use of TFs to activate neuronal genes has also been combined with the use of microRNAs (miRNAs) (Vasan et al., 2021). miRNAs are short non-coding RNAs that act as post-transcriptional regulators, either by inducing mRNA degradation or by inhibiting translation (Bartel, 2004). By repressing the genes that are not normally expressed in neural lineages, many miRNAs play a critical role for neuronal differentiation during CNS development (Lang and Shi, 2012). Some of these

miRNAs have also been shown to contribute to neuronal reprogramming when coupled with TFs (Pascale et al., 2022). For example, miR-9-5p/3p and miR-124 promote the direct conversion of human fibroblasts into neurons and the effect is enhanced when they are co-expressed with the TFs, NeuroD2, Ascl1, and Myt1l (Yoo et al., 2011). miR-128 together with the TFs Ascl1, NeuroD1 and LIM Homeobox transcription factor 1 alpha (Lmx1a) leads to enhanced astrocyte-to-neuron conversion *in vivo* (Rivetti di Val Cervo et al., 2017). In addition, in neural cells miR-124 represses the expression of the polypyrimidine tract-binding protein 1 (Ptbp1), an RPB that exerts its alternative splicing function also on neuronal genes (Makeyev et al., 2007; Min et al., 1995; Xue et al., 2013; Xue et al., 2016). It has been reported that repression of Ptbp1 alone is sufficient to promote fibroblast-to-neuron reprogramming (Xue et al., 2013). Another important aspect to consider for efficient induction of neuronal reprogramming is the metabolic change that occurs during the cell fate conversion (Gascon et al., 2016). While astrocytes, fibroblasts and other proliferative cells rely on anaerobic glycolysis and β-oxidation, neurons rely on an oxidative metabolism (McKay et al., 1983; Tsacopoulos and Magistretti, 1996). The rapid metabolic switch is thought to be responsible for the observed increased production of reactive oxygen species (ROS) during the conversion process, which increases lipid peroxidation (Lip-Ox) and leads to significant cell death by ferroptosis (Gascon et al., 2016). Co-expression of reprogramming TFs with the anti-apoptotic protein Bcl-2 or treatment with antioxidants has been shown to reduce Lip-Ox, thereby improving cell fate conversion and survival (Gascon et al., 2016).

1.2.2 Reprogramming somatic cells into neurons

In addition to astrocytes, another cell type suitable for direct and efficient neuronal reprogramming is the olfactory ensheathing cells (OECs), a type of specialised glial cells that shares properties with astrocytes (Ramon-Cueto and Avila, 1998; Sun et al., 2019). Neurog2 alone has been shown to induce the direct conversion of OECs into synapses forming-neurons with electrophysiological properties *in vitro* (Sun et al., 2019). Additionally, OEC-derived neurons successfully integrated after transplantation into normal or injured mouse spinal cord *in vivo* (Sun et al., 2019). Much progress has been made in converting also cells originating from different germ layers into neurons *in vitro*. Mesoderm-derived mouse embryonic and postnatal fibroblasts were reprogrammed into functional neurons *in vitro* by a combinatorial expression of three TFs, Ascl1, Brn2 and Myt1l (called BAM factors) (Vierbuchen et al., 2010). The induced neurons also formed synapses that can fire action potentials (Vierbuchen et al., 2010). Although Ascl1 alone is capable of inducing direct

fibroblast-to-neuron conversion, the combination of BAM TFs is required to achieve more efficient neuronal conversion (Chanda et al., 2014; Treutlein et al., 2016; Vierbuchen et al., 2010). When combined with the TF NeuroD1, the BAM factors elicit the conversion of fetal and postnatal human fibroblasts into neurons (Pang et al., 2011). The BAM cocktail, alone or in combination with other factors, was used to induce neuronal conversion of several other somatic cell types in addition to fibroblasts. Forced expression of the BAM factors directly induces neuronal reprogramming of postnatal mouse adipocyte progenitor cells (APCs) and hepatocytes (Marro et al., 2011; Yang et al., 2013). When combined with the TF, T Cell Leukemia Homeobox 3 (Tlx3) and the miR-124, the BAM factors have also been shown to directly convert human brain vascular pericytes (HBVPs) into cholinergic neurons (Cheng et al., 2009; De Pietri Tonelli et al., 2008; Liang et al., 2018). Partial neuronal conversion of mouse and human pluripotent stem cell-derived cardiomyocytes into neuronal-like cells induced by the combination of NeuroD1 and BAM factors has also been reported (Chuang et al., 2017).

1.2.3 Neuronal reprogramming *in vivo* – achievements and challenges

The *in vitro* neuronal reprogramming studies were accompanied by *in vivo* protocols to investigate the effects of the diseased brain on the direct conversion and the integration of the generated neurons into the pre-existing circuits. Indeed, *in vitro* experiments are limited in their ability to replicate the altered environment created by disease or trauma conditions, such as reactive gliosis and inflammation, which can significantly affect the reprogramming process (Bocchi et al., 2022). *Buffo* and colleagues provided the first evidence of *in vivo* neuronal conversion of proliferating glial cells driven by Pax6 following stab wound (SW) injury in the adult mouse brain (Buffo et al., 2005). Similar to *in vitro* studies, significant progress has been made with *in vivo* reprogramming of reactive glia, including Neuron-Glia antigen 2-expressing glial cells (NG2 glia) and astrocytes, into neurons mainly using the bHLH TFs, such as Neurog2, Ascl1 and NeuroD1 (Vasan et al., 2021). Neurog2 alone was shown to reprogram proliferating glial cells into neurons in an injured brain *in vivo*, but with limited efficiency (Gascon et al., 2016; Grande et al., 2013). Some studies revealed that combining Neurog2 with other factors led to increased reprogramming efficiency. For example, the expression of Neurog2 in combination with (i) exposure to fibroblast growth factor 2 (FGF2) and epidermal growth factor (EGF) (Grande et al., 2013), (ii) expression of the anti-apoptotic protein Bcl2 or treatment with antioxidants, *e.g.* Calcitriol or αT3 (Gascon et al., 2016), (iii) expression of Nuclear receptor-related 1 protein (Nurr1) (Mattugini et al., 2019). Ascl1 in combination with Sox2 or Sox2 alone elicited neuronal reprogramming of

resident NG2 glia in the injured adult cerebral cortex (Heinrich et al., 2014). In the dopamine-depleted striatum, Ascl1, in combination with Lmx1a and Nurr1, drives the reprogramming of endogenous NG2 glia into neurons that resemble fast-spiking, parvalbumin-containing interneurons (Pereira et al., 2017). NeuroD1 can reprogramme cortical NG2 cells and astrocytes into neurons in the injured brain and in a mouse model of Alzheimer's disease (Guo et al., 2014). Also, when co-expressed with Dlx2, NeuroD1 elicits the conversion of striatal astrocytes into GABAergic neurons in a mouse model of Huntington's disease (Wu et al., 2020). NeuroD1-driven neuronal reprogramming of reactive astrocytes also contributes to reverse the effects of glial scar formation in the injured cortex back to normal neural tissue (Zhang et al., 2020). Importantly, some of the evidence for direct astrocyte-to-neuron conversion *in vivo* has been challenged by a recent publication (Chen et al., 2020; Liu et al., 2020; Wang et al., 2021a; Wang et al., 2021b; Xiang et al., 2021). Using multiple lineage tracing strategies, the authors could not validate the previously reported neuronal conversion induced by the overexpression of NeuroD1 *in vivo* (Wang et al., 2021a). However, the authors still acknowledged the general potential of NeuroD1 as neurogenic TF to induce neuronal conversion under other conditions, such as in cell culture (Pataskar et al., 2016; Zhang et al., 2015). This study highlights the importance of monitoring cell fate changes when studying cell fate conversion *in vivo*, using live imaging, labelling of pre-existing endogenous neurons or lineage tracing of the starter cell type (Bocchi et al., 2022; Wang et al., 2021a). Taken together, these studies demonstrate the great progress that has been made in identifying several factors that influence direct neuronal reprogramming, both *in vitro* and *in vivo*. Further investigations are underway to optimise reprogramming approaches for future potential therapeutic use.

1.3 Aims

Major advances in direct neuronal reprogramming are revealing its great therapeutic potential for cell replacement in the diseased or injured brain. Many *in vitro* and *in vivo* studies have highlighted the striking ability of key neurogenic TFs to instruct direct lineage conversion of diverse cell sources towards neuronal fate. However, the contribution of post-transcriptional regulation of gene expression to neuronal reprogramming remains largely unexplored. As discussed above, RBPs have the potential to regulate gene expression through a variety of post-transcriptional mechanisms, not only in mature neurons but also in embryonic neurogenesis. Evidence for the involvement of RBPs in cell fate commitment during neurogenesis raises the question of whether they are also involved in establishing neuronal fate in the context of direct neuronal reprogramming. Elucidating the role of post-transcriptional regulators in neuronal reprogramming is therefore key to gaining new insight into the underlying mechanisms of cell fate conversion.

In this PhD thesis, I focused on the two well-established RBPs Pum2 and Stau2 to unravel their (potential) role in astrocyte-to-neuron reprogramming.

In particular, I aimed to answer the following questions:

(i) Do Pum2 and Stau2 contribute to the successful fate conversion of astrocytes into neurons?
(ii) Do they have different or redundant roles in cell fate conversion?
(iii) What is the temporal requirement for their function during neuronal reprogramming?
(iv) What are the molecular mechanisms underlying the contribution of these RBPs to the reprogramming process?

2 MATERIAL AND METHODS

2.1 Material

The materials used in this study are listed in the following tables.

Table 1: List of buffers, media and solutions used in this study.

Buffer/Medium/Solution	***Components***
2xBES-buffered saline (BBS); pH 7.10-7.15	50 mM BES pH 7.15-7.30; 1.5 mM Na_2HPO_4; 280 mM $NaCl_2$
4% paraformaldehyde	16% (w/v) PFA in HBSS 1X pH 7.4
Astrocyte medium	DMEM/F12 (1:1) (1X); 10% (v/v) FCS; 1X B27 supplement; 1% (v/v) D-(+)-Glucose 45%; 1% (v/v) GlutaMAX™-I (100x); 1% (v/v) Pen Strep
B27 differentiation medium	DMEM/F12 (1:1) (1X); 1X B27 supplement; 1% (v/v) D-(+)-Glucose 45%; 1% (v/v) GlutaMAX™-I (100x); 1% (v/v) Pen Strep
Blocking solution	10X PBS; 2% (w/v) BSA; 2% (v/v) FCS; 0.2% (v/v) fish gelatine
BSA packaging medium	DMEM (1X) + FCS; 1.2% (w/v) BSA
DAPI solution	DAPI (2µg/ml) in 1xPBS
Dissection medium	10 mM HEPES Buffer solution (1M); HBSS 1X
DMEM + FCS	DMEM (1X); 3.7g/L Sodium bicarbonate; 1% (w/v) sodium pyruvate; 1% (v/v) GlutaMAX supplement; 10% (v/v) FCS;
DMEM + FCS (0 medium)	DMEM (1X) + GlutaMAX™-I; 10% (v/v) FCS;
DMEM + HS	DMEM (1X) + 10% (v/v) HS; 1% (v/v) pyruvate; 1% (v/v) GlutaMAX™-I (100x)
Growth medium	DMEM (1X) + GlutaMAX™-I; 10% (v/v) FCS; Geneticin (50 mg/ml); Tetracyclin (1mg/ml); Puromycin (10 mg/ml);
NMEM + B27	1xMEM; 1X B27 supplement; 0.22% (w/v) $NaHCO_3$; 0.6% (w/v) D-glucose; 1% (w/v) sodium pyruvate; 1% (v/v) GlutaMAX
TBS5 buffer	Tris-HCl, pH 7.8; NaCl 5M; KCl 1M; $MgCl_2$ 1M
Transfection medium, pH 7.4 (lentivirus production)	MEM (10X); 1mM sodium pyruvate; 15 mM HEPES pH 7.3; 1% (v/v) GlutaMAX™-I (100x); 1X B27 supplement; 33 mM D-glucose

Transfection medium (retrovirus production)	DMEM (1X) + GlutaMAX™-I

Table 2: List of plasmids used in this study.

Construct	***Vector***
CAG-GFP	CAG-GFP
CAG-Neurog2-IRES-GFP	CBIG
CAG-DsRedExpress2	RV-CAG-Dest (M.Götz laboratory)
CAG-Neurog2-IRES-DsRedExpress2	RV-CAG-Dest (M.Götz laboratory)
pFu3a-H1-shNTC-pCAG-tagRFP	Fu3a tagRFP
pFu3a-H1-shPum2-pCAG-tagRFP	Fu3a tagRFP
pFu3a-H1-shStau2-pCAG-tagRFP	Fu3a tagRFP

Table 3: List of antibodies used in this study.

Primary antibody	***Host Species***	***Manufacturer***	***Dilution***
anti-DCX polyclonal IgG	Guinea pig	Merck	1:2000
anti-DCX polyclonal IgG	Rabbit	Abcam	1:1000
anti-GFAP monoclonal IgG	Mouse	Sigma-Aldrich	1:1000
anti-GFAP polyclonal IgG	Goat	Abcam	1:1000
anti-Pum2 polyclonal IgG	Rabbit	Abcam	1:500
anti-RFP polyclonal IgG	Rabbit	Thermo Fisher	1:1000
anti-Stau2 monoclonal IgG	Mouse	Kiebler Lab (selfmade)	1:500
Secondary Antibody-Conjugate	***Host Species***	***Manufacturer***	***Dilution***
anti-Goat IgG – AlexaFluor488	*Calf*	Dianova	1:1000
anti-Guinea pig IgG – AlexaFluor488	Goat	Thermo Fisher	1:1000
anti-Guinea pig IgG – AlexaFluor647	Goat	Thermo Fisher	1:1000
anti-Mouse IgG – AlexaFluor647	Donkey	Thermo Fisher	1:1000
anti-Rabbit pig IgG – AlexaFluor488	Donkey	Thermo Fisher	1:1000
anti-Rabbit pig IgG – AlexaFluor555	Donkey	Thermo Fisher	1:1000

anti-Rabbit pig IgG – AlexaFluor647	Donkey	Thermo Fisher	1:1000

Table 4: List of chemicals used in this study.

Chemical	***Manufacturer***
BES	Merck
BSA	Gerbu Biotechnik
Calcium chloride	Merck
DAPI	Sigma-Aldrich/Carl Roth
D-(+)-Glucose (in transfection medium, LV)	Merck
D-(+)-Glucose solution (45%)	Sigma-Aldrich
Dismozon® pur	Hartmann/Carl Roth
FBS, Qualified, HI	Thermo Fisher Scientific
Fish gelatine	Sigma-Aldrich
Fluoromount™ Aqueous Mounting	Sigma-Aldrich
GenJet™ Plus DNA Transfection Reagent	SignaGen Laboratories
Gibco™ B27® Supplement (50X)	ThermoFisher Scientific
Gibco™ DMEM	Thermo Fisher Scientific
Gibco™ DMEM (1X) + GlutaMAX™-I [+] 4.5 g/L D-glucose, 25mM HEPES	Thermo Fisher Scientific
Gibco™ DMEM/F12 (1:1) (1X)	Thermo Fisher Scientific
Gibco™ DPBS (1X) [-] Calcium, Magnesium	Thermo Fisher Scientific
Gibco™ Geneticin®	Thermo Fisher Scientific
Gibco™ GlutaMAX™-I (100x)	Thermo Fisher Scientific

Gibco™ GlutaMAX Supplement (in DMEM+FCS solution)	Thermo Fisher Scientific
Gibco™ HBSS (1X) [+] Calcium, Magnesium	Thermo Fisher Scientific
Gibco™ HEPES Buffer Solution (1M)	Thermo Fisher Scientific
Gibco™ HI Horse Serum	Thermo Fisher Scientific
Gibco™ MEM (10X)	Thermo Fisher Scientific
Gibco™ Pen Strep	Thermo Fisher Scientific
Gibco™ Puromycin	Thermo Fisher Scientific
Gibco™ Recombinant Human Basic Fibroblast Growth Factor (bFGF)	Thermo Fisher Scientific
Gibco™ Recombinant Human Epidermal Growth Factor (EGF)	Thermo Fisher Scientific
Gibco™ 0.5% Trypsin/EDTA solution (10X)	Thermo Fisher Scientific
HEPES	Sigma-Aldrich
Magnesium chloride solution	Sigma-Aldrich
Opti-MEM™	Thermo Fisher Scientific
Paraformaldehyde powder	Merck
Poly-D-lysine hydrobromide	Sigma-Aldrich
Potassium chloride solution	Sigma-Aldrich
Sodium bicarbonate	Sigma-Aldrich
Sodium chloride solution	Sigma-Aldrich
Sodium pyruvate	Sigma-Aldrich
Tetracycline hydrochloride	Sigma-Aldrich
Triton X-100	Carl Roth
Trizma® hydrochloride solution	Sigma-Aldrich

Table 5: List of consumable material used in this study.

Consumable	***Manufacturer***
Cell Culture Plate, 24-Well	Eppendorf
CELLSTAR® 100/20 mm cell culture dish	Greiner Bio-One
CELLSTAR® 35/10 mm cell culture dish	Greiner Bio-One
CELLSTAR® cell culture flasks, 25 cm^2	Greiner Bio-One
CELLSTAR® tubes, 15 ml	Greiner Bio-One
CELLSTAR® tubes, 50 ml	Greiner Bio-One
EndoFree Plasmid Maxi Kit	Qiagen
Glass coversplis, 12 mm	VWR-Marienfeld
Microscope slides	Thermo Fisher Scientific
Nunc™ 60/15 mm cell culture dish	Thermo Fisher Scientific
Nunc™ cell culture flask 75 cm^2	Thermo Fisher Scientific
Nunc™ cell culture untreated 12 well plate	Thermo Fisher Scientific
Nunc EasYFlask™ 175 cm^2	Thermo Fisher Scientific
Polypropylene centrifuge tubes	Beckman Coulter

Table 6: List of instruments and equipment used in this study.

Instrument/Equipment	***Manufacturer***
Avanti J-26S XP Highspeed Centrifuge	Beckman Coulter
Axio Observer Z1 inverted phase contrast fluorescence microscope	Zeiss
Axiocam 506 mono camera	Zeiss
Axiovert 10 inverted light microscope	Zeiss
Blades	Carl Roth
Centrifuge 5417 R	Eppendorf
Centrifuge 5424 R	Eppendorf

Centrifuge 5810 R	Eppendorf
Bio-Safety Cabinet class II: B-[Max-Pro]^2-130	Berner
Bio-Safety Cabinet class II: B-[Max-Pro]^2-160	Berner
CO_2 incubator	Binder
CO_2 incubator	Eppendorf
COLIBRI.2 LED	Zeiss
Cycler: S1000TM Thermal cycler	Bio-Rad
DMI LED microscope	Leica
Graefe Forceps	FST
Innova® 44 shaking incubator	Eppendorf
JLA-10.500 rotor + tubes	Beckman Coulter
Milli-Q® Direct Water Purification System	Merck
Multifuge X3R Centrifuge	Thermo Fisher Scientific
NanoDrop™ 2000c	Thermo Fisher Scientific
Optima™ XPN-80 Ultracentrifuge	Beckman Coulter
pH meter FiveEasy™ F20	Mettler Toledo
plan-Apochromat 63x/1.40 NA Ph3 M27 8/0.17 oil immers. objective	Zeiss
Student Dumont #5 Forceps	FST
Student Dumont #7 Forceps	FST
Student Fine Forceps - Angled	FST
Student Fine Scissors	FST
Student Surgical Scissors	FST
Student Vannas Spring Scissors	FST
SW32Ti rotor + tubes	Beckman Coulter

2.2 Astrocyte cell culture

Primary mouse astrocyte cell cultures were generated according to the established protocol previously described by (Heinrich et al., 2011). In detail, grey matter tissue of the cerebral cortex was dissected from the brain of postnatal, 6 days old (P6) C57BL/6J mice after removal of the subventricular region, meninges, hippocampus and white matter. The entire procedure was performed in cold dissection medium. The tissue was then mechanically

dissociated using fire-polished Pasteur pipettes, centrifuged at 300g for 5 min at 4°C, resuspended and cultured in uncoated flasks in prewarmed astrocyte medium. The medium was supplemented with epidermal growth factor (EGF) (10 µg/ml) and basic fibroblast growth factor (bFGF) (10 µg/ml). The cells were maintained in culture at 37°C in a humidified and CO_2-enriched (5%) atmosphere for an expansion period of 7 days. At day 4, the medium was replaced with fresh prewarmed astrocyte medium supplemented with growth factors. At day 7, culture flasks were harshly shaken several times to remove contaminating oligodendrocyte progenitor cells and were passaged with trypsin/EDTA. Afterwards, cells were seeded onto poly-D-lysine (PDL) coated glass coverslips at a density of 50.000 cells per coverslip, in prewarmed astrocyte medium supplemented with EGF and bFGF. The day after seeding, the purity of the astrocyte culture was ensured by performing immunostaining for the astrocyte marker Glial Fibrillary Acidic Protein (GFAP) and the immature neuron marker Doublecortin (Dcx). All experiments were performed on cultured astrocytes the day after seeding. All procedures concerning animals were performed conform to the German Animal Protection Law and were approved by the local authority (*Regierung von Oberbayern*).

2.3 Neuron cell culture

Primary rat neuronal cultures were prepared by Karl Bauer, Ulrike Kring and Sabine Thomas and maintained as previously described (Goetze et al., 2003). In detail, hippocampi were dissected from embryonic day 17 (E17) Sprague-Dawley rat embryos (Charles River Laboratories). Tissue was washed with warm HBSS and dissociated with trypsin-EDTA and mechanical trituration with two different fire-polished Pasteur pipettes. Cells were then plated on poly-L-lysine-coated glass coverslips at a density of approximately 74 cells/mm^2. Neurons were cultured in NMEM+B27 medium, at 36.5°C in a humidified and CO_2-enriched (5%) atmosphere. After 3 days, hippocampal neurons on coverslips were transferred to dishes that were previously seeded with glial cells. Glial cells were cultured from the cortex of E17 rat brains and grown for one week in a flask containing DMEM+HS, at 36.5°C in a humidified and CO_2-enriched (5%) atmosphere. After 7 days, the cells were split 1:3 into a new flask. After a further 7 days in culture, the cells were plated into cell culture dishes (60mm) at a density of 20.000 cells/dish. For single cell imaging experiments on glial cells, cells were plated on poly-L-lysine-coated glass coverslips at a density of 20.000 cells/coverslip. Experiments were performed with cultured neurons 10-16 days *in vitro* (DIV).

All procedures concerning animals were performed conform to the German Animal Protection Law and were approved by the local authority (*Regierung von Oberbayern*).

2.4 Plasmids

The retroviral plasmids CAG-GFP and CAG-Neurog2-IRES-GFP were ordered from Addgene. The vectors were amplified in DH5α bacteria and selected for antibiotic resistance using LB medium containing ampicillin (100 µg/ml). The retroviral plasmids CAG-DsRedExpress2 and CAG-Neurog2-IRES-DsRedExpress2 were generated in the laboratory of Magdalena Götz at the BMC (Heinrich et al., 2011). The lentiviral plasmids pFu3a-H1-shNTC-pCAG-tagRFP, pFu3a-H1-shPum2-pCAG-tagRFP and pFu3a-H1-shStau2-pCAG-tagRFP were generated by exchanging the CamKIIα promoter for the CAG promoter in the previously published pFu3a-H1-shNTC-pCamKIIα-tagRFP vector (Fernandez-Moya 2021, Schieweck et al. 2021). The vectors were amplified in Stbl2 bacteria and selected for antibiotic resistance using LB medium containing ampicillin (100 µg/ml). All plasmids were purified using plasmid DNA extraction kits and DNA concentrations were determined by measuring the absorbance at 260nm on a *NanoDrop™ ND-1000c* spectrophotometer. All plasmid sequences were validated by Sanger sequencing at *Eurofins Genomics*. Sequencing primers were ordered from *Eurofins Genomics.*

2.5 Astrocyte-to-neuron reprogramming

Astrocyte-to-neuron reprogramming was performed according to the published protocol (Heinrich et al., 2011). Briefly, the day after seeding astrocytes on coverslips, cells were transduced with a retroviral vector encoding the neurogenic fate determinant Neurogenin2 (Neurog2) (Neurog2-IRES-GFP) and the corresponding control (CAG-GFP). After 36 h, the astrocyte medium was replaced with fresh prewarmed B27 differentiation medium. Cells were cultured at 37°C, in a humidified and CO_2-enriched (5%) atmosphere for 7 days. At 7 days post-infection (DPI), the cells were washed twice with prewarmed DPBS1X washing buffer and fixed with 4% paraformaldehyde (PFA). At 7 DPI, the reprogramming efficiency was assessed by performing immunostaining for the neuronal marker Dcx.

2.6 Short hairpin RNA-mediated knockdown

To knockdown Pum2 or Stau2 during reprogramming, short hairpin (sh) RNA-mediated interference was performed. In detail, seeded astrocytes were transduced with lentiviral vectors expressing either a shRNA with no known targets in the mammalian genome

(shNTC) or a Pum2/Stau2-specific shRNA (shPum2/shStau2). Lentiviral transduction was performed either simultaneously with the Neurog2-expressing retrovirus (Neurog2-IRES-GFP) or two days later. The reprogramming procedure was performed as described above. The efficiency of the knockdown was assessed by immunostaining on mouse cortical astrocytes, rat glial cells (astrocytes) and rat hippocampal neurons at different time points (4 and 6 DPI).

2.7 Retrovirus production

Control CAG-GFP and Neurog2-expressing retroviral particles were obtained from HEK 293GPG cells (gift from the laboratory of Magdalena Götz). Cells were plated at a density of $6x10^6$ per 10cm plate in prewarmed growth medium supplemented with antibiotics for cell selection: Geneticin, Tetracycline and Puromycin. Two days later, the medium was replaced with fresh prewarmed DMEM+FCS (0 medium) without antibiotics and the cells were incubated for 2 h at 37°C, in a humidified and CO_2-enriched (5%) atmosphere. GenJet™ Plus DNA Transfection Reagent was used for an efficient gene delivery into cells. A solution of transfection medium containing 180 µl of GenJet™ was slowly added to a solution of transfection medium previously mixed with 120 µg of the delivery plasmid. The final solution was gently swirled several times and incubated at RT for 15 min. The solution was then added dropwise to the HEK 293GPG cells. At one and four days post-transfection (DPT), the medium was replaced with fresh prewarmed DMEM+FCS (0 medium). At six DPT, the cell medium containing viral particles was collected, filtered through 0.45µm PVDF syringe filter and concentrated by ultracentrifugation at 27.000 rpm for 2 h at 4°C. The virus pellet obtained was resuspended in TBS5 buffer and stored at -80°C.

2.8 Lentivirus production

Control shNTC- shStau2- and shPum2-expressing lentiviral particles were obtained from HEK293T cells (gift from the laboratory of Magdalena Götz). Cells were plated at a density of $1.5x10^6$ per 10cm plate in DMEM+FCS medium and two days later they were co-transfected with the packaging plasmids psPAX2, pcDNA3.1-VSV-G (Heraud-Farlow et al., 2013) and the respective pFu3a plasmids: either H1-shNTC-pCAG-tagRFP or H1-shPum2-pCAG-tagRFP or H1-shStau2-pCAG-tagRFP. Transfection was performed using calcium phosphate (Ca_4PO_3) co-precipitation as previously described (Goetze et al., 2004). Briefly, a total of 36 µg of DNA plasmid (from the three delivery vectors) was mixed with freshly diluted 2.5M $CaCl_2$ and H_2O to a final volume of 720 µl. The same amount of 2×BES (pH

7.15 - 7.30) (720 µl) was slowly added to the $CaCl_2$/DNA solution, and then mixed by introducing air bubbles with the pipette. The solution was added dropwise to the HEK cells in prewarmed transfection medium. After 5 h of incubation, the medium was replaced with fresh BSA packaging medium. At two DPT, the cell medium containing viral particles was collected, filtered through 0.45µm PVDF syringe filter and concentrated by ultracentrifugation at 23.000 rpm for 2 h and 20 min at 4°C. The virus pellet obtained was resuspended in Opti-MEM™ and stored at -80°C.

2.9 Immunostaining

Astrocytes and reprogrammed neurons seeded on coverslips were washed twice with pre-warmed DPBS 1X and fixed with 4% PFA for 15 min. Fixed cells were washed three times for 5 min with DPBS 1X and permeabilised with cold 0.1% Triton X-100 in HBSS (1X) for 5 min. Cells were washed again three times for 5 minutes with DPBS 1X and blocked with 100% blocking solution for at least 30 min at RT. The cells were then incubated with primary antibodies, overnight at 4°C. The primary antibodies were diluted in 10% blocking solution in HBSS (1X). The next morning, the cells were washed three times for 5 min with DPBS 1X and incubated with the appropriate fluorophore-coupled secondary antibody for 45 min at RT. The secondary antibodies were diluted in 10% blocking solution in HBSS (1X). The cells were then washed three times for 5 min with DPBS 1X and counterstained with 2 µg/ml DAPI solution for 5 min at RT. After DAPI staining, the cells were washed three times for 5 min with DPBS 1X. The coverslips were mounted on glass microscope slides using mounting medium.

2.10 Fluorescence microscopy and image processing

Fluorescence images of fixed astrocytes and induced neurons were acquired using the microscopy software ZEN2.6 pro (blue edition, Zeiss) on a Zeiss Axio Observer.Z1 inverted phase contrast fluorescence microscope equipped with a Plan-Apochromat 63x/1.40 Ph3 M27 oil immersion objective and a 20x objective as well as a COLIBRI.2 LED light source and an Axiocam 506 mono camera. Fluorescence imaging was performed using the 63x Plan-Apochromat oil immersion objective or the 20x objective. Astrocytes and induced neurons were selected on the basis of general cell characteristics, such as morphology and size, and expression of fluorescent transduction markers. The LED wavelengths with excitation maxima of 385 nm, 470 nm, 555 nm, 625 nm were used with acquisition times ranging from 10 to 300 milliseconds. All raw images were analysed using ZEN 3.2 (blue

edition, Zeiss). For the purpose of presentation, images were not edited beyond adjustment of intensity levels, brightness, contrast and magnification ratio. The scale bars in the images correspond to 20 µm or 50 µm.

2.10.1 Endogenous expression of Pum2 and Stau2 protein in astrocytes and induced neurons

To evaluate the Pum2 or Stau2 protein expression patterns during reprogramming, astrocytes and induced neurons (transduced with either control or Neurog2 viruses) positive for the fluorescent transduction marker were imaged using the Plan-Apochromat 63×/1.40 Ph3 M27 oil immersion objective. Images were acquired separately using phase contrast and channels with emission spectra equivalent to Cy5, Cy3 or EGFP and DAPI. Three coverslips were included as technical replicates for each experimental condition. For the analysis of the reprogramming condition, two cell populations of Neurog2-transduced cells were considered, (i) cells with non-neuronal morphology, still in fate transition or failed to be reprogrammed, (ii) successfully converted cells with typical neuronal morphology and positive for neuron-specific Dcx (Gascon et al., 2016). For each cell selected, a region of interest (ROI) was manually drawn based on phase contrast and fluorescence channels: the perinuclear region of astrocytes and the soma of induced neurons. For each ROI, measurements of the area and the mean fluorescence were acquired. For background subtraction, a region without fluorescence signal adjacent to the cell was manually selected. In the case of induced neurons lying on top of astrocytes, the background ROI was selected next to the neuron, on the underlying astrocyte. To account for the different cell size of astrocytes and induced neurons, the integrated density of the fluorescence signal was quantified. The integrated density of fluorescence represents the total fluorescence measured in an area, independent of size differences in the area measured in the different cell types. The integrated density was calculated by multiplying the mean fluorescence intensity by the ROI (μm^2) of the considered cell (*Integrated Density: Intensity Mean Value X Area*). Background subtraction was then performed using the following formula:

Corrected Total Cell Fluorescence (CTCF) = Integrated Density – (ROI of selected cell X Intensity Mean of background ROI)

The same quantification method was also used to evaluate the efficiency of shRNA-mediated knockdown on mouse cortical astrocytes, rat glial cells (astrocytes) and rat hippocampal neurons.

2.10.2 Colocalisation assay in astrocytes

To evaluate the colocalisation of endogenous Pum2 and Stau2 in astrocytes, healthy cells showing positive staining for both proteins were imaged using the Plan-Apochromat 63x/1.40 Ph3 M27 oil immersion objective. Images were acquired separately using phase contrast and channels with emission spectra equivalent to Cy5, EGFP and DAPI. Two or three coverslips were included as technical replicates. For each astrocyte, a Z-stack consisting of 20 slices with 0.26 µm step size was acquired in the Cy5 and EGFP channels. Images were deconvolved using the deconvolution module of the ZEN 2.6 software (blue edition, Zeiss) with the following settings:

Method = Deconvolution (adjustable); Algorithm = Constrained iterative; Set Strength Manually (Medium 5.0); Corrections = Background.

In each deconvolved image, a ROI was selected according to specific criteria: a 10 x 10 µm square (70x70 pixel image size) was drawn approximately halfway between the nucleus and one tip of the cell by using the “Create Image Subset” tool. Pum2 and Stau2 particle colocalisation was quantified in the ROI using an automated analysis pipeline in the Arivis Vision4D 3.5 software. In details, particles were detected using the tool “blob finder” tool with the following setting:

Pum2: Particle diameter = 0.2 µm; Probability threshold = 4%; Split sensitivity = 100%; Volume: VoxelCount > 4;

Stau2: Particle diameter = 0.2 µm; Probability threshold = 5%; Split sensitivity = 100%; Volume: VoxelCount > 5;

Detected Pum2 particles with a volume smaller than 4 voxels and Stau2 particles with a volume smaller than 5 voxels were excluded as they were considered residual background. Given the fact that the ROI considered was only a small part of the cell, particles at the edges were also excluded to avoid missing potential colocalisation events beyond the edges. The overlapping volume of Pum2 and Stau2 particles was measured. An overlapping volume larger than 30% was scored as a colocalisation event.

2.10.3 Colocalisation assay in induced neurons

To evaluate the colocalisation of endogenous Pum2 and Stau2 in induced neurons, healthy cells positive for Neurog2-expressing fluorescent reporter and showing positive staining for both proteins were imaged using the Plan-Apochromat 63×/1.40 Ph3 M27 oil immersion objective. Images were acquired separately using phase contrast and channels with emission spectra equivalent to Cy5, Cy3, EGFP and DAPI. Two or three coverslips were included as technical replicates. For each neuron, a Z-stack consisting of 32 slices with 0.29

µm step size was acquired in the Cy5 and Cy3 channel. Images were deconvolved using the deconvolution module of the ZEN 2.6 software (blue edition, Zeiss) with the following settings:

Method = Deconvolution (adjustable); Algorithm = Constrained iterative; Set Strength Manually (Strong 10.0); Corrections = Background.

In each deconvolved image, a ROI was selected according to specific criteria: a 10µm long rectangular region was drawn in the proximal section of a neuronal process, by using the “Create Image Subset” tool. Pum2 and Stau2 particle colocalisation was quantified in the ROI using an automated analysis pipeline in the Arivis Vision4D 3.5 software. In detail, particles were detected using the tool “blob finder” tool with the following setting:

Pum2: Particle diameter = 0.1 µm; Split sensitivity = 100%; Volume: VoxelCount > 2;

Stau2: Particle diameter = 0.1 µm; Split sensitivity = 100%; Volume: VoxelCount > 3;

The probability threshold for the detection of both Pum2 and Stau2 particles was adjusted for each cell with values ranging between 2% and 7%. Detected Pum2 particles with a volume smaller than 2 voxels and Stau2 particles with a volume smaller than 3 voxels were excluded as they were considered residual background. The overlapping volume of Pum2 and Stau2 particles was measured. An overlapping volume larger than 30% was scored as a colocalisation event.

2.10.4 Reprogramming efficiency

To get a representative estimate of the reprogramming efficiency, cells fixed on coverslips were imaged using a 20x objective. Images were acquired from nine fixed spots on each coverslip using channels with emission spectra equivalent to Cy5, Cy3, EGFP and DAPI. Three coverslips were included as technical replicates for each experimental condition. The induced neurons were evaluated by morphology and Dcx staining, based on previously published criteria (Gascon et al., 2016). In detail, only those Dcx-positive cells with ellipsoid soma and at least one thin process three times longer than the soma were scored as successfully converted neurons. The proportion of successfully converted cells among the cells positive for Neurog2-expressing fluorescent reporter is defined as reprogramming efficiency. Only cells showing good viability by DAPI staining were included in the cell count. The reprogramming efficiency in either the Stau2- or Pum2-depleted condition was evaluated by quantifying the proportion of successfully converted cells among the cells positive for both Neurog2 and shRNA-expressing fluorescent reporters. The absolute numbers of Neurog2- and shRNA-positive cells that were successfully converted and those that failed to undergo reprogramming were also quantified. To estimate cell death, the

absolute numbers of DAPI-positive cells and the Neurog2-positive cells were quantified. In addition, cells positive for both Neurog2 and shRNA were normalised to the total number of Neurog2-positive cells.

2.10.5 Morphological analysis of induced neurons

Morphological analysis of successfully induced neurons was performed after 7 days of reprogramming under Pum2-depleted conditions. Those Neurog2- and shRNA-transduced cells considered as successfully converted neurons were evaluated by distinguishing bipolar from multipolar neurons. Induced neurons that exhibited only two neuronal processes extending from the soma towards opposite poles were scored as bipolar neurons. Those showing multiple neuronal extensions from the soma were scored as multipolar neurons. Neurons that could not be properly scored were excluded from the analysis. Nucleus integrity was assessed qualitatively based on DAPI staining pattern and nuclear shape. The area of the nucleus and soma of induced neurons was also quantified.

2.10.6 Morphological analysis of cells failing reprogramming

Morphological analysis of non-reprogrammed cells was performed after 7 days of reprogramming under Pum2-depleted conditions. Based on qualitative evaluation, the Neurog2- and shRNA-transduced cells that did not undergo a successful reprogramming were categorised into cells with normal astrocyte morphology and cells with aberrant morphology. The morphology considered as normal included both the typical astrocyte morphology and the elongated transitional shape typical of cells undergoing reprogramming. On the other hand, cells were considered to have aberrant morphology if they exhibited atypical features that deviated from the expected astrocyte morphology. These characteristics included smaller size, shrivelled shape and the presence of abnormal cell protrusions. Cell morphology with one or more of these atypical features was considered aberrant. A quantitative assessment of the cell size (μm^2) of both categories was also performed. Cells that overlapped with surrounding cells, making it therefore impossible to distinguish the entire cell area, were excluded from the measurement. The proportion of cells with normal and aberrant morphology among all non-reprogrammed cells was evaluated in the Pum2-depleted condition compared to the control. In addition, the expression of the neuronal marker Dcx was evaluated among the cells with an aberrant morphology.

2.11 Statistical analysis

Data processing was performed in Microsoft Excel; GraphPad Prism 8 was used for data plotting and statistical analysis. In addition, RStudio 4.2.1 was used for data processing and plotting of the colocalisation assay and for the comparative analysis of the gene lists from published data. For fluorescence intensity measurements, the statistical analysis was performed after Log10 transformation of the raw data. Data were tested for normal distribution by the Shapiro-Wilk normality test. In each experiment, the statistical analysis was performed on the mean of three technical replicates for each independent biological replicate. Paired Student's t-test (for normally distributed data) and Wilcoxon matched-pairs signed rank test (for non-normally distributed data) were used to test for significance of differences in the mean of different biological replicates between two conditions. Estimated *p*-values less than 0.05 were considered as statistically significant and are indicated by asterisks in the figures (*$p < 0.05$, **$p < 0.01$, ***$p < 0.001$, ns ≥ 0.05).

3 RESULTS

3.1 Astrocyte-to-neuron reprogramming *in vitro*

To study the role of RBPs in neuronal reprogramming, astrocyte-to-neuron conversion was used as the experimental system of choice. Specifically, I employed the established protocol described by Heinrich and colleagues in 2011 (Heinrich et al., 2011). This allows the direct conversion of postnatal mouse cortical astrocytes into glutamatergic neurons *in vitro* by inducing the expression of the single neurogenic TF Neurog2. After the forced expression of Neurog2, the neuronal identity is typically acquired between 5-7 days (Heinrich et al., 2011). The experimental procedure starts with the isolation of astrocytes from the cerebral cortex of P6 mice followed by an expansion phase in culture (**Figure 4A**). After 7 days, the proliferating cells were either analysed to confirm the astrocytic identity or transduced with a retrovirus expressing Neurog2 in order to induce the cell fate conversion (**Figure 4A, 5A**). Immunostaining for the astrocytic marker GFAP and the immature neuronal marker Dcx showed that the majority of the cultured cells were GFAP-positive astrocytes and that Dcx-positive cells were absent, confirming the purity of the astrocyte culture (**Figure 4B,C**). The reprogramming efficiency was assessed by morphology and Dcx immunostaining at 7 days post-infection (DPI) (**Figure 5A**). Only Dcx-positive cells with an ellipsoid soma and at least one thin process three times longer than the soma were scored as successfully converted neurons (Gascon et al., 2016). While cells infected with the control retroviral vector did not generate any Dcx-positive neurons, the forced expression of Neurog2 induced the conversion of infected cells with an average efficiency of 39% (**Figure 5B,C**). Therefore, this system provided a suitable tool to study the role of RBPs in neuronal reprogramming.

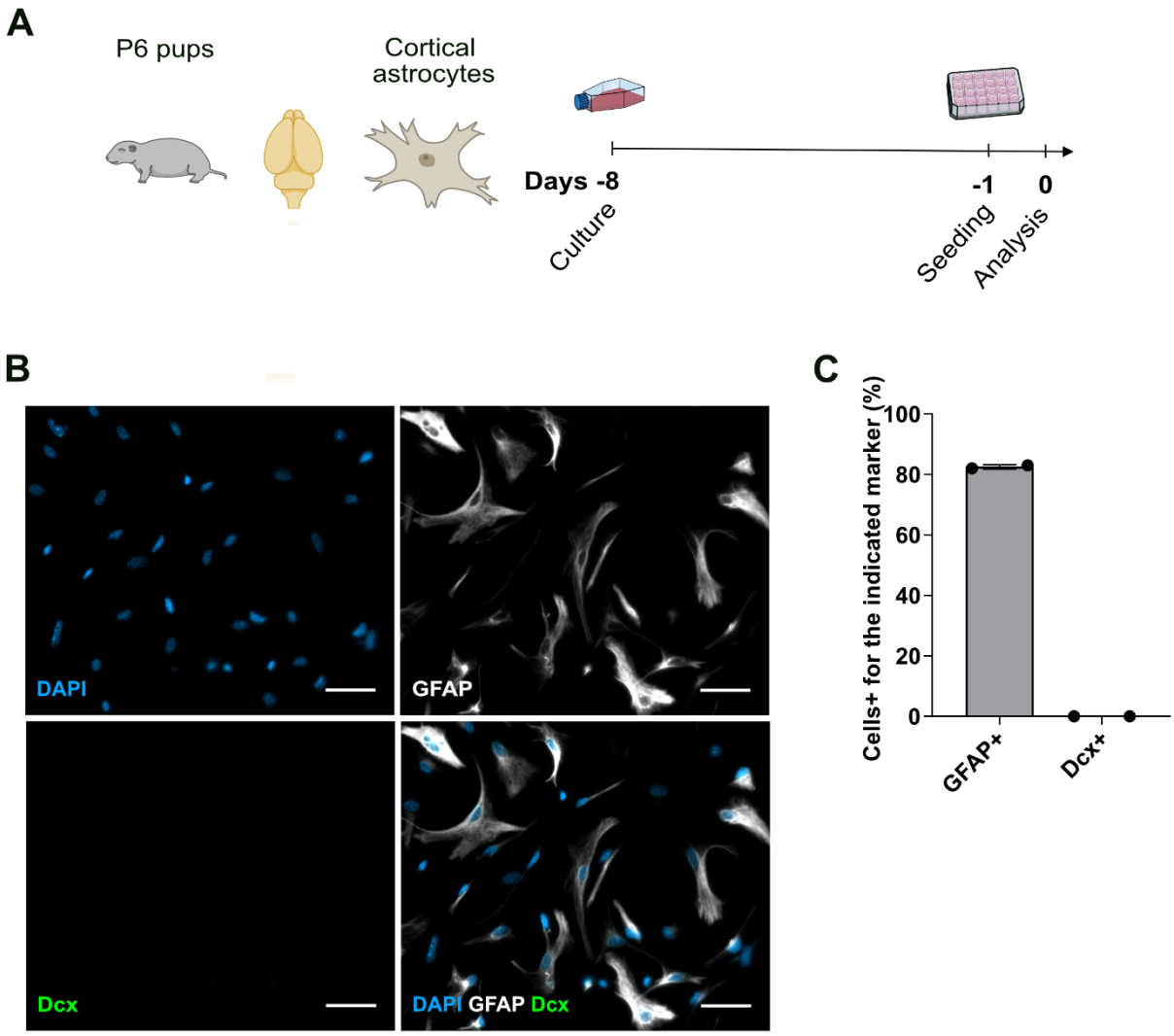

Figure 4: Cultured astrocyte purity was confirmed by the enrichment of GFAP-positive cells and the absence of Dcx-positive cells

(A) Experimental outline of the cortical astrocyte culture. **(B)** Representative examples of GFAP and Dcx immunostaining, DAPI staining and merged images of mouse cortical astrocytes after 7 days in culture. Scale bars: 50 µm. **(C)** Bar plot displaying percentage of cells positive for GFAP or Dcx. Black circles indicate independent biological replicates (n = 2). Mean and Standard Deviation are shown. Flask icon modified from Marcel Tisch, licenced under Creative Commons CC0 1.0 Universal. 24-well plate icon modified from Database Center for Life Science, licenced under Creative Commons Attribution 4.0 International, https://creativecommons.org/licenses/by/4.0/

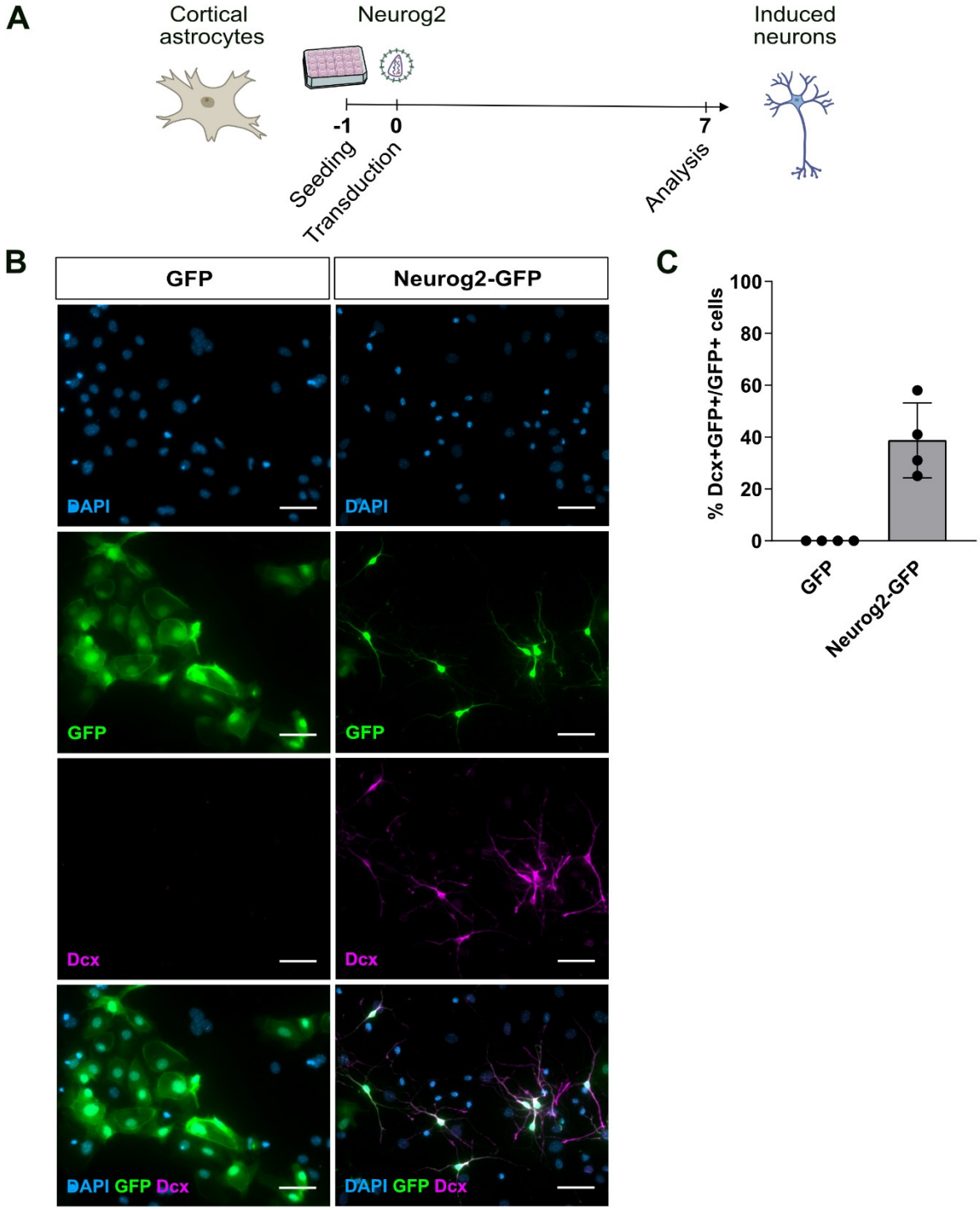

Figure 5: Forced expression of Neurog2 induces direct conversion of cortical astrocytes into neurons

(A) Experimental outline of astrocyte-to-neuron reprogramming. **(B)** Representative examples of GFP fluorescence, Dcx immunostaining, DAPI staining and merged images of control (GFP only) or Neurog2-GFP-positive cells. Scale bars: 50 µm. **(C)** Bar plot displaying the proportion of Dcx-positive neurons (Dcx+) among GFP-positive-cells under control (GFP only) or Neurog2-induced conditions at 7 DPI. Black circles indicate independent biological replicates (n = 4). Mean and Standard Deviation are shown. 24-well plate icon modified from Database Center for Life Science, licenced under Creative Commons Attribution 4.0 International, https://creativecommons.org/licenses/by/4.0/

3.2 Protein expression patterns of Pum2 and Stau2 in astrocytes and mature neurons

To explore the role of Pum2 and Stau2 in astrocyte-to-neuron reprogramming, I first examined their endogenous expression patterns in the initial cell population before the conversion process. Cortical astrocytes were immunostained for endogenous Pum2 or Stau2 after 7 days in culture (**Figure 6A**). Immunostaining revealed expression of both RBPs with a predominant cytoplasmic localisation and a punctate staining pattern (**Figure 6B,C**). Interestingly, a similar staining and protein localisation pattern was also observed in cultured mature rat hippocampal neurons (**Figure 6D,E**). Indeed, in neurons Pum2 and Stau2 have previously been reported to assemble their target mRNAs into RNPs (also often referred to as RNA granules), typically enriched in the somatodendritic compartment (Duchaine et al., 2002; Kiebler and Bassell, 2006; Vessey et al., 2006). This suggests that Pum2 and Stau2 share comparable cytoplasmic localisation and distribution of RNA granules in different brain cell types. To investigate whether Pum2 and Stau2 not only localise in the cytoplasm of astrocytes, but also potentially interact, their colocalisation was investigated in detail. Therefore, cortical astrocytes were immunostained for endogenous Pum2 and Stau2 after 7 days in culture (**Figure 7A**), and Pum2- and Stau2-containing particles were examined for colocalisation events in the selected cytoplasmic regions (**Figure 7B**). Only particles with more than 30% overlapping volume were considered to colocalise. Based on this analysis, on average, approximately 15% of Pum2-containing particles were found in close contact with Stau2-containing particles (**Figure 7C**). This result suggests that Pum2 and Stau2 do not show substantial interaction in the cytoplasmic compartment of astrocytes.

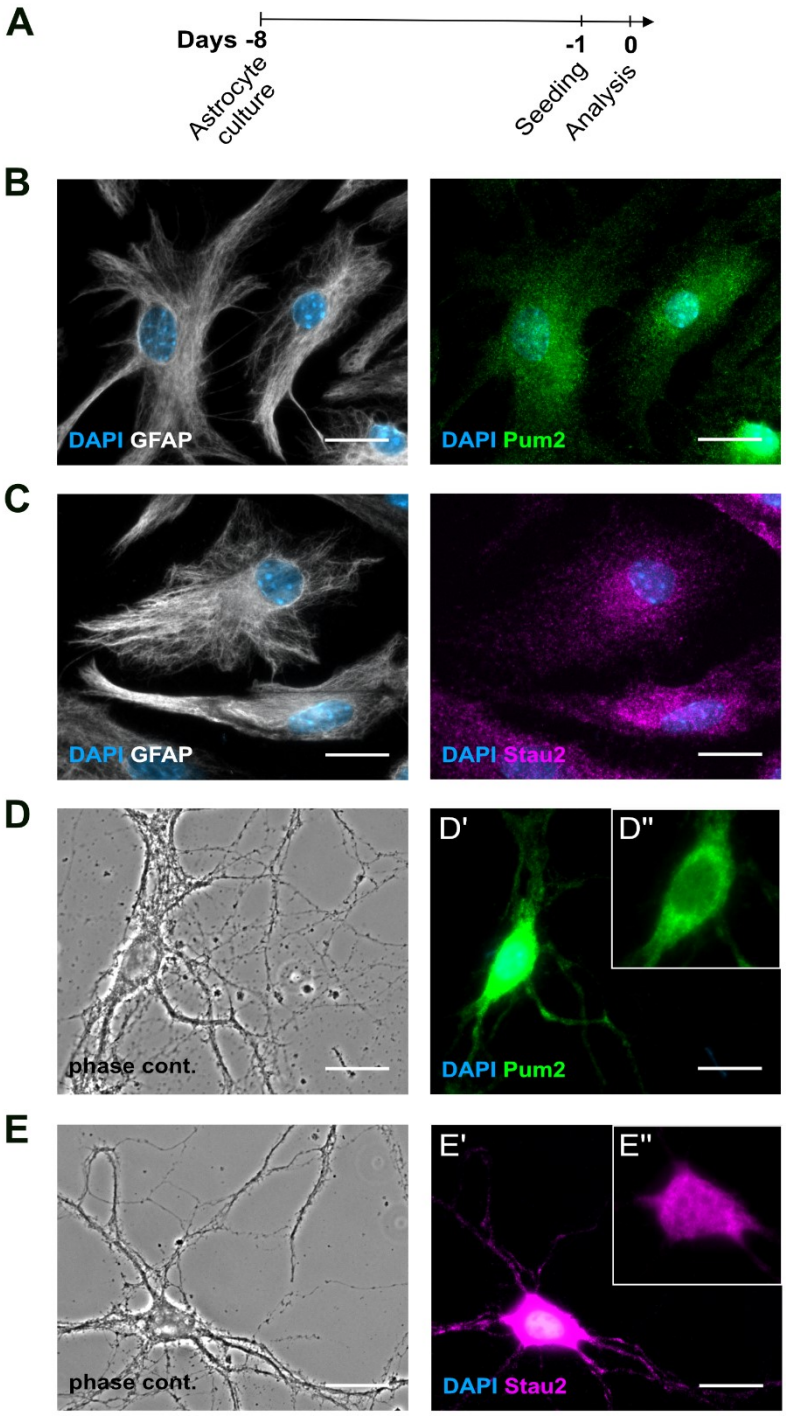

Figure 6: Predominant cytoplasmic localisation of Pum2 and Stau2 in astrocytes

(A) Experimental outline of astrocyte culture. **(B,C)** Representative examples of GFAP and Pum2 or Stau2 immunostaining and DAPI staining images of mouse cortical astrocytes after 7 days in culture. Scale bars: 20 µm. **(D,E)** Representative examples of Pum2 or Stau2 immunostaining, DAPI staining and phase contrast images of rat hippocampal neurons after 16 days in culture. D',E' Increased signal to better visualise neuronal processes. D",E" Boxed regions in images represent magnified insets of the soma. Scale bars: 20 µm.

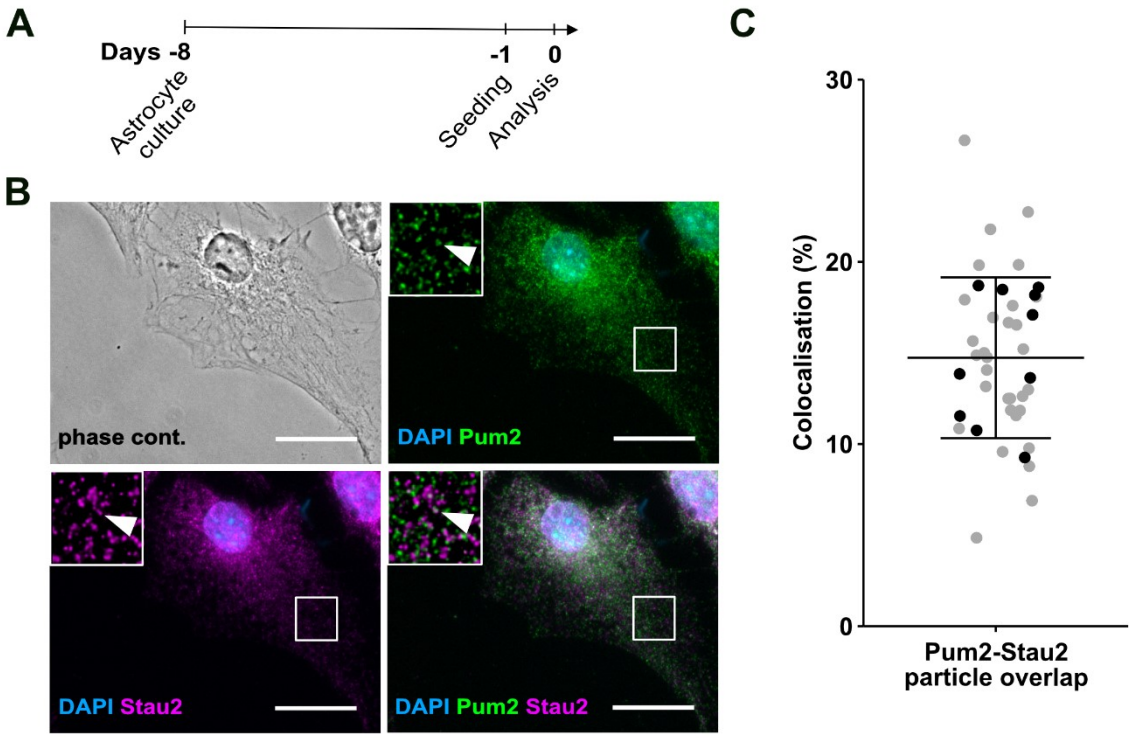

Figure 7: Most Pum2 and Stau2 particles do not colocalise in the cytoplasmic compartment of astrocytes

(A) Experimental outline of astrocyte culture. **(B)** Representative examples of Pum2 and Stau2 co-immunostaining, DAPI staining, merged and phase contrast images of mouse cortical astrocytes after 7 days in culture. Scale bars: 20 µm. Boxed regions in images are displayed as magnified insets processed separately by image deconvolution. White arrowhead indicates one example for colocalisation between Pum2 and Stau2. **(C)** Dot plot displaying percentage of Pum2 particles overlapping with Stau2 particles (defined by more than 30% volume overlap) in mouse cortical astrocytes after 7 days in culture. Grey and black circles indicate individual cells from two independent biological replicates (n = 2). Mean and Standard Deviation are shown.

3.3 Changes in Pum2 and Stau2 protein expression patterns during astrocyte-to-neuron reprogramming

3.3.1 Pum2 protein levels are increased in cells undergoing conversion but stable in successfully induced neurons

To get first insight into the role of Pum2 in neuronal reprogramming, the expression pattern of Pum2 protein during the reprogramming process was examined. To this end, cultured cortical astrocytes were transduced with a retrovirus expressing Neurog2 and an immunostaining for endogenous Pum2 was performed at different time points, 3, 5 and 7 DPI (**Figure 8A**). These time points represent key steps in the conversion process. Indeed, it's been shown that the major changes in gene expression necessary to induce the reprogramming occur during the first 48h upon forced expression of Neurog2 (Masserdotti et al., 2015). Within 3 days, the cells have already started the morphological transition towards the neuronal identity (Gascon et al., 2016; Masserdotti et al., 2015). When Neurog2 forced expression is induced, immature neuronal identity is reached between 5-7 days (Gascon et al., 2016; Heinrich et al., 2011). At each time point, Pum2 protein levels were assessed in two different cell populations: the Neurog2-transduced cells with non-neuronal morphology, still in fate transition or failed to be reprogrammed, and those successfully converted, showing typical neuronal morphology and positive staining for neuron-specific Dcx (Gascon et al., 2016) (**Figure 8B-D**). Fluorescence analysis showed a slight but significant increase in Pum2 protein levels in the cells that were still in the transition phase (displaying non-neuronal morphology) at 5 DPI compared to the control condition (GFP only) (**Figure 8F**). In contrast, there was no significant variation in the same category of cells at 3 and 7 DPI (**Figure 8E,G**). Interestingly, no change in Pum2 protein levels was observed in successfully converted neurons at 5 and 7 DPI compared to the control condition (GFP only) (**Figure 8F,G**). Notably, the decreased Pum2 levels observed in induced neurons at 3 DPI (**Figure 8E**), could be explained by the fact that the small number of prematurely converted neurons at day 3 are unlikely to survive or complete the typical maturation process required to develop into functional neurons. Taken together, these results are consistent with the idea of a Pum2 involvement in the reprogramming process. In addition, the dynamic protein expression observed in the cells undergoing reprogramming at 5 DPI suggests that its role may be more pronounced during the late stages of the conversion process than in the early stages.

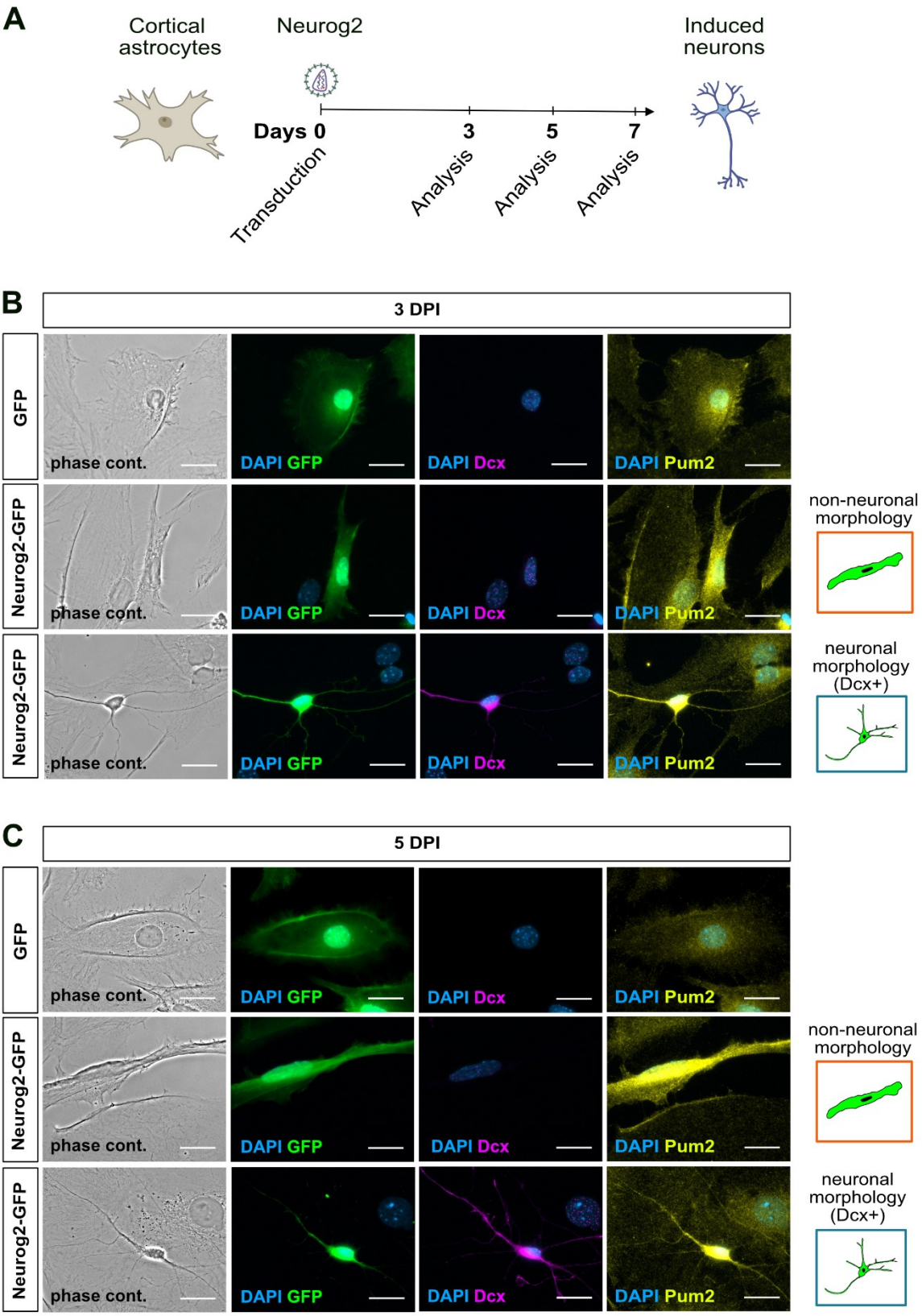
A
Cortical astrocytes
Neurog2
Induced neurons
Days 0
3
5
7
Transduction
Analysis
Analysis
Analysis
B
3 DPI
GFP
Neurog2-GFP
Neurog2-GFP
phase cont.
DAPI GFP
DAPI Dcx
DAPI Pum2
non-neuronal morphology
neuronal morphology (Dcx+)
C
5 DPI
GFP
Neurog2-GFP
Neurog2-GFP
phase cont.
DAPI GFP
DAPI Dcx
DAPI Pum2
non-neuronal morphology
neuronal morphology (Dcx+)

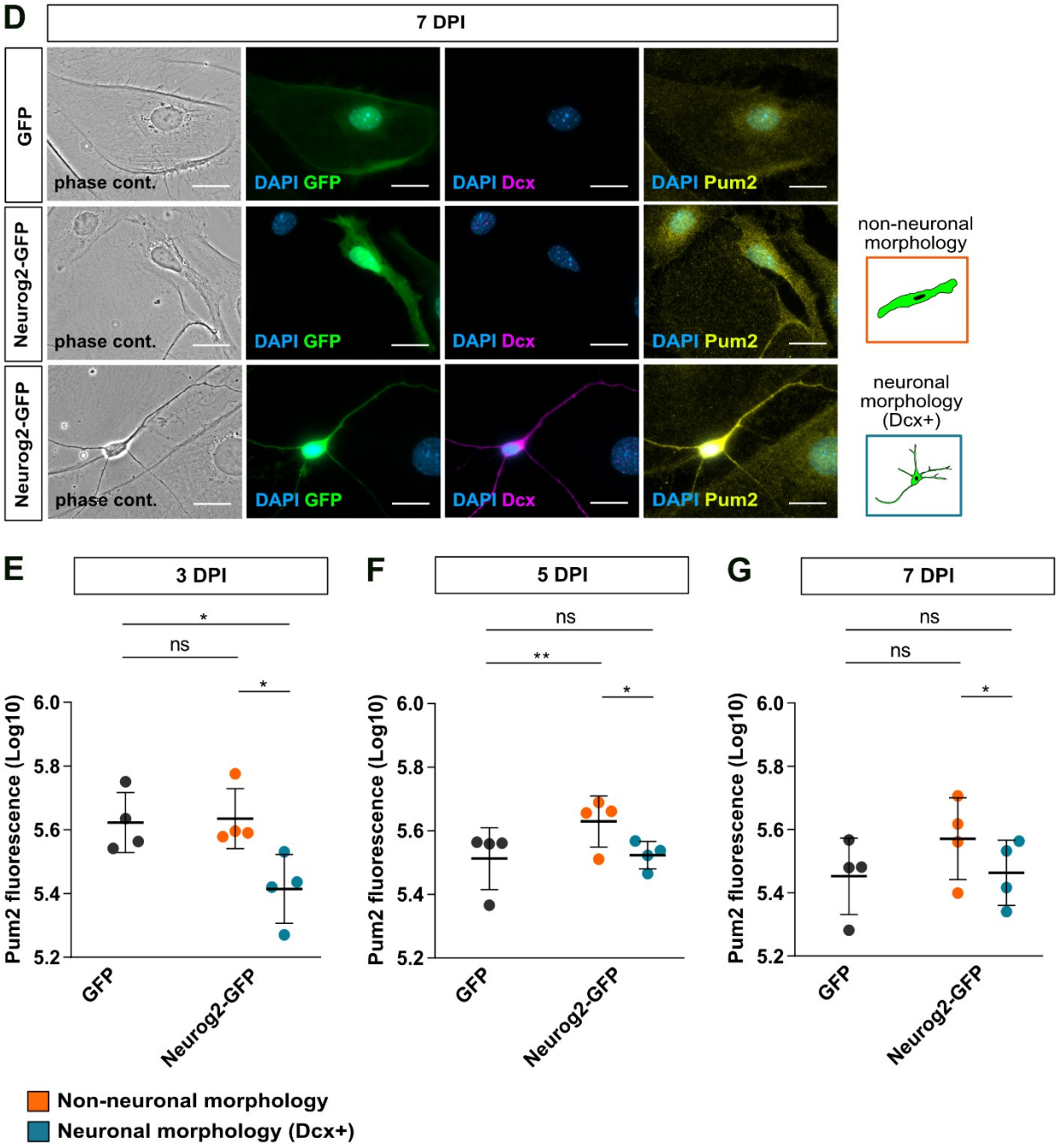

Figure 8: Pum2 protein levels are increased in cells undergoing conversion

(A) Experimental outline of astrocyte-to-neuron reprogramming. **(B,C,D)** Representative examples of Pum2 and Dcx immunostaining, GFP fluorescence, DAPI staining and phase contrast images of control- (GFP only) or Neurog2-GFP-positive cells at 3 (DPI) **(B)**, 5 DPI **(C)** and 7 DPI **(D)**. Scale bars: 20 µm. **(E,F,G)** Dot plot displaying Pum2 total fluorescence (Log10 scale) in control- (GFP only) or Neurog2-GFP-positive cells at 3 DPI **(E)**, 5 DPI **(F)** and 7 DPI **(G)**. Control- (GFP only) positive cells are displayed in dark grey circles. Sub-categories of Neurog2-GFP-positive cells are displayed in orange (GFP+ cells with non-neuronal morphology) and blue (GFP+Dcx+ cells with neuronal morphology) circles. Mean and Standard Deviation are shown. Circles indicate independent biological replicates (n = 4). Asterisks represent *p*-values obtained by paired Student's t-test (*$p < 0.05$, **$p < 0.01$, ns ≥ 0.05). Total fluorescence was measured in the perinuclear region which differed in size between different cell types (panels B-D).

3.3.2 Selective increase in Stau2 protein levels in successfully induced neurons

To compare the protein expression dynamics of different RBPs during the reprogramming process, I repeated the same experiment presented for Pum2 in the previous chapter, this time for endogenous Stau2. As for Pum2 (**Figure 8A**), reprogramming was induced by the forced expression of Neurog2, and Stau2 protein levels were evaluated in Neurog2-transduced cells with non-neuronal morphology and successfully induced neurons (Dcx-positive) at 3, 5, and 7 DPI (**Figure 9A-C**). Immunofluorescence analysis revealed a significant increase in Stau2 protein levels in successfully induced neurons at 7 DPI compared to the control condition (DsRed-Expressed2, hereafter indicated as DsRed) (**Figure 9F**). It's noteworthy that a similar trend of increased Stau2 protein levels was already observed at 5 DPI, compared to 3 DPI (**Figure 9D,E**). In contrast, a decrease in Stau2 protein levels was detected in the category of cells with non-neuronal morphology at 3 and 7 DPI compared to the control condition (DsRed) (**Figure 9D,F**). A similar trend of decrease in Stau2 protein levels was also observed at 5 DPI, although not statistically significant. This may be due to the lower number of biological replicates available at 5 DPI compared to 3 and 7 DPI. These results suggest that also Stau2, in addition to Pum2, may be involved in the reprogramming process. Furthermore, the observed dynamic protein expression in both non-reprogrammed and successfully reprogrammed cells suggests that Stau2 involvement may span across different stages of the conversion process. Noteworthy, the observed distinct protein expression patterns of Pum2 and Stau2 during reprogramming may reflect their roles in different stages and aspects of the conversion process.

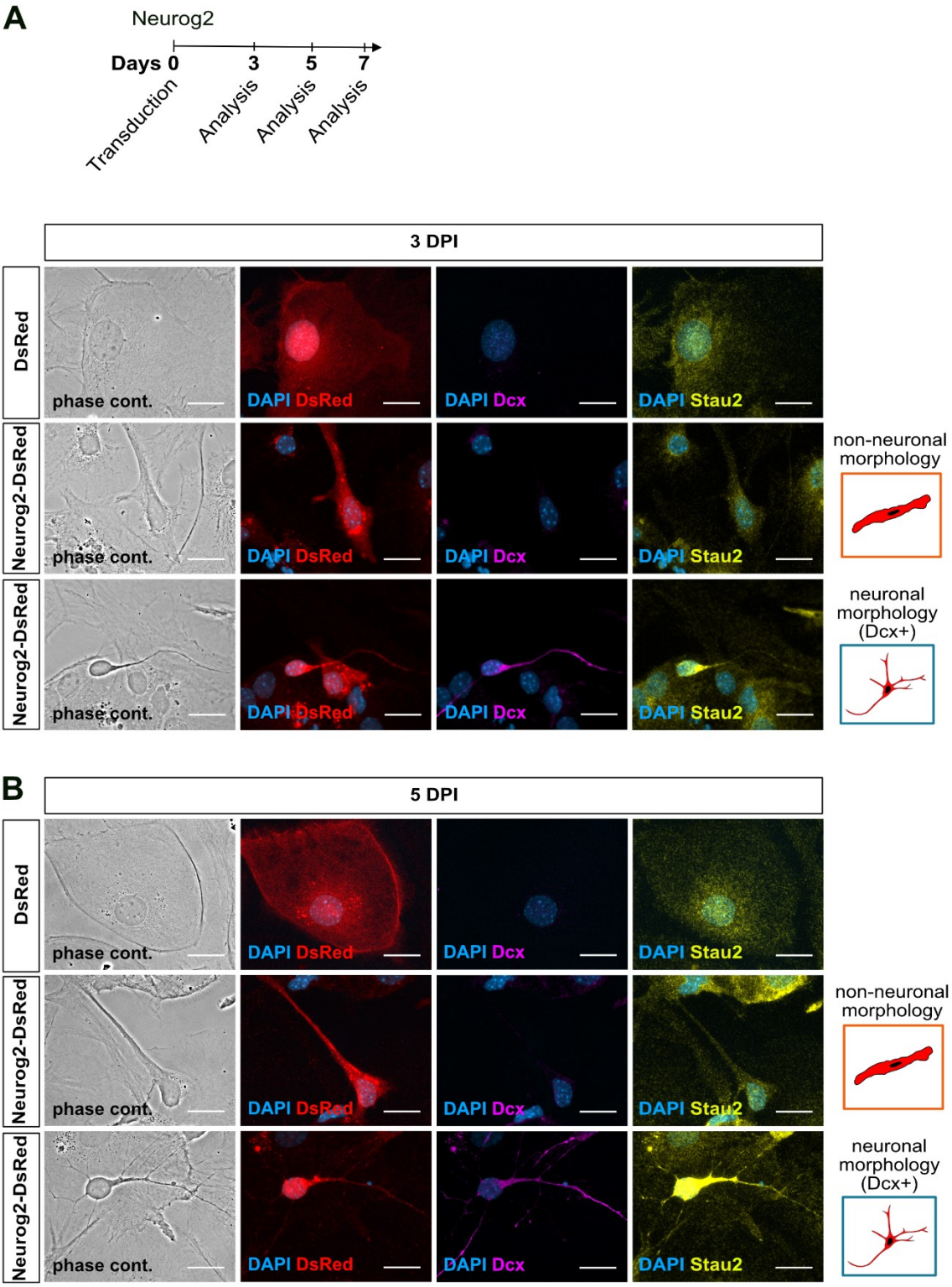
A
Neurog2
Days 0
3
5
7
Transduction
Analysis
Analysis
Analysis
3 DPI
DsRed
Neurog2-DsRed
Neurog2-DsRed
phase cont.
DAPI DsRed
DAPI Dcx
DAPI Stau2
non-neuronal morphology
neuronal morphology (Dcx+)
B
5 DPI
DsRed
Neurog2-DsRed
Neurog2-DsRed
phase cont.
DAPI DsRed
DAPI Dcx
DAPI Stau2
non-neuronal morphology
neuronal morphology (Dcx+)

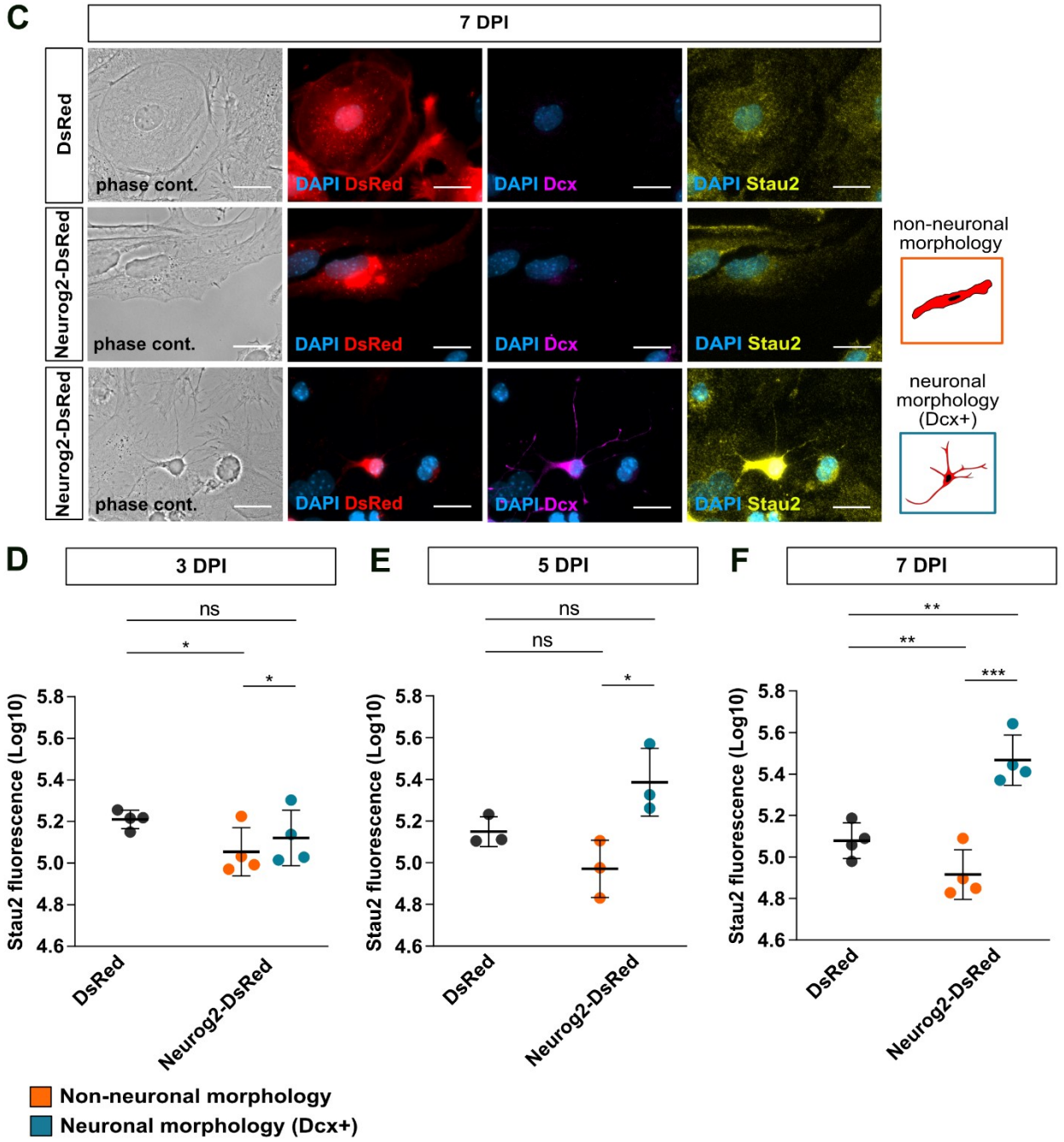

Figure 9: Stau2 protein levels are increased in successfully induced neurons

(A,B,C) Experimental outline of astrocyte-to-neuron reprogramming and representative examples of Stau2 and Dcx immunostaining, DsRed fluorescence, DAPI staining and phase contrast images of control- (DsRed only) or Neurog2-DsRed-positive cells at 3 (DPI) **(A)**, 5 DPI **(B)** and 7 DPI **(C)**. Scale bars: 20 µm. **(D,E,F)** Dot plot displaying Stau2 total fluorescence (log10 scale) in control- (DsRed only) or Neurog2-DsRed-positive cells at 3 DPI **(D)**, 5 DPI **(E)** and 7 DPI **(F)**. Control- (DsRed only) positive cells are displayed in dark grey circles. Sub-categories of Neurog2-DsRed-positive cells are displayed in orange (DsRed+ with non-neuronal morphology) and blue (DsRed+Dcx+ with neuronal morphology) circles. Mean and Standard Deviation are shown. Circles indicate independent biological replicates (n = 4 in **D;F**, n = 3 in **E**). Asterisks represent *p*-values obtained by paired Student's t-test (*$p < 0.05$, **$p < 0.01$, ***$p < 0.001$; ns ≥ 0.05). Total fluorescence was measured in the perinuclear region which differed in size between different cell types (panels D-F).

3.3.3 Enhanced colocalisation of Pum2 and Stau2 particles in successfully induced neurons

Despite the different protein expression patterns of Pum2 and Stau2 observed during reprogramming, I examined their potential interaction. Neuronal reprogramming was induced by the forced expression of Neurog2, followed by immunostaining for endogenous Pum2 and Stau2 at 7 DPI (**Figure 10A,B**). Colocalisation events were examined in the proximal region of neuronal processes of successfully converted neurons (**Figure 10C**). Similar to the approach used in cortical astrocytes (**Figure 7A,B**), only particles with more than 30% overlapping volume were considered to colocalise. Colocalisation analysis revealed that, on average, approximately 43% of Pum2-containing particles were found in close contact with Stau2-containing particles (**Figure 10D**). Notably, the extent of colocalisation between Pum2 and Stau2 in induced neurons after reprogramming showed an increase compared to the previously observed colocalisation in cortical astrocytes (**Figure 7C**). This degree of colocalisation between Pum2 and Stau2 particles in induced neurons may indicate potential interaction between these two RBPs, despite their distinct expression patterns along the conversion process.

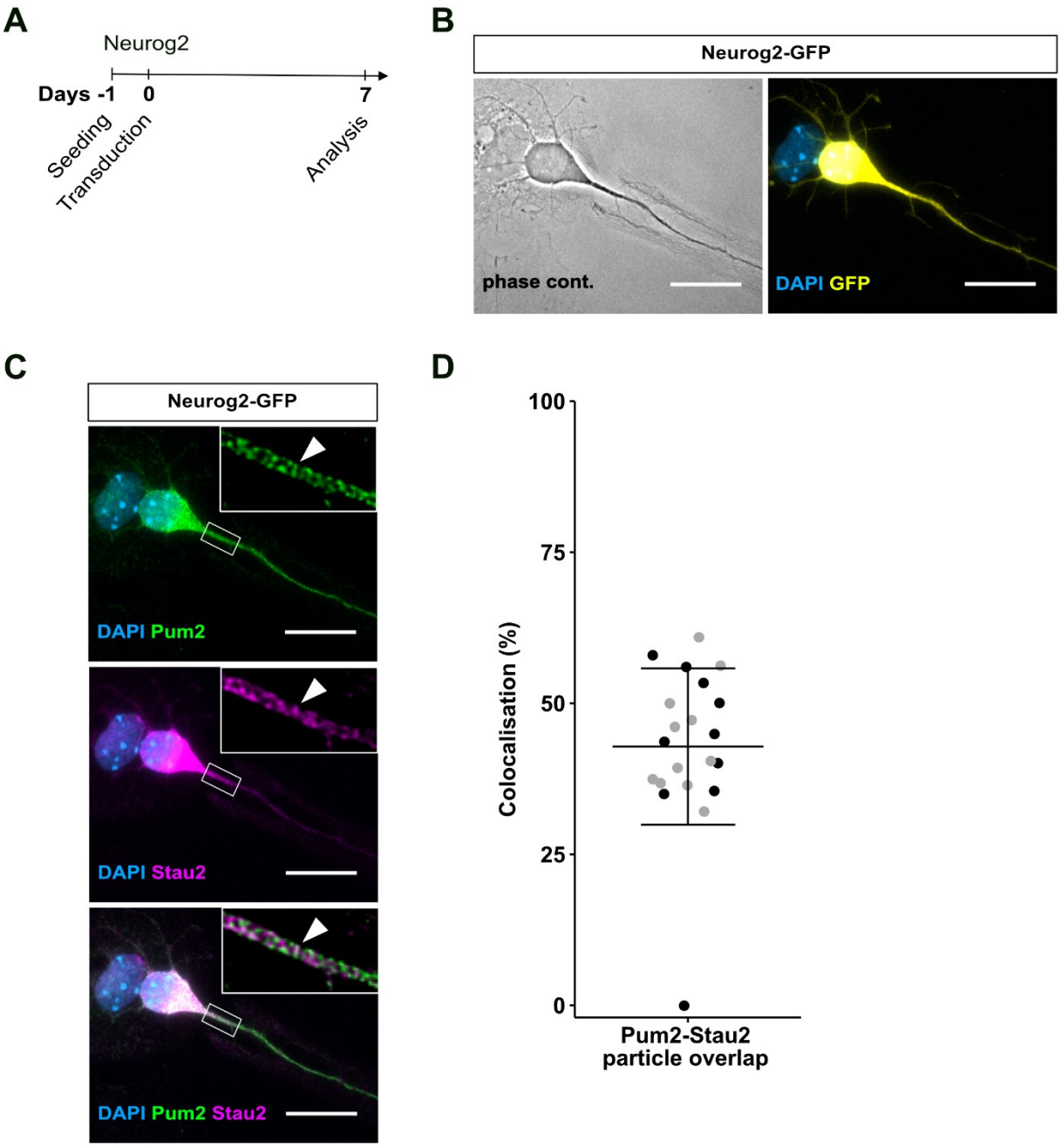

Figure 10: Colocalisation of Pum2 and Stau2 particles in induced neurons

(A) Experimental outline of astrocyte-to-neuron reprogramming. **(B)** Representative examples of GFP fluorescence, DAPI staining and phase contrast images of Neurog2-GFP-positive cells at 7 DPI. **(B)** Representative examples of Pum2 and Stau2 co-immunostaining, DAPI staining and merged images of Neurog2-GFP-induced neurons at 7 DPI. Scale bars: 20 µm. Boxed regions in images represent magnified insets processed separately by image deconvolution. White arrowhead indicates one example for colocalisation between Pum2 and Stau2. **(B)** Dot plot displaying percentage of Pum2 particles overlapping with Stau2 particles (defined by more than 30% volume overlap) in Neurog2-GFP-induced neurons after 7 days of reprogramming. Grey and black circles indicate individual cells from two independent biological replicates (n = 2). Mean and Standard Deviation are shown.

3.4 Neuronal reprogramming efficiency is impaired upon Pum2 or Stau2 depletion

To investigate whether Pum2 contributes to a successful cell fate conversion during reprogramming, the efficiency of astrocyte-to-neuron conversion was determined in the absence of Pum2 or Stau2. To this end, cortical astrocytes were simultaneously transduced with (i) a retrovirus expressing Neurog2 and (ii) a lentivirus expressing well-characterized shRNAs targeting either *Pum2* or *Stau2* mRNA (Goetze et al., 2006; Vessey et al., 2010) (**Figure 11A**). The efficacy of knockdown of these shRNAs was further confirmed in cortical astrocytes after 7 days in culture, showing a 50% and 35% reduction in Pum2 and Stau2 protein levels, respectively, at 4 DPI (data not shown). The proportion of successfully converted neurons among the cells positive for both Neurog2 (GFP+) and shRNA (RFP+) fluorescent reporters was evaluated at 7 DPI (**Figure 11A,B**). Only those cells that were positive for the neuronal marker Dcx and also exhibited neuronal morphology were scored as successfully converted neurons (Gascon et al., 2016) (**Figure 11B**). Interestingly, shRNA-mediated downregulation of Pum2 resulted in a significant reduction in the proportion of neurons among co-infected cells (approximately by 43%) compared to the control condition (shNTC) (**Figure 11C**). Surprisingly, Stau2 knockdown also resulted in a reduction in reprogramming efficiency (approximately by 24%), although less pronounced compared to Pum2 (**Figure 11C**). These results highlight the importance of both Pum2 and Stau2 in the process of neuronal reprogramming, with Pum2 having a greater impact on the successful cell fate conversion. These results provide additional support for the potentially distinct contributions of Pum2 and Stau2 to the reprogramming process. Due to the more robust effect of Pum2 on reprogramming efficiency, further experiments were performed to investigate how this RBP contributes to neuronal reprogramming.

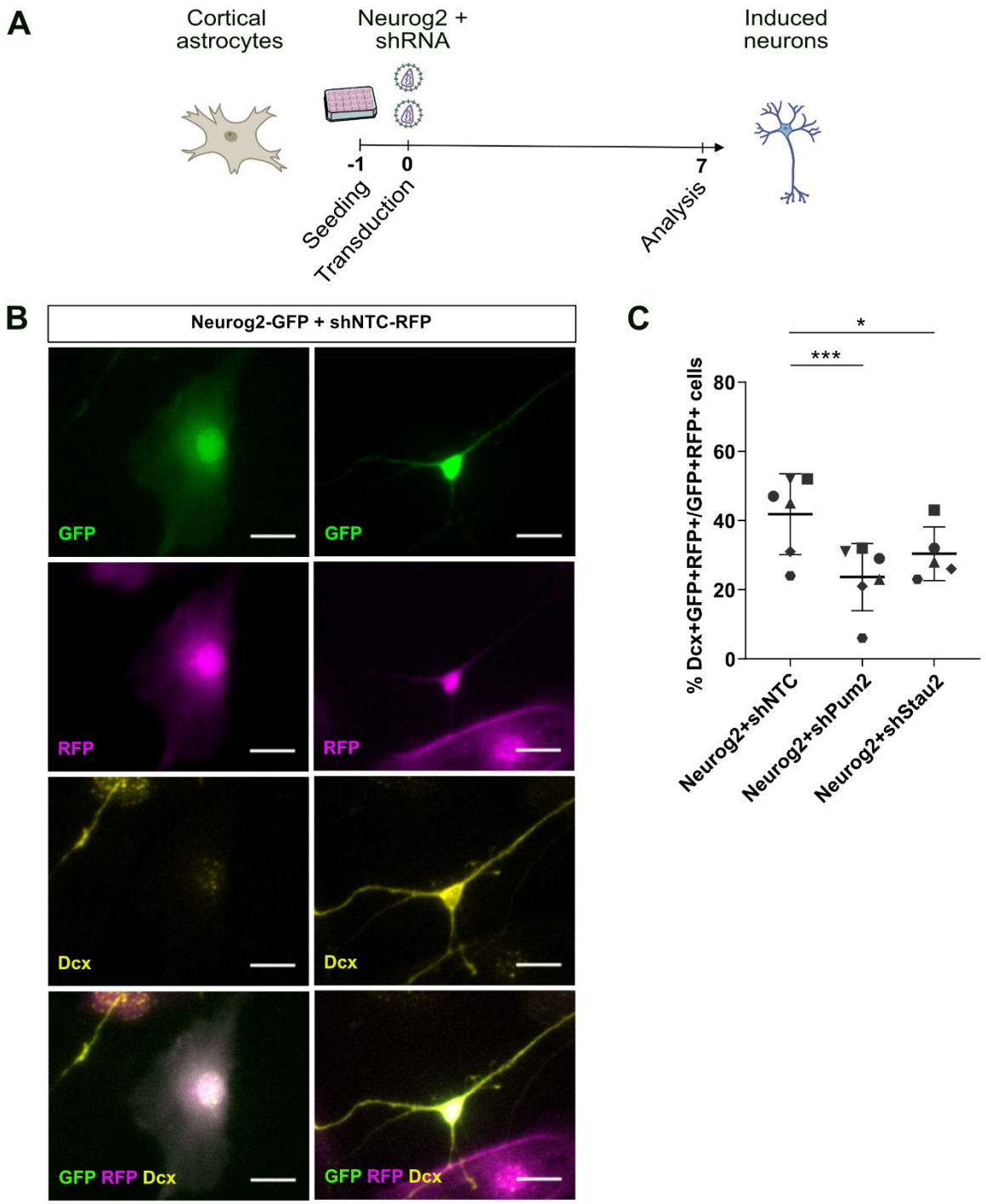

Figure 11: Pum2 and Stau2 depletion differentially affects successful reprogramming **(A)** Experimental outline of astrocyte-to-neuron reprogramming under Pum2 or Stau2-depleted conditions. **(B)** Representative examples of GFP and RFP fluorescence, Dcx immunostaining and merged images of Neurog2-GFP and shNTC-RFP-positive cells. Scale bars: 20 µm. **(C)** Dot plot displaying the proportion of neurons (Dcx+) among Neurog2-GFP and shRNA-RFP-positive cells under control (Neurog2+shNTC) or under Pum2 or Stau2-depleted conditions (Neurog2+shPum2/shStau2) at 7 DPI. Grey symbols indicate independent biological replicates (n = 6 for shPum2 and n = 5 for shStau2). Mean and Standard Deviation are shown. Asterisks represent *p*-values obtained by paired Student's t-test (*$p < 0.05$, ***$p < 0.001$). 24-well plate icon modified from Database Center for Life Science, licenced under Creative Commons Attribution 4.0 International, https://creativecommons.org/licenses/by/4.0/

3.4.1 Cell death is not the cause of reduced reprogramming efficiency upon Pum2 depletion

To elucidate the underlying cause of the decreased reprogramming efficiency in the absence of Pum2, I first investigated whether cell death was a possible contributing factor. In brief, I reevaluated the existing data obtained from the reprogramming experiment under Pum2-depleted condition at 7DPI (**Figure 12A**). First, the total number of live cells, identified by positive DAPI staining, was quantified both in the presence and absence of Pum2. The analysis revealed no significant change in the total number of DAPI-positive cells under Pum2-depleted condition (shPum2) compared to the control (shNTC) (**Figure 12B**). Therefore, reprogramming, at least at a general level, did not cause substantial cell death after Pum2 depletion. For a more accurate assessment of cell death, further quantification was performed on the cells positive for both Neurog2 (GFP+) and shRNA (RFP+) fluorescent reporters, which were previously considered for the evaluation of reprogramming efficiency. This subset of cells (GFP+RFP+) was normalised to the total population of cells transduced with Neurog2-expressing retrovirus (GFP+). Indeed, this normalisation takes into account any possible variations in the total number of Neurog2-positive cells, allowing a clearer understanding of the impact of cell death on the reprogramming process upon Pum2 depletion. If cell death were a significant factor, it would lead to a reduction of this ratio. Interestingly, the analysis showed no significant variation in the ratio of Neurog2 and shRNA-positive cells to Neurog2-positive cells under Pum2 depleted condition (shPum2) compared to the control (shNTC) (**Figure 12C**). Moreover, no change of the absolute number of Neurog2-positive cells was detected upon Pum2 knockdown (**Figure 12D**). Taken together, these results indicate that cell death is most likely not a major contributor to the reduction in reprogramming efficiency observed in the absence of Pum2.

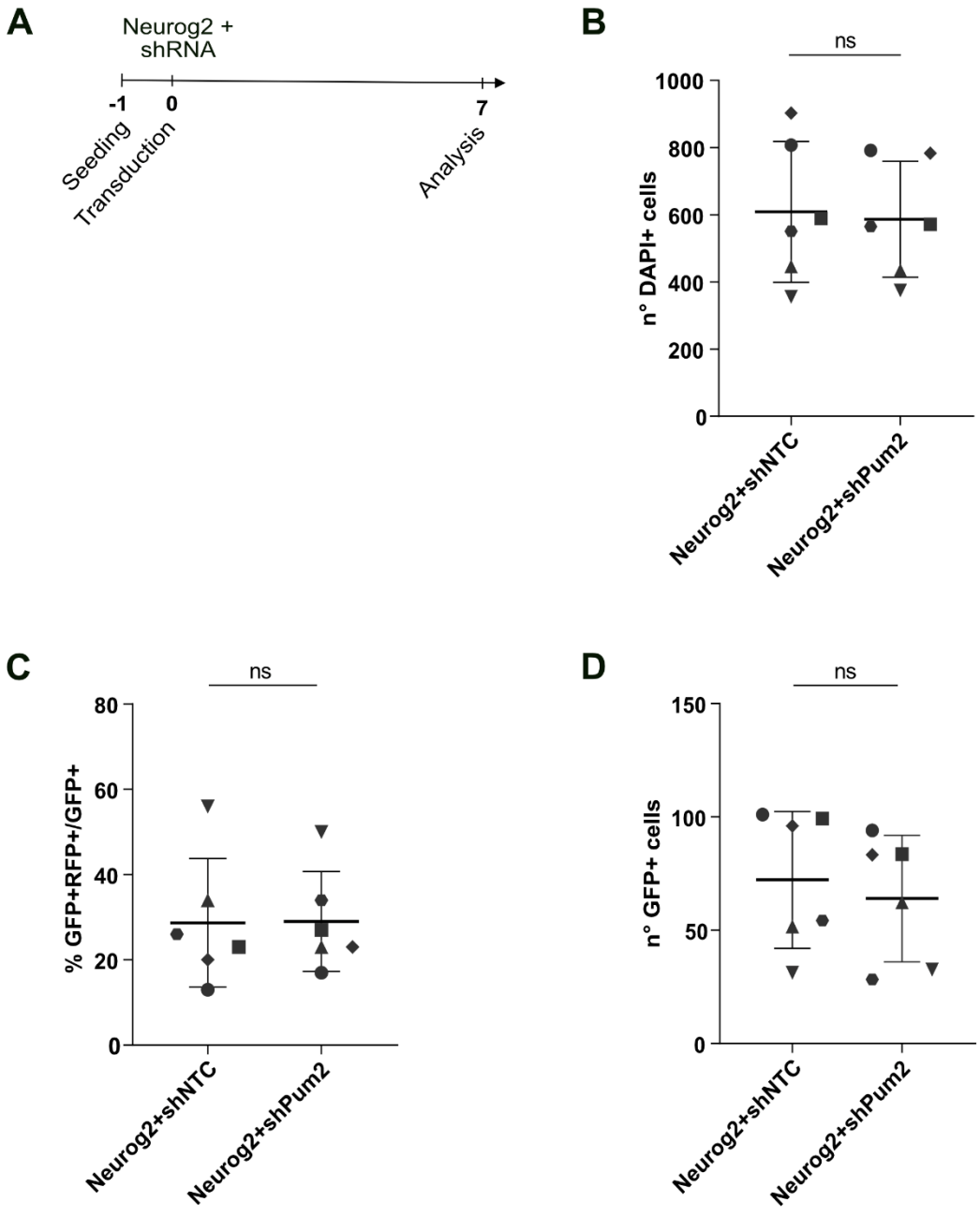

Figure 12: Cell death is not the major contributor to reduced reprogramming efficiency upon Pum2 depletion

(A) Experimental outline of neuronal reprogramming under Pum2-depleted condition. **(B,C,D)** Dot plot displaying number of DAPI-positive cells **(B)**, normalisation of Neurog2-GFP and shRNA-RFP-positive cells to Neurog2-GFP-positive cells **(C)** and number of Neurog2-GFP-positive cells **(D)** under control (Neurog2+shNTC) and Pum2-depleted condition (Neurog2+shPum2) at 7DPI. Grey symbols indicate independent biological replicates (n = 6). Mean and Standard Deviation are shown. Statistics obtained by paired Student's t-test (ns $\geq$ 0.05).

3.4.2 Reduced generation of neurons upon Pum2 depletion in astrocyte-to-neuron reprogramming

To investigate the cellular dynamics underlying the reduced reprogramming efficiency upon Pum2 depletion, I performed a detailed analysis of reprogramming in the absence of Pum2 at 7 DPI (**Figure 13A**). Specifically, I quantified the absolute numbers of the two categories of cells involved in the reprogramming process: (i) cells that failed to reprogram and (ii) successfully converted neurons (**Figure 13A**). As mentioned above, the reprogramming efficiency was quantified as proportion of successfully converted neurons (Dcx-positive cells showing neuronal morphology) among the cells positive for both Neurog2 and shRNA fluorescent reporters (GFP+RFP+). As first step, I quantified the total number of double-positive cells (GFP+RFP+) without distinguishing between non-reprogrammed and reprogrammed cells. The analysis showed no significant reduction in the total number of double-positive cells in the Pum2-depleted condition (shPum2) compared to the control (shNTC) (**Figure 13B**). Notably, this result is consistent with previous evidence that no major cell loss occurs during reprogramming upon Pum2 depletion. I then individually quantified the absolute number of cells that failed to become neurons (showing non-neuronal morphology) (**Figure 13C**) and successfully converted cells (Dcx-positive with typical neuronal morphology) (**Figure 13D**). This analysis revealed a decrease in the number of induced neurons and a concomitant slight increase in the population of cells that failed to reprogram in the absence of Pum2 compared to the control. Taken together, these findings reveal the dynamics of the cells involved in reprogramming upon Pum2 depletion, in particular how the absence of Pum2 negatively affects neuron generation.

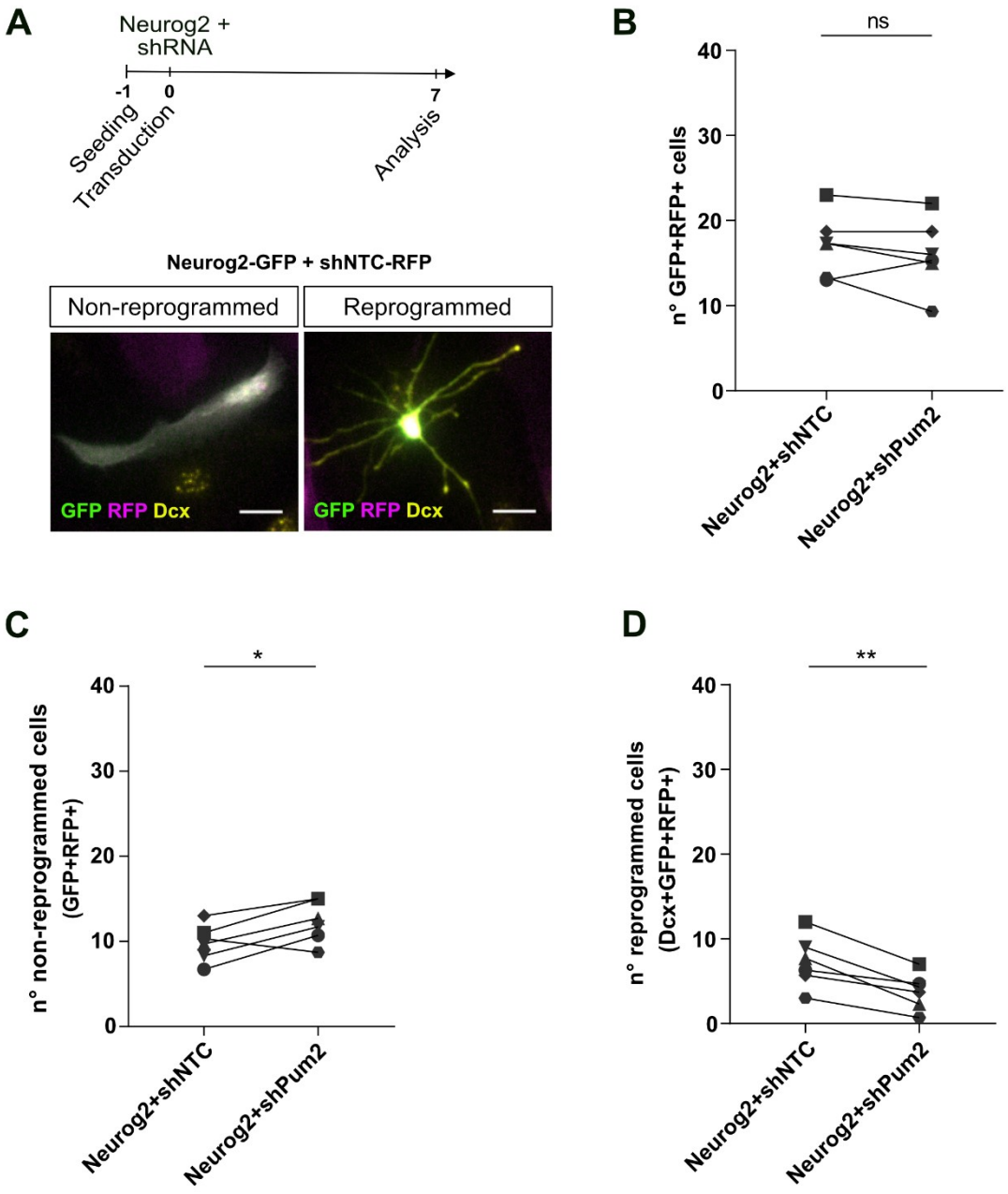

Figure 13: Pum2 depletion results in reduced generation of neurons and increase of non-reprogrammed cells

(A) Experimental outline of neuronal reprogramming under Pum2-depleted condition and representative examples of GFP and RFP fluorescence, Dcx immunostaining merged images of non-reprogrammed and reprogrammed Neurog2-GFP and shNTC-RFP-positive cells. **(B,C,D)** Dot plots displaying number of Neurog2-GFP and shRNA-RFP-positive cells **(B),** number of non-reprogrammed Neurog2-GFP and shRNA-RFP-positive cells **(C),** number of reprogrammed Neurog2-GFP, shRNA-RFP and Dcx-positive cells **(D)** under control (Neurog2+shNTC) or Pum2-depleted conditions (Neurog2+shPum2) at 7 DPI. Grey symbols indicate independent biological replicates (n = 6). Asterisks represent *p*-values obtained by paired Student's t-test (*$p < 0.05$, **$p < 0.01$, ns ≥ 0.05).

3.5 The effects of Pum2 on reprogramming manifest after 5 days of conversion process

Reprogramming of astrocytes into neurons, triggered by the forced expression of a neurogenic cell fate determinant, such as Neurog2, leads to the acquisition of neuronal identity within 5-7 days. Typically, by day 5 many reprogrammed cells have acquired the expression of neuronal markers and show typical neuronal morphology as a sign of successful conversion (Gascon et al., 2016; Heinrich et al., 2011). To determine, at which time point of the reprogramming process Pum2 is required for successful fate conversion, the reprogramming efficiency was assessed in Pum2-depleted conditions at 5 DPI, instead of the conventional 7 DPI. This would allow a closer examination of the potential role of Pum2 in the early phase of reprogramming. Cortical astrocytes were simultaneously transduced with a retrovirus expressing Neurog2 and a lentivirus expressing a shRNA targeting *Pum2* mRNA (Figure 11A). The proportion of successfully converted neurons among the cells positive for both Neurog2 (GFP+) and shRNA (RFP+) fluorescent reporters was evaluated at 5 DPI (**Figure 14A,B**). Successful conversion was again determined based on the expression of the neuronal marker Dcx and the manifestation of a well-defined neuronal morphology (Gascon et al., 2016) (**Figure 14B**). Interestingly, this analysis showed no significant change in reprogramming efficiency upon Pum2 depletion (shPum2) compared to the control (shNTC) (**Figure 14C**). The decrease in reprogramming efficiency observed at 7 DPI (**Figure 11C**), but not yet at 5 DPI, suggests that Pum2 may contribute to reprogramming in the late stages of conversion, rather than in the critical initial steps required to initiate cell fate conversion.

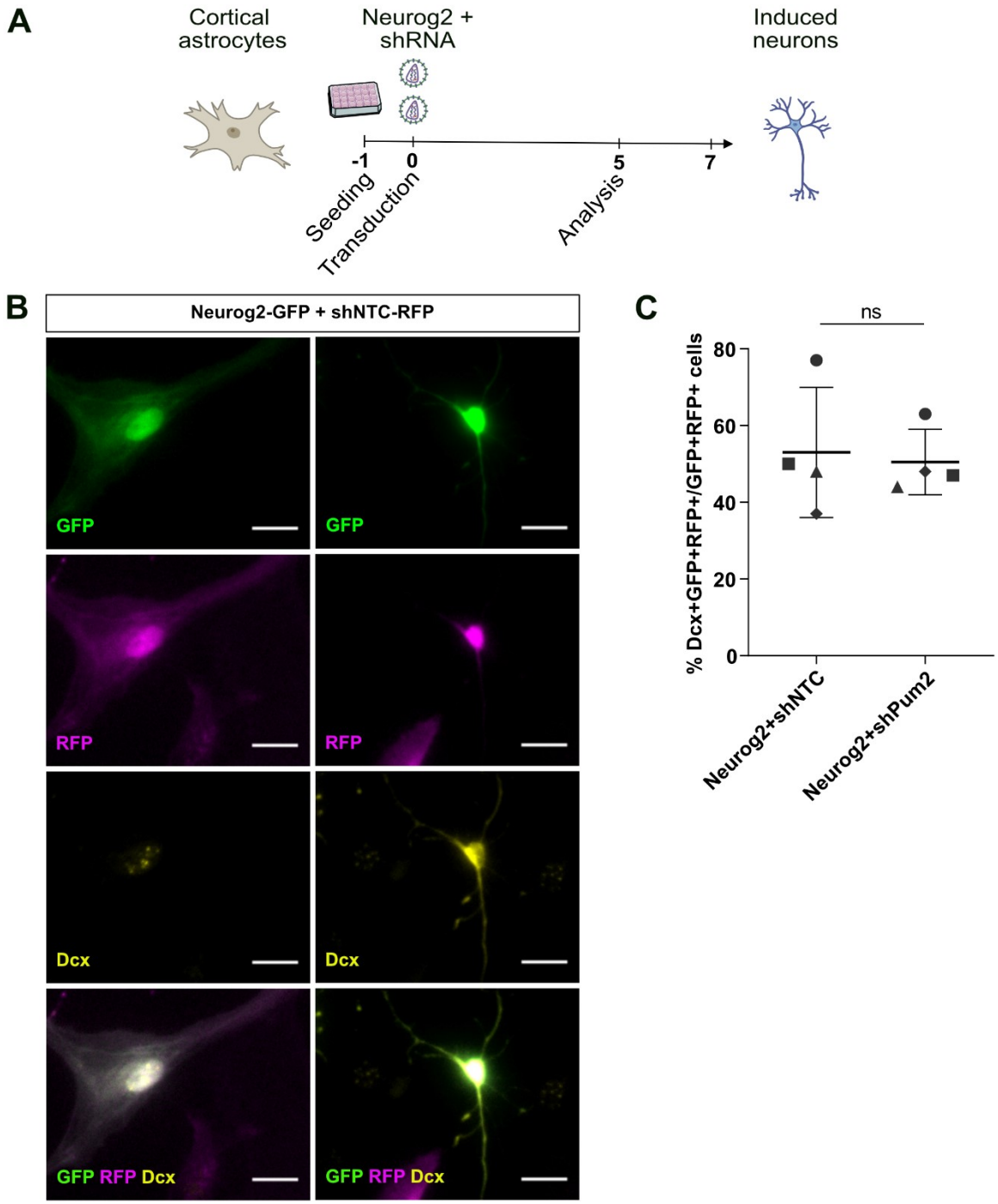

Figure 14: Reduction in reprogramming efficiency upon Pum2 depletion does not occur at day 5

(A) Experimental outline of astrocyte-to-neuron reprogramming under Pum2-depleted condition. **(B)** Representative examples of GFP and RFP fluorescence, Dcx immunostaining and merged images of Neurog2-GFP and shNTC-RFP-positive cells. Scale bars: 20 µm. **(C)** Dot plot displaying the proportion of neurons (Dcx+) among Neurog2-GFP and shRNA-RFP-positive cells under control (Neurog2+shNTC) or Pum2-depleted conditions (Neurog2+shPum2) at 5 DPI. Mean and Standard Deviation are shown. Grey symbols indicate independent biological replicates (n = 4). Statistics obtained by paired Student's t-test (ns ≥ 0.05). 24-well plate icon modified from Database Center for Life Science, licenced under Creative Commons Attribution 4.0 International, https://creativecommons.org/licenses/by/4.0/

3.6 Pum2 is required in the late phase of astrocyte-to-neuron reprogramming

To further investigate whether Pum2 is involved in the late phase of neuronal reprogramming, Pum2 downregulation was induced two days after the forced expression of Neurog2. Indeed, the early Neurog2-mediated transcriptional changes necessary for the change of cellular identity occur during the first 48h of direct neuronal reprogramming (Masserdotti et al., 2015). Cortical astrocytes were first transduced with a retrovirus expressing Neurog2, followed two days later by a second transduction with a lentivirus expressing a shRNA targeting *Pum2* mRNA (**Figure 15A**). The reprogramming efficiency was evaluated at 7 DPI, considering Neurog2- and shRNA-transduced cells (GFP+RFP+) positive for neuron-specific Dcx and showing neuronal morphology as successfully converted (**Figure 15B**). Interestingly, the analysis revealed a reduction of approximately 40% in the proportion of neurons among co-infected cells upon Pum2 depletion (shPum2) compared to the control (shNTC) (**Figure 15C**). Noteworthy, the interference with Pum2 expression two days after Neurog2 overexpression reduced the reprogramming efficiency similarly to the continuous loss of Pum2 observed previously (**Figure 11C**). These data point towards a role of Pum2 in the late phase of the cell fate conversion, when the early transcriptional changes associated with neuronal fate have already been implemented.

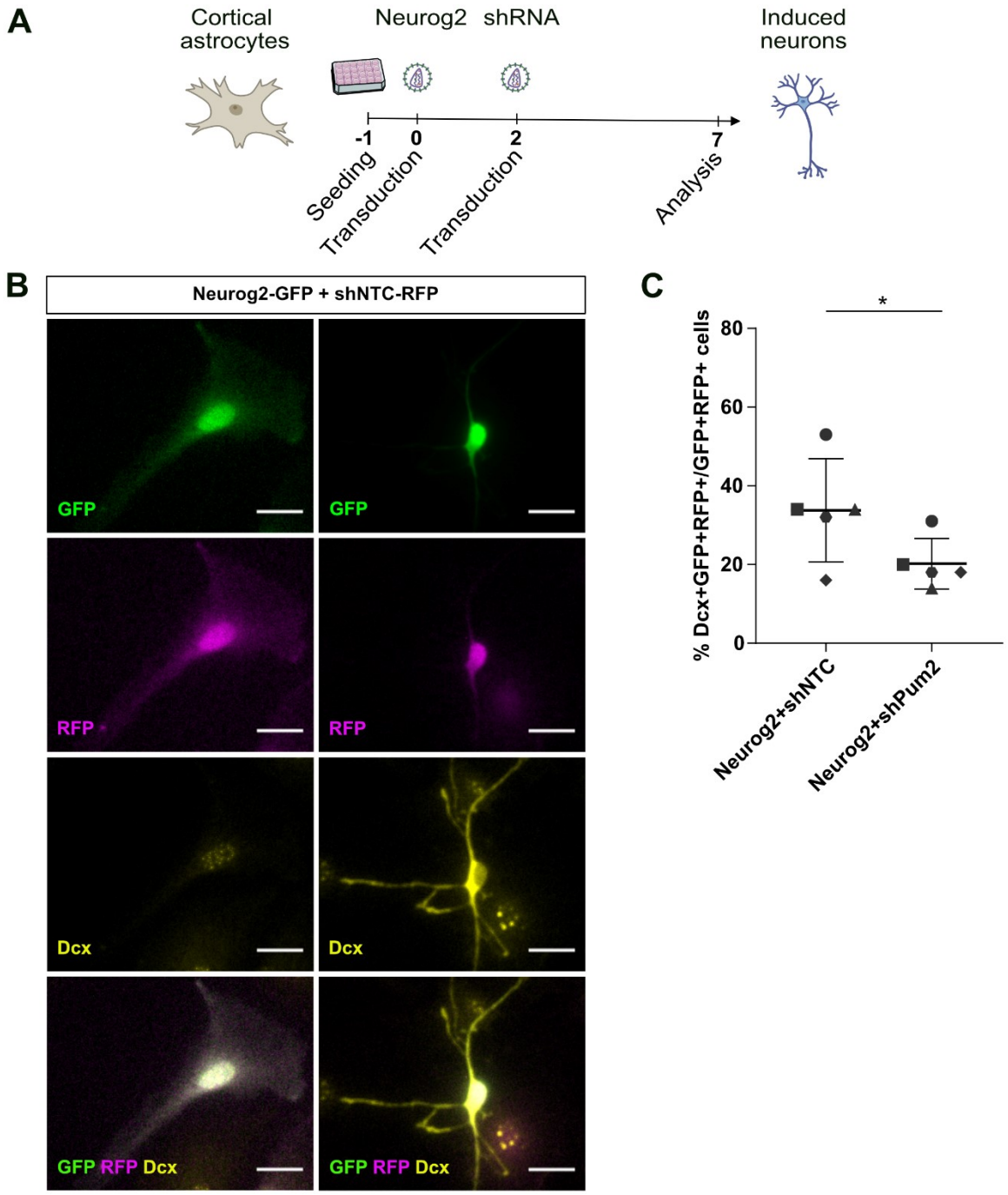

Figure 15: Reduced Pum2 expression upon Neurog2 overexpression diminishes reprogramming efficiency

(A) Experimental outline of Pum2 knockdown induced two days after Neurog2 overexpression. **(B)** Representative examples of GFP and RFP fluorescence, Dcx immunostaining and merged images of Neurog2-GFP and shNTC-RFP-positive cells. Scale bars: 20 µm. **(C)** Dot plot displaying the proportion of neurons (Dcx+) among Neurog2-GFP and shRNA-RFP-positive cells under control (Neurog2+shNTC) or Pum2-depleted conditions (Neurog2+shPum2) at 7 DPI. Grey symbols indicate independent biological replicates (n = 5). Mean and Standard Deviation are shown. Asterisks represent *p*-values obtained by paired Student's t-test (*$p < 0.05$). 24-well plate icon modified from Database Center for Life Science, licenced under Creative Commons Attribution 4.0 International, https://creativecommons.org/licenses/by/4.0/

3.7 Pum2 does not have a significant effect on successfully induced neurons

Having established that Pum2 is involved in the late phase of reprogramming, I investigated whether this RBP had an effect on the subset of cells that, after the forced expression of Neurog2, achieved a proper cell fate conversion (Dcx-positive and exhibiting neuronal morphology). To this end, morphological analysis was performed on successfully induced neurons 7 days after reprogramming in the absence of Pum2 (**Figure 16A**). I first examined whether Pum2 affected the overall integrity of the Neurog2 and shRNA-positive cells successfully converted, by evaluating the nucleus and the cytoplasm (**Figure 16B**). Preliminary qualitative evaluation revealed no obvious change in the DAPI staining pattern or aberrant shape of the nucleus in the Pum2-depleted condition compared to control (**Figure 16B**). Furthermore, quantitative analysis of the nucleus size (μm^2) of induced neurons revealed no significant differences between the control and Pum2-depleted condition (**Figure 16C**). Interestingly, a slight but significant decrease in the size of the soma (μm^2) was observed in induced neurons under Pum2-depleted condition compared to the control (**Figure 16D**). Taken together, these results suggest that Pum2 does not affect the general well-being of induced neurons, while it may be involved in regulating neuronal growth. Additionally, I investigated whether Pum2 affects the establishment of neuronal polarity. Successfully converted neurons were evaluated by distinguishing between bipolar and multipolar neurons (**Figure 17A,B**). This analysis revealed that almost all induced neurons showed a multipolar morphology both in the presence and absence of Pum2, while only a minority of neurons were bipolar (**Figure 17C**). This result indicates that Pum2 does not significantly affect the establishment of neuronal polarity during neuronal reprogramming. In summary, these results suggest that the depletion of Pum2 has only a minimal effect on the general morphology of neurons that have been successfully induced.

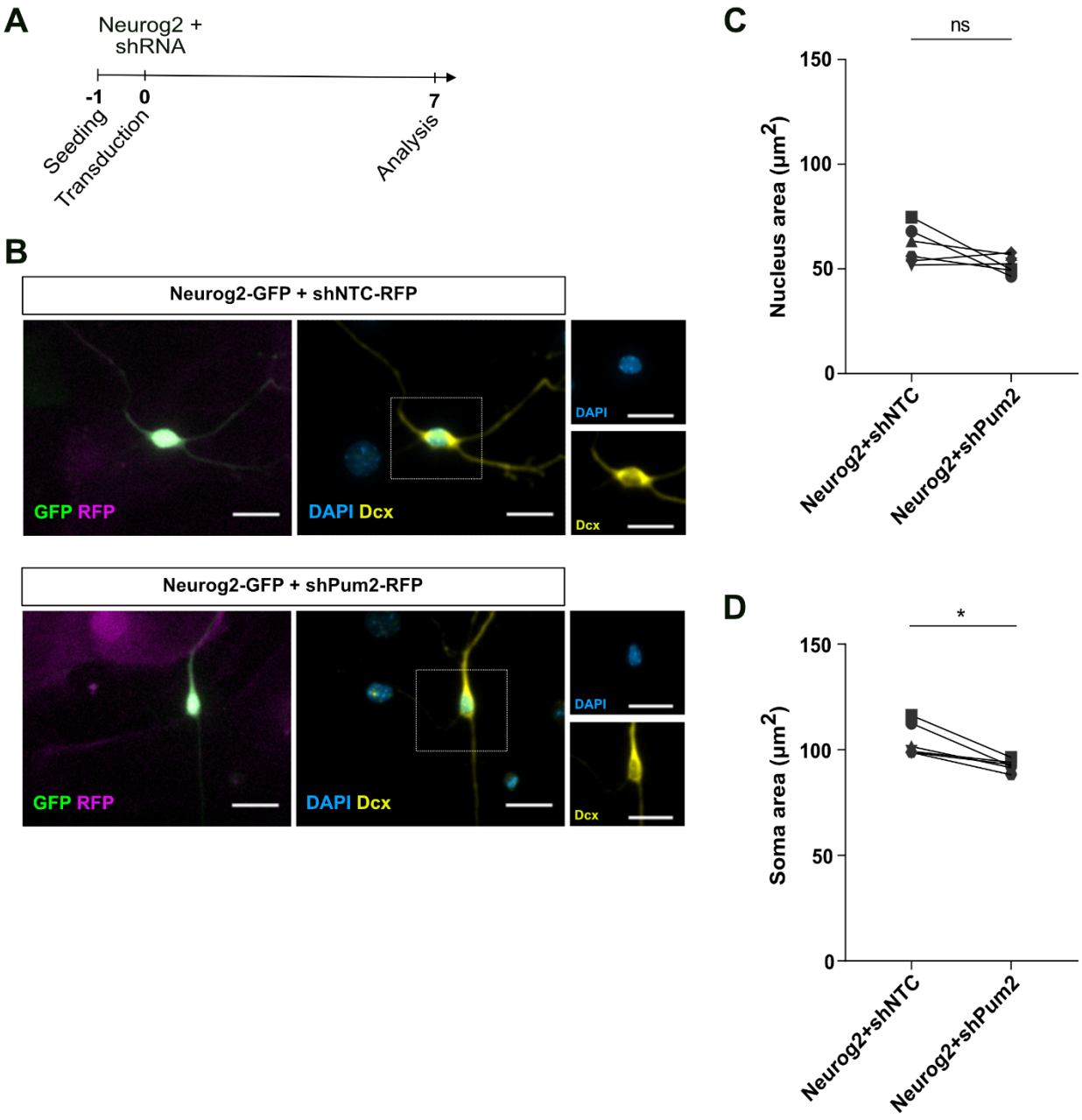

Figure 16: Pum2 depletion does not affect the integrity of successfully induced neurons

(A) Experimental outline of astrocyte-to-neuron reprogramming under Pum2-depleted conditions. **(B)** Representative examples of GFP and RFP fluorescence, DAPI staining and Dcx immunostaining images of Neurog2-GFP and shNTC or shPum2-RFP-positive cells. Boxed regions in images represent magnified insets. Scale bars: 20 µm. **(C,D)** Dot plot displaying nuclear **(C)** and somatic compartment **(D)** areas (µm^2) of Neurog2-GFP-induced neurons (Dcx+) under control (Neurog2+shNTC) or Pum2-depleted conditions (Neurog2+shPum2). Grey symbols indicate independent biological replicates (n = 6). Asterisks represent *p*-values obtained by paired Student's t-test **(C)** and Wilcoxon matched-pairs signed rank test **(D)** (*$p < 0.05$, ns ≥ 0.05).

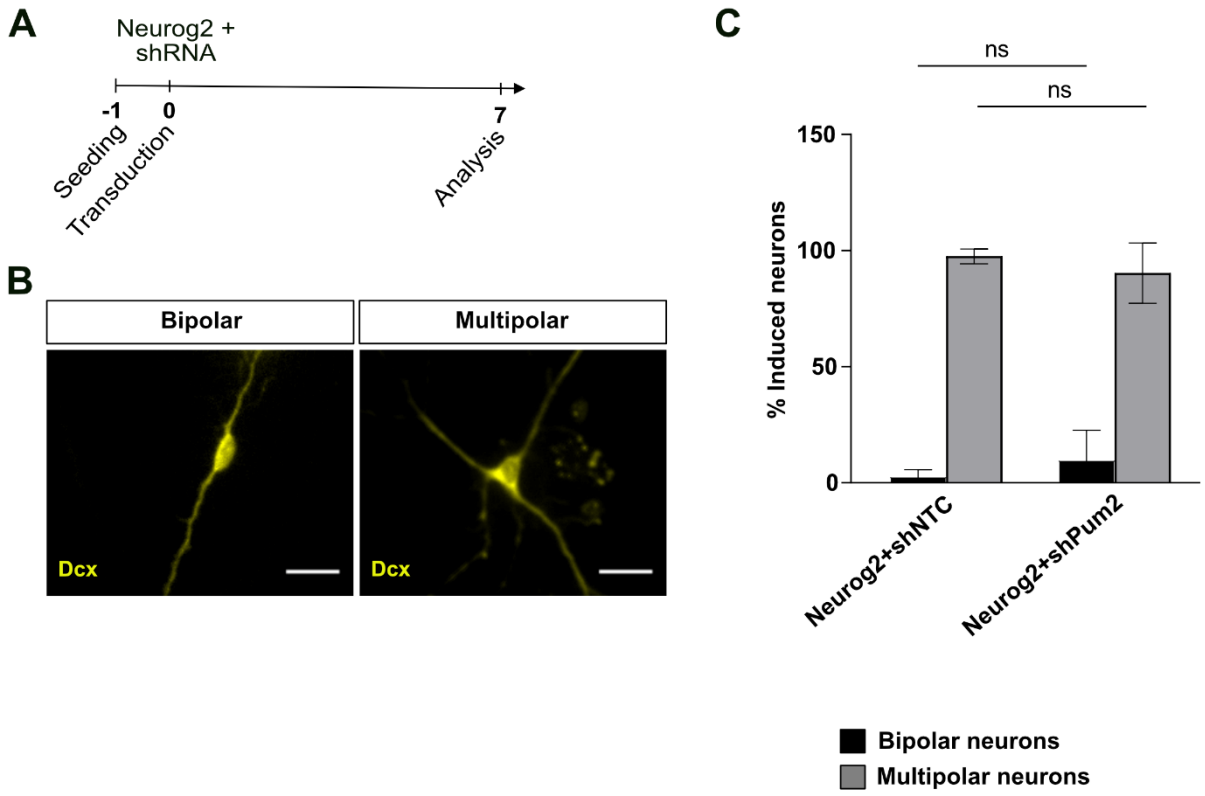

Figure 17: Pum2 does not affect the establishment of neuronal polarity during reprogramming

(A) Experimental outline of astrocyte-to-neuron reprogramming under Pum2-depleted conditions. **(B)** Representative examples of Dcx immunostaining images of successfully induced neurons. Scale bars: 20 µm. **(C)** Bar plot displaying percentage of Neurog2-GFP-induced neurons (Dcx+) showing bipolar and multipolar morphology under control (Neurog2+shNTC) or Pum2-depleted conditions (Neurog2+shPum2). Mean and Standard Deviation are shown. n = 6 biologically independent experiments. Statistics obtained by paired Student's t-test (ns ≥ 0.05).

3.8 Pum2 depletion leads to an increased amount of aberrant non-reprogrammed cells

To gain a deeper understanding of how Pum2 influences neuronal reprogramming in the late phase of conversion, the morphological analysis on induced neurons was combined with a parallel analysis of the cells that failed to undergo successful reprogramming. Again, the morphological analysis was performed after 7 days of reprogramming under Pum2-depleted conditions (**Figure 18A**). Based on a preliminary qualitative evaluation, the non-reprogrammed cells positive for both Neurog2 (GFP+) and shPum2 (RFP+) fluorescent reporters were categorised into cells with normal astrocyte morphology (**Figure 18B**) and cells with aberrant morphology (**Figure 18C**). A more detailed qualitative analysis classified cells with normal morphology exhibiting either typical astrocyte morphology or the elongated transitional shape typical of cells undergoing reprogramming (Gascon et al., 2016; Heinrich et al., 2011) (**Figure 19A**). Instead, cells with aberrant morphology exhibited atypical features that were clearly distinct from the so far observed astrocyte morphology (**Figure 19B,C**). Specifically, cells with aberrant morphology were often characterised by small size, shrivelled shape with uneven surface, and/or the presence of abnormal cell protrusions (**Figure 19B,C**). The morphology classified as aberrant exhibited these features individually or in combination. Indeed, a quantitative assessment of the cell area of non-reprogrammed cells showed a significant decrease in the cells with aberrant morphology compared to the cells with normal morphology (**Figure 19D**). In addition, the majority of non-reprogrammed cells with aberrant morphology did not express the neuronal marker Dcx (**Figure 19E**). Interestingly, a quantitative analysis of the abundance of cells with aberrant morphology among all non-reprogrammed cells revealed a slight but significant trend of increase in the Pum2-depleted condition compared to the control (**Figure 19F**). Conversely, the number of cells with normal morphology among all the non-reprogrammed cells decreased in the Pum2-depleted condition compared to the control (**Figure 19G**). Taken together, these results indicate that the absence of Pum2 not only leads to a reduction in the generation of neurons, but also results in an increased presence of non-reprogrammed cells exhibiting atypical morphology.

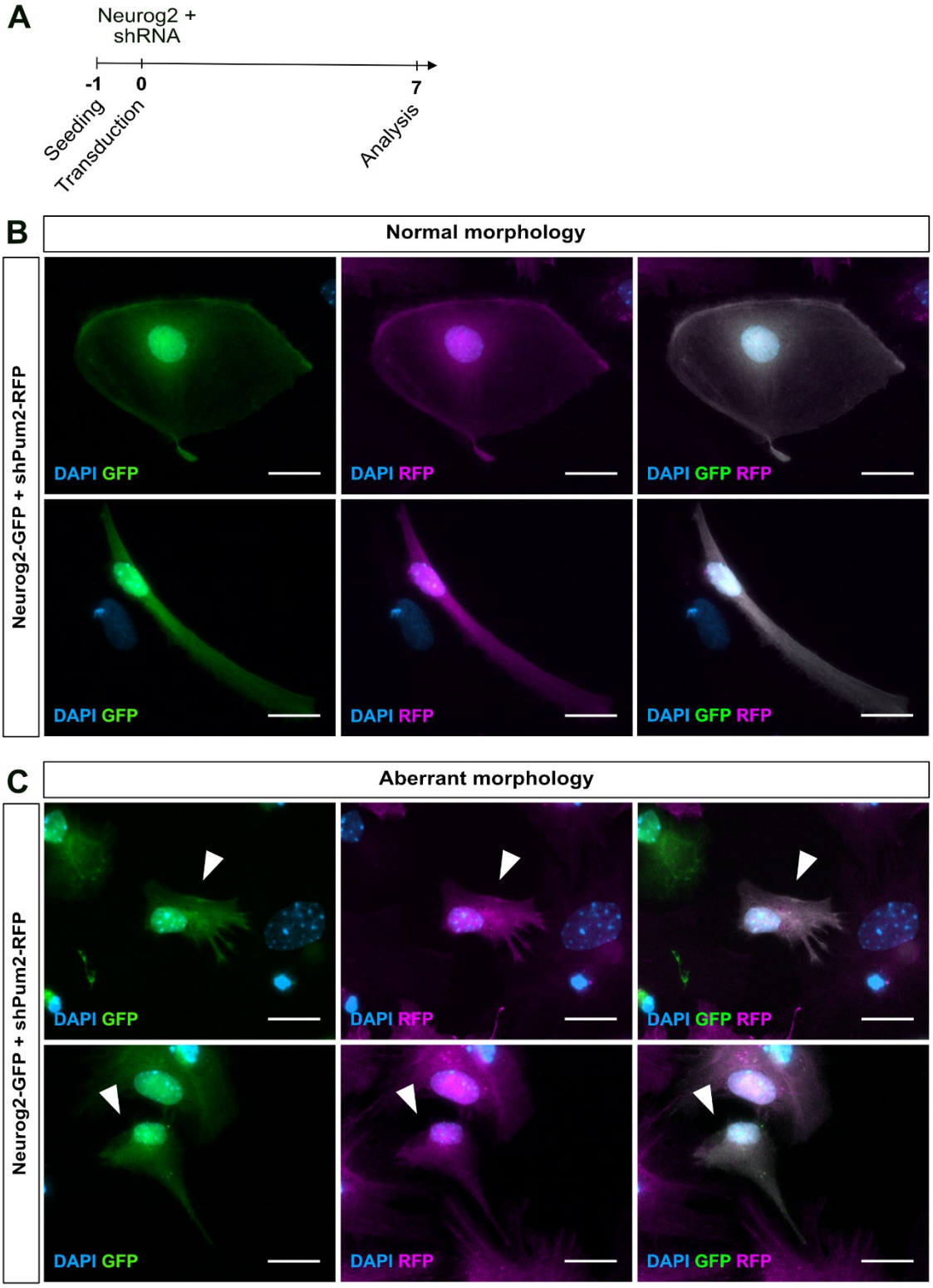

Figure 18: Different morphological phenotypes of non-reprogrammed cells upon Pum2 depletion

(A) Experimental outline of astrocyte-to-neuron reprogramming under Pum2-depleted conditions. **(B,C)** Representative examples of GFP and RFP fluorescence, DAPI staining and merged images of Neurog2-GFP and shPum2-RFP-positive cells showing normal **(B)** and aberrant morphology **(C)**. White arrowhead indicates examples of cells with aberrant morphology **(C)**. Scale bars: 20 µm.

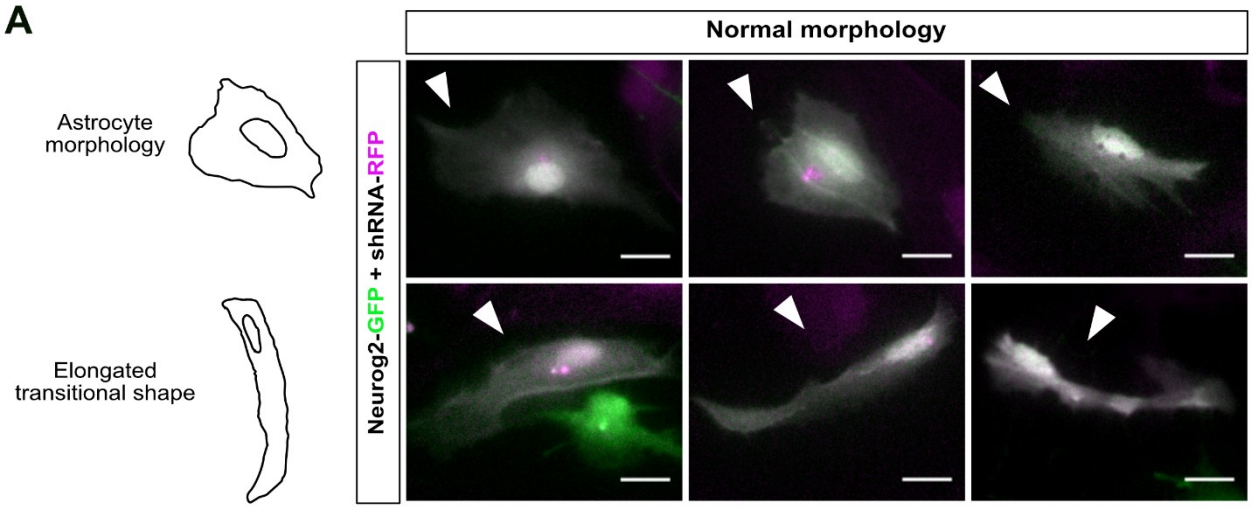
A
Normal morphology
Astrocyte morphology
Elongated transitional shape
Neurog2-GFP + shRNA-RFP

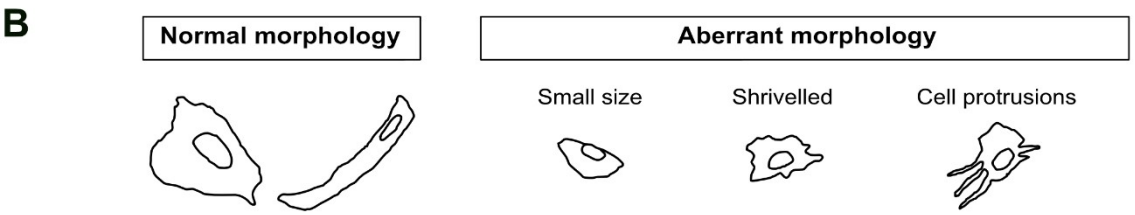
B
Normal morphology
Aberrant morphology
Small size
Shrivelled
Cell protrusions

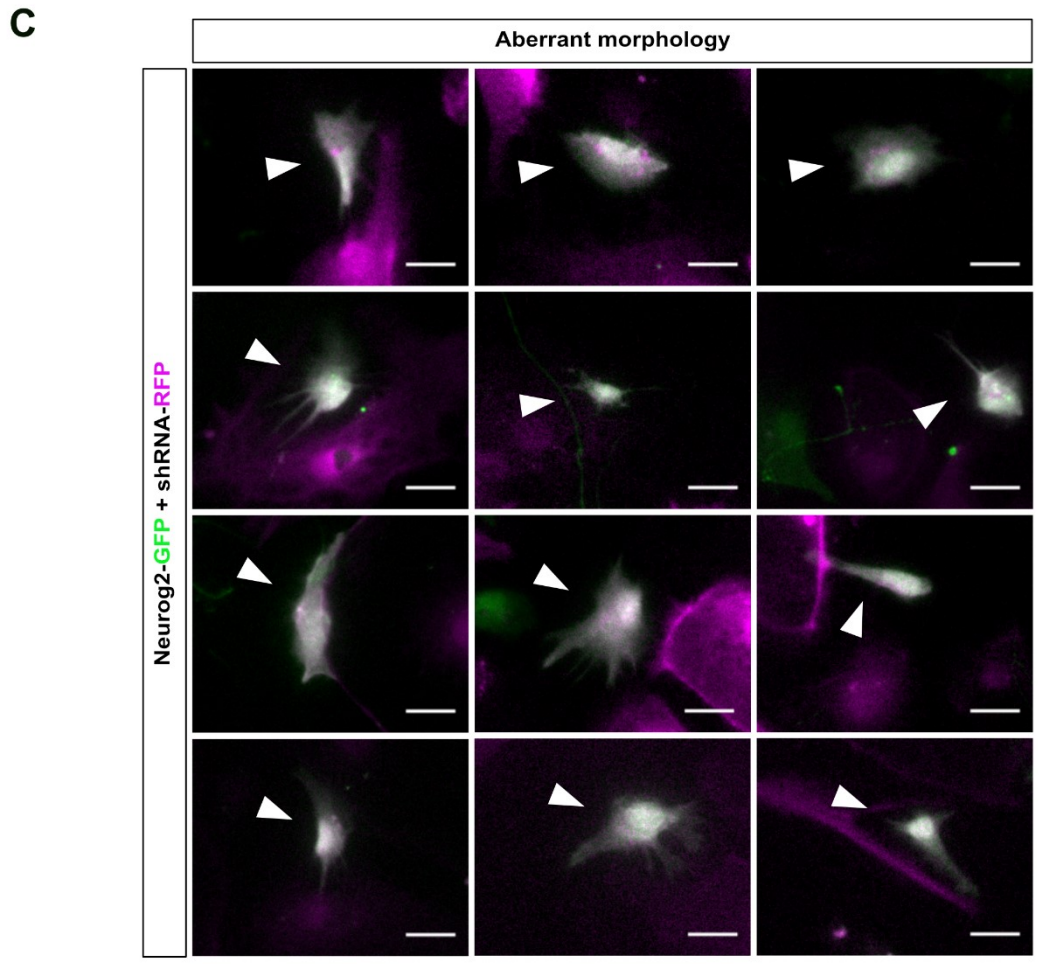
C
Aberrant morphology
Neurog2-GFP + shRNA-RFP

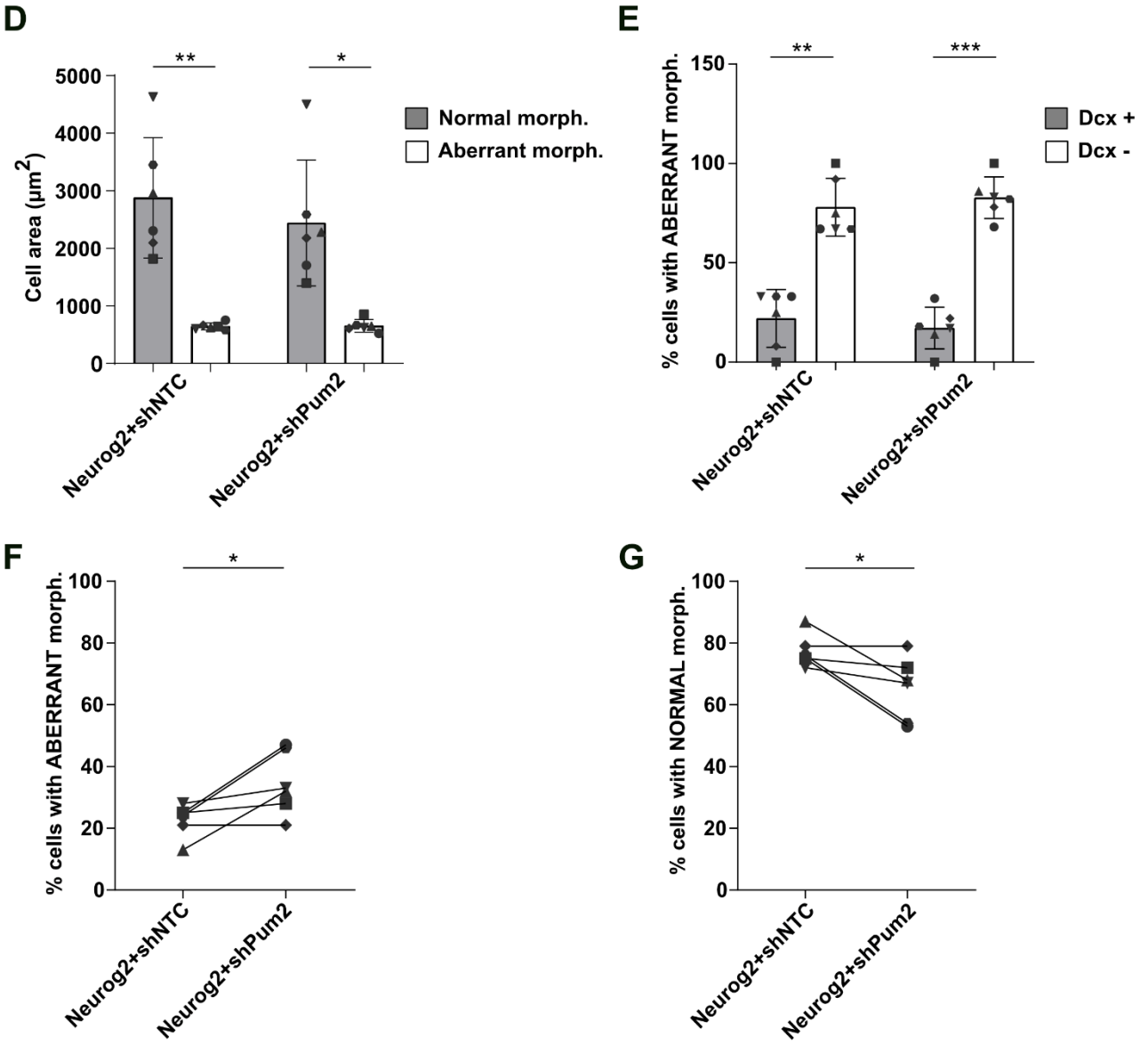

Figure 19: Aberrant non-reprogrammed cells increase upon Pum2 depletion

(A) Schematic drawings depicting astrocyte morphology and elongated shape as reference for normal morphology (left). Representative examples of GFP and RFP fluorescence merged images of Neurog2-GFP and shRNA-RFP-positive cells (right). White arrowheads indicate examples of cells with normal morphology. Scale bars: 20 µm. **(B)** Schematic drawings depicting normal or aberrant morphology identified by small size, shrivelled shape and cell protrusions. **(C)** Representative examples of GFP and RFP fluorescence merged images of Neurog2- and shRNA-RFP-positive cells. White arrowheads indicate examples of cells with aberrant morphology. Scale bars: 20 µm. **(D)** Bar plot displaying area of cells (μm^2) with normal and aberrant morphology under control (shNTC) or Pum2-depleted conditions (shPum2). **(E)** Bar plot displaying percentage of cells with aberrant morphology expressing Dcx under control (shNTC) or Pum2-depleted conditions (shPum2). **(F,G)** Dot plot displaying percentage of cells with aberrant **(F)** and normal **(G)** morphology under control (shNTC) or Pum2-depleted conditions (shPum2). **(D,E,F,G)** Grey symbols indicate independent biological replicates (n = 6). Mean and Standard Deviation are shown in **D**,**E**. Asterisks represent *p*-values obtained by paired Student's t-test (*$p < 0.05$, **$p < 0.01$, ***$p < 0.001$, ns ≥ 0.05).

3.9 Identification of genes commonly regulated by Neurog2 and Ascl1 that are potential Pum2 or Stau2 targets during neuronal reprogramming

RBPs can regulate complex pathways involved in neuronal development and neuronal homeostasis (Schieweck et al., 2021a). Indeed, in addition to its function in post-mitotic neurons, Pum2 has been shown to be involved in crucial aspects of embryonic neurogenesis (Vessey et al., 2012; Zahr et al., 2018). In the early stages of direct neuronal reprogramming, rapid and dynamic transcriptional changes occur to ensure the cell fate conversion (Masserdotti et al., 2015). It is also known that the forced expression of different key neurogenic TFs, such as Neurog2 and Ascl1, induces distinct transcriptional programs with only a small subset of commonly regulated targets, some of which play crucial roles in mediating neuronal reprogramming (Masserdotti et al., 2015). To gain further insight into the involvement of Pum2 in neuronal reprogramming, I compared the common Neurog2-Ascl1 downstream targets within the first 24h of the reprogramming process (Masserdotti et al., 2015) with Pum2 mRNA targets from E12 mouse cortex, obtained from previously published data (Zahr et al., 2018). Interestingly, cross-referencing the two datasets revealed that 4 genes commonly regulated by Neurog2 and Ascl1 were also targets of Pum2 during mouse embryonic corticogenesis (**Figure 20A**). Of note, the TF Prox1, a homologue of the *Drosophila* Prospero protein and known Stau target, has been described as an essential downstream effector in astrocyte-to-neuron reprogramming (Li et al., 1997; Masserdotti et al., 2015; Vessey et al., 2012). On the other hand, Ankyrin repeat and SAM domain-containing protein 1 (Anks1), Down syndrome cell adhesion molecule-like protein 1 (DscamI1) and Slit homolog 1 protein (Slit1) have important neurodevelopmental functions, including axon guidance and neuronal remodelling (Fuerst et al., 2009; Gonda et al., 2020; Sachse et al., 2019; Shin et al., 2007; Southall and Brand, 2009). These findings provide additional support for the involvement of Pum2 in neuronal reprogramming and suggest a role in implementing post-transcriptional control on specific neurogenic mRNA targets. To compare the potential targets of different RBPs during the reprogramming process, I performed the same analysis for Stau2 as well. Indeed, similar to Pum2, also Stau2 has been shown to make a crucial contribution to cell fate specification during embryonic neurogenesis (Chowdhury et al., 2021; Kusek et al., 2012; Vessey et al., 2012). I performed a comparative analysis of the common Neurog2-Ascl1 downstream targets within the first 24h of the reprogramming process (Masserdotti et al., 2015) with Stau2 mRNA targets from different time points during mouse embryonic corticogenesis, derived from previously published data (Chowdhury et al., 2021). The analysis revealed that a subset of 13 genes,

which are commonly regulated by Neurog2 and Ascl1, were also targets of Stau2 during corticogenesis (**Figure 20B**). Some of these common genes encode factors that are highly associated with the regulation of neurogenesis, such as Hes5, Hes6 and Trnp1(Gratton et al., 2003; Hatakeyama et al., 2004; Vaid and Huttner, 2020). Other common genes encode proteins involved in axon guidance, synaptic formation and plasticity, such as the cytoplasmic/membrane factors Semaphorin-5A (Sema5a), Cell adhesion molecule 3 (Cadm3), Alpha-synuclein (Snca) (Biederer et al., 2002; Cheng et al., 2011; Kantor et al., 2004; Niederkofler et al., 2010). Notably, only two potential targets (*Slit1* and *Dscaml1*) are shared between Pum2 and Stau2. This result provides additional support that Stau2 may also play a role during neuronal reprogramming, perhaps with a different contribution than Pum2. Future studies are clearly needed to consolidate whether this is indeed the case and which relevant transcripts are regulated by Pum2 and Stau2 during direct astrocyte-to-neuron reprogramming.

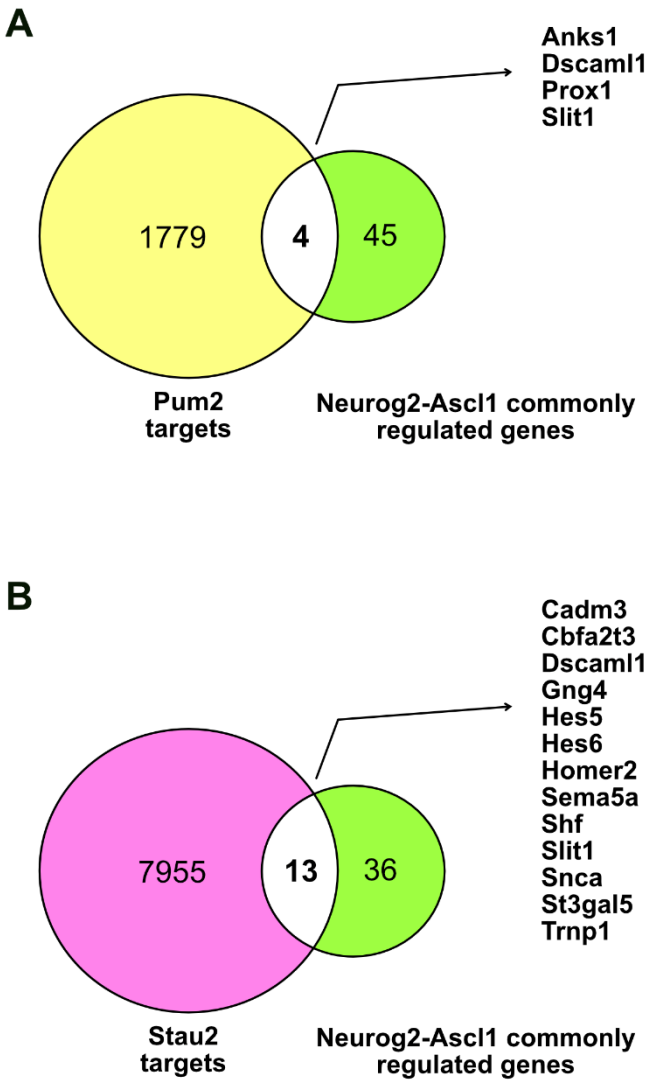

Figure 20: Several genes regulated during reprogramming are Pum2 or Stau2 target mRNAs during mouse embryonic corticogenesis

(A) Venn diagram of Pum2 mRNA targets in embryonic corticogenesis (Zahr et al., 2018) and genes commonly regulated by Neurog2 and Ascl1 at 24h of reprogramming (Masserdotti et al., 2015). Arrow indicates the 4 shared genes **(B)** Venn diagram of Stau2 mRNA targets in embryonic corticogenesis (Chowdhury et al., 2021) and genes commonly regulated by Neurog2 and Ascl1 at 24h of reprogramming (Masserdotti et al., 2015). Arrow indicates the 13 shared genes.

4 DISCUSSION

4.1 The regulatory potential of RBPs in neuronal reprogramming

Over the past two decades, significant progress has been made in unravelling the intricacies of the transcriptional networks, epigenetic events, key signalling pathways and metabolic hurdles underlying cell fate conversion in the context of direct neuronal reprogramming (Bocchi et al., 2022). While these efforts have undoubtedly advanced the knowledge in the field, there is a notable gap in our understanding of how the downstream mechanisms of post-transcriptional gene regulation contribute to cell fate conversion. In addition to the central role of lineage-specific TFs, evidence for the impact of post-transcriptional mechanisms mediated by regulatory RNAs and RBPs in promoting cell fate conversion during reprogramming has been reported. For example, neuron-specific miRNAs, such as miR-9/9* and miR-124, have been used alongside TFs to generate functional neurons from human fibroblasts (Yoo et al., 2011). In this context, the miRNA-dependent silencing of mRNA translation orchestrates the repression of negative neuronal fate effectors, thereby promoting the establishment of neuronal identity (Lee et al., 2018; Yoo et al., 2011). Furthermore, suppression of the RBP Ptbp1, described as repressor of neuron-specific splicing, can induce the conversion of multiple cell types into neuronal-like cells, including the direct reprogramming of fibroblasts into functional neurons (Spellman and Smith, 2006; Xue et al., 2013). In this context, Ptbp1 was reported to be extensively involved in modulating miRNA targeting in addition to its role in alternative splicing (Xue et al., 2013). Despite this, our understanding about specific mechanisms that exert post-transcriptional regulation during neuronal reprogramming remains limited. It is widely accepted that post-transcriptional gene regulation, orchestrated by RBPs, provides sophisticated mechanisms to control neuronal development and functionality (Schieweck et al., 2021a). In addition to their well-studied role in neuronal transmission and synaptic plasticity in mature neurons, RBPs have been identified as key players in embryonic neurogenesis. In fact, beyond the intricate transcriptional events, the dynamic activity of RBPs is of great importance for the spatiotemporally controlled protein expression required during progressive neurogenesis (Parra and Johnston, 2022; Schieweck et al., 2021a). In this context, Pum2 and Stau2 are of special interest due to their emerged pivotal roles as cell fate regulators in mammalian cortical development (Chowdhury et al., 2021; Kusek et al., 2012; Vessey et al., 2012; Zahr et al., 2018). Stau2 and Pum2 were first reported to form an RNA complex that regulates localisation and expression of proneurogenic mRNAs during RGCs division (Vessey et al.,

2012). In this context, the asymmetric distribution of Stau2 and Pum2-containing RNA complex has a major impact on fate commitment by determining stem cell maintenance versus neuronal differentiation (Chowdhury et al., 2021; Kusek et al., 2012; Vessey et al., 2012). Other important studies have reported that Pum2 is required for NSCs proliferation, survival and differentiation in the hippocampus as well as for the temporal specification of different neuronal subtypes in the developing cortex (Zahr et al., 2018; Zhang et al., 2017). The intriguing role of Pum2 and Stau2 in the context of neurogenesis makes them ideal candidates to study the role of RBPs in the process of direct fate conversion of non-neuronal cells into neurons.

4.2 Pum2 and Stau2 contribute differently to direct neuronal reprogramming

In neurons, RBPs associate with mRNAs to form RNPs (also often referred to as RNA granules) and influence many aspects of RNA metabolism, including stability, localisation, translation control and local protein synthesis, ultimately contributing to neuronal homeostasis (Doyle and Kiebler, 2011; Kiebler and Bassell, 2006; Schieweck et al., 2021a). Both Pum2 and Stau2 form RNPs that localise in the somatodendritic compartment of hippocampal neurons (Duchaine et al., 2002; Vessey et al., 2006). Interestingly, Pum2 and Stau2 consistently show a distribution in RNA granules and a predominant cytoplasmic localisation also in the initial reprogramming population, cortical astrocytes, and in the successfully induced neurons. In addition, while Pum2 and Stau2 particles do not colocalise significantly in the cytoplasmic compartment of astrocytes, a remarkable degree of colocalisation was observed in the neuronal processes of induced neurons after reprogramming. This observation raises the intriguing possibility of a functional interaction between these two RBPs during reprogramming. This is consistent with previous findings that Pum2 colocalises with Stau2-RNPs in distal dendrites of mature hippocampal neurons, supporting the hypothesis that Stau2-mediated RNA transport within neuronal dendrites is closely linked to Pum2-mediated translational repression (Dahm and Kiebler, 2005; Fritzsche et al., 2013). As mentioned above, Pum2 and Stau2 interaction has also been reported in neuronal precursor cells where they contribute to cell fate determination during cortical development (Vessey et al., 2012). Notably, their conserved interaction also extends to conserved roles in different cellular contexts. Indeed, Stau2 and Pum2 have been implicated in RNA localisation and translation regulation, respectively, in both embryonic corticogenesis and post-mitotic neurons (Vessey et al., 2012; Zahr et al., 2018). Therefore, it is likely that Pum2 and Stau2 maintain a conserved interaction and function also in direct neuronal reprogramming. In fact, their involvement in critical aspects of RNA dynamics and

regulation in different cellular states indicates their versatility and importance in orchestrating key cellular events, which could extend to the complex process of direct cell fate conversion. The hypothesis that Pum2 and Stau2 are involved in neuronal reprogramming is experimentally supported by their dynamic protein expression patterns along critical time points during astrocyte-to-neuron reprogramming (3, 5 and 7 DPI). Interestingly, both Pum2 and Stau2 protein levels are increased at later stages of the reprogramming process (5-7 DPI) rather than at early stages, albeit in two different categories of cells. Indeed, while Pum2 protein levels are increased in cells undergoing reprogramming (at 5 DPI), that have not yet successfully converted, Stau2 protein levels are prominently increased in successfully induced neurons (at 7 DPI). Also, in contrast to the selective increase observed in induced neurons, a decrease in Stau2 protein levels was detected in non-reprogrammed cells (still in fate transition or failed to be reprogrammed) at both early and late stages (3 and 7 DPI). The different protein expression patterns observed for Pum2 and Stau2 during reprogramming suggest that they are likely to exert their functions in different aspects of cell fate conversion and possibly through different regulatory roles. This would be consistent with the different roles that Pum2 and Stau2 play during neuronal development and in mature neurons, with Pum2 involved in translation regulation and Stau2 in RNA localisation and stability (Heraud-Farlow et al., 2013; Kiebler et al., 1999; Kusek et al., 2012; Schieweck et al., 2021b; Vessey et al., 2012; Zahr et al., 2018). The important role of Pum2 and Stau2 in neuronal reprogramming is confirmed by the finding that depletion of either Pum2 or Stau2 leads to a reduction in reprogramming efficiency. Interestingly, Pum2 and Stau2 don’t contribute equally to successful cell fate conversion, with Pum2 having a greater effect than Stau2. Although they have different effects on astrocyte-to-neuron conversion, these results suggest that both Pum2 and Stau2 play a pivotal role in regulating cellular plasticity during cell fate decision. In this scenario, Pum2 and Stau2 seem to shape transcriptional changes that are induced by TFs to induce cell fate commitment, as previously shown during neurogenesis (Chowdhury et al., 2021; Kusek et al., 2012; Vessey et al., 2012; Zahr et al., 2018; Zhang et al., 2017). Although the mechanisms guiding reprogramming and embryonic neurogenesis are fairly distinct (Masserdotti et al., 2016), it is more than plausible that Pum2- and Stau2-dependent cellular plasticity critically contributes to both processes. Furthermore, as already suggested by the different protein expression patterns observed during reprogramming, the divergent effects of Pum2 and Stau2 on successful fate conversion further support the hypothesis that they play non-redundant roles in reprogramming. It is interesting to note that Pum2 depletion had no significant effect on cell survival, indicating

that cell death is not the major contributor to the observed reduced reprogramming efficiency. This is in contrast to previously published findings showing increased cell death associated with reduced hippocampal neurogenesis upon Pum1 and Pum2 depletion (Zhang et al., 2017). This may indicate a compensatory effect of Pum1, or, alternatively, a context-specific effect of Pum2 knockdown. Furthermore, my results show that the reduced reprogramming efficiency upon Pum2 depletion is primarily due to a decrease in the number of induced neurons, accompanied by a slight increase in the population of cells that did not successfully undergo reprogramming. These observations highlight the key role of Pum2 in orchestrating critical aspects of the reprogramming process necessary for the accurate establishment of neuronal fate. Supportive for this notion is the evidence showing that Pum2 is required for the differentiation of neural progenitors into neurons during hippocampal neurogenesis (Zhang et al., 2017).

4.3 A late function of Pum2 influences successful neuronal reprogramming

Reprogramming is a gradual process, in which dynamic and hierarchical regulation of gene expression support the distinct maturational steps that underlie the change in cell identity (Heinrich et al., 2011; Masserdotti et al., 2015). Analysis of the transcriptional programs elicited by proneural TFs, such as Neurog2, revealed substantial transcriptome changes occurring at early stages of astrocyte-to-neuron reprogramming (Masserdotti et al., 2015). My data argue for a role of Pum2 at later stages of the reprogramming rather than at early stages, when the initial transcriptional changes associated with neuronal fate have already been implemented. This scenario is supported by the finding that the decrease in reprogramming efficiency observed after 7 days of reprogramming in Pum2-depleted conditions, did not yet manifest on day 5. This hypothesis was further tested by depleting Pum2 two days after the overexpression of the TF-driving reprogramming, Neurog2. Indeed, the early transcriptional changes mediated by Neurog2 occur during the first 48h of neuronal reprogramming (Masserdotti et al., 2015). Surprisingly, interfering with Pum2 expression upon Neurog2 overexpression reduced the reprogramming efficiency similar to the continuous loss of Pum2 observed previously. Thus, these results clearly indicate that Pum2 is likely to exert its function during the late stages of the conversion process. Moreover, the alleged involvement of Pum2 at later stages of reprogramming echoes its protein expression dynamics along the conversion process, where increased protein levels were observed 5 days after the onset of the reprogramming. Regarding the potential function of Pum2 at later stages of reprogramming, the examination of its impact on successfully induced neurons did not reveal any discernible effects on neuronal integrity, polarity or structural complexity. The

only notable effect was a slight reduction in the soma size of the induced neurons in the absence of Pum2. This is consistent with recent research highlighting Pum2 as a regulator of neuronal growth (Schieweck et al., 2021c). While it's conceivable that Pum2 may have an additional independent role as a growth factor for induced neurons, it seems plausible that Pum2 does not significantly contribute to define the establishment of proper neuronal morphology of successfully converted neurons. It is therefore reasonable to hypothesise that Pum2 might be involved in the mechanisms for stabilising and maintaining the neuronal fate acquired by reprogrammed cells.

4.3.1 Pum2 as a potential contributor to the irreversible commitment of reprogrammed cells to neuronal fate

The results discussed so far are compatible with a working hypothesis that Pum2 is involved during the late stages of neuronal reprogramming to ensure the irreversible commitment of reprogrammed cells to neuronal fate. In the field of reprogramming of somatic cells into iPSCs, the irreversible commitment to the acquired pluripotent state has been associated with a crucial point in the reprogramming process called "point of no return" (Nagy and Nagy, 2010). This has been defined as the time point of reprogramming beyond which the cells can't longer revert to their original state (Nagy and Nagy, 2010). In this context, distinct factors have been reported to be required to maintain the acquired pluripotent state (Samavarchi-Tehrani et al., 2010). While the concept of a definitive "point of no return" in the field of direct neuronal reprogramming remains still somewhat speculative, it is plausible that distinct signalling networks are required to stabilise the newly acquired neuronal identity. This view is supported by the evidence that although Ascl1 can initiate direct fibroblast-to-neuron reprogramming, reliance on this TF alone is inefficient in maintaining converted cells in the neuronal lineage. Therefore, the authors suggested that intermediate stages of cell fate conversion are unstable and that addiction factors are necessary to guide cells towards a permanent acquisition of neuronal identity. This prevents them from reverting to their original state or straying into alternative cell fates (Treutlein et al., 2016). My hypothesis is that Pum2 takes part to the molecular mechanisms that are crucial for stabilising neuronal fate in astrocyte-to-neuron reprogramming. In this scenario, the overexpression of Neurog2 induces the successful conversion of astrocytes into young developing neurons by day 5, which I assume are not yet irreversibly committed. The presence of Pum2 contributes to the irreversible commitment of young neurons by day 7, allowing them to proceed with maturation and become functional neurons. In the absence of Pum2, the conversion process proceeds normally until day 5, resulting in the proper generation of young neurons. Indeed,

at this time point of conversion process, a proper reprogramming efficiency was detected even in the absence of Pum2. However, in the absence of Pum2, I hypothesise that the newly generated young neurons are not irreversibly committed to a neuronal fate, thereby losing their neuronal identity and reverting to their original astrocyte identity **(Figure 21)**. Thus, the young neurons observed at day 5 do not reach the fully committed stage by day 7. This could explain the observed reduced presence of induced neurons at day 7 in the absence of Pum2 without a concomitant increase in cell death events. However, it is important to emphasise that this working model depends on the observation of a substantial downregulation of Pum2 in young neurons at day 5, a critical aspect that requires further investigation. Interestingly, in addition to the reduced generation of neurons observed in the absence of Pum2, an increased presence of non-reprogrammed cells with atypical morphology was also observed. These aberrant morphological phenotypes appear clearly to be distinct from the initial astrocyte morphology or the elongated transitional shape typical of cells undergoing reprogramming (Gascon et al., 2016; Heinrich et al., 2011). Hence, it is conceivable that these non-reprogrammed cells with such unique phenotypes do not simply represent astrocytes that failed to progress towards a neuronal fate. Instead, they may represent cells in a transient state on their way back to the astrocyte identity **(Figure 21)**. Notably, the majority of these cells do not express the immature neuronal marker Dcx, suggesting a possible initial expression followed by subsequent loss of this marker during their transitional phase. However, it is utmost importance to investigate whether these non-reprogrammed cells are positive for astrocytic markers such as GFAP. Indeed, the hypothesis that these cells are reverting to their original astrocytic identity would be supported by the fact that they are GFAP positive. It is also possible that, irrespective of the expression of astrocytic markers, these non-reprogrammed cells may never fully revert to an astrocytic identity, potentially facing cell death while stuck in this transient state. While qualitative examination of DAPI staining of these non-reprogrammed cells on day 7 did not reveal any sign of imminent cell death, it still remains possible that observation of these cells a few days later in the reprogramming process may reveal subsequent of cell death events.

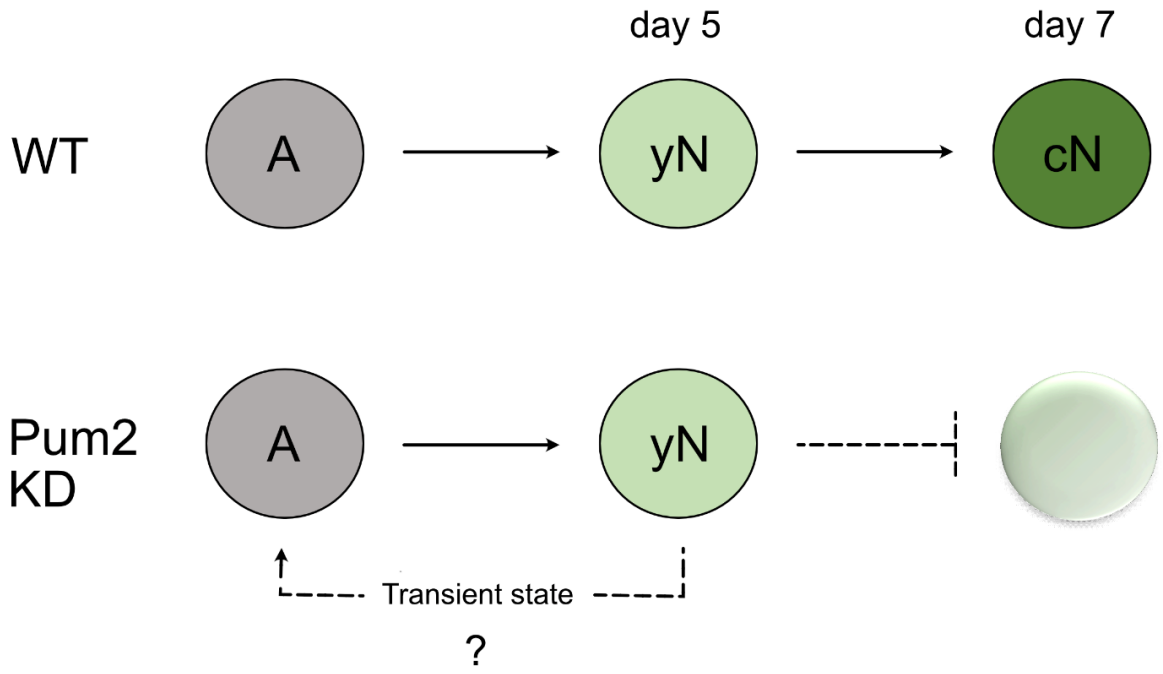

A = Astrocyte
yN = young developing Neuron
cN = committed Neuron

Figure 21: Pum2 is required for irreversible commitment of reprogrammed cells to neuronal fate

Forced expression of Neurog2 can effectively convert astrocytes into young developing neurons (yN) within 5 days. The yN must develop into irreversibly committed neurons (cN) by day 7 in order to continue their maturation and become functional neurons (upper panel). In the absence of Pum2, a proper conversion of astrocytes into yN can be still detected on day 5. However, the absence of Pum2 seems to interfere with the critical process of irreversible commitment. As a result, yN fail to progress to the stage of fully committed neurons by day 7 (lower panel). As a consequence of this failure in achieving irreversible neuronal fate commitment, the yN lose their neuronal identity and revert to their original astrocyte state. During this transition, it is conceivable that the cells could enter transient and undefined states, representing a phase of uncertainty and instability in their cellular identity.

4.4 Conclusions and future perspectives

By shedding new light on the implications of RBP-mediated post-transcriptional gene regulation in astrocyte-to-neuron reprogramming, the data presented in this thesis provide sophisticated novel molecular and mechanistic insight into the underlying mechanisms of neuronal lineage conversion. While not ignoring the potential role of Stau2, my results highlight the pivotal role of Pum2 due to its more pronounced and robust effect on successful cell fate conversion. In this regard, my results provide a novel perspective that positions Pum2 as key player in guiding converted cells towards a permanent acquisition of neuronal identity. Furthermore, by investigating the potential role of Pum2 in the later stages of reprogramming, my data shed light on another critical phase of cell fate conversion that has not yet been explored in the field. Although my data clearly indicate a late-stage role for Pum2, a complementary approach would be helpful to confirm this evidence. In this case, I propose to downregulate Pum2 prior to the initiation of Neurog2-driven reprogramming, followed by a subsequent rescue of Pum2 expression three days after reprogramming induction. This would allow me to specifically reduce Pum2 expression during the initial phase of cell fate conversion in order to confirm that it does not play key roles at this stage. In addition, further studies are clearly necessary to confirm the proposed hypothesis that Pum2 is required for the irreversible commitment of converted cells to a neuronal fate. In this context, the use of single-cell tracking with time-lapse videomicroscopy appears to be the preferred approach. Indeed, time-lapse analysis has already been shown to be extremely valuable in the context of astrocyte-to-neuron reprogramming (Gascon et al., 2016; Heinrich et al., 2011). By directly visualising the sequential progression of neuronal reprogramming events in the absence of Pum2, this approach would undoubtedly reveal the reason for the reduced number of induced neurons observed and elucidate the origin and the ultimate fate of the aforementioned non-reprogrammed cells that display distinctly aberrant phenotype. Importantly, by confirming the role of Pum2 as a key factor in the irreversible commitment of induced neurons, this working model would also substantiate the critical “point of no return” hypothesis in the field of neuronal reprogramming as described above. Moreover, future studies should focus on unravelling the relevant targets of Pum2 and the underlying mechanisms of post-transcriptional regulation by which Pum2 operates in this critical phase of reprogramming. An insightful cross-reference analysis presented in my data revealed that four genes commonly regulated by Neurog2 and Ascl1 during early stages of reprogramming are also targets of Pum2 during mouse embryonic corticogenesis (Masserdotti et al., 2015; Zahr et al., 2018). Among these, *Prox1* is a critical regulator of

neural development by promoting neural stem cell differentiation, while *Anks1*, *DscamI1* and *Slit1* play roles in other crucial neurodevelopmental processes, such as axon guidance and neuronal remodelling (Fuerst et al., 2009; Gonda et al., 2020; Sachse et al., 2019; Shin et al., 2007; Southall and Brand, 2009). Of particular interest is the potential target *Prox1*, whose knockdown during Neurog2-induced reprogramming resulted in reduced neuron generation, highlighting its crucial contribution to cell fate conversion (Masserdotti et al., 2015). Therefore, a logical and promising starting point would be to validate whether these neurogenic mRNAs are directly regulated by Pum2 during the process of neuronal reprogramming. However, given the low level of overlap between the genes regulated by Neurog2 during reprogramming and in the developing cerebral cortex (Gohlke et al., 2008; Masserdotti et al., 2015), I expect Pum2 to regulate a substantially broader set of mRNA targets than those identified in the cross-reference analysis. Consequently, it is crucial to elucidate how Pum2 regulates the metabolism of these mRNA targets. It is now clear that RBPs have a broad post-transcriptional regulatory potential and they are required for multiple pathways in both embryonic neurogenesis and mature neurons (Schieweck et al., 2021a). As described above, Pum acts as a regulator of RNA translation in many organisms and different cellular contexts (Schieweck et al., 2021a). The reported role of Pum2 in translational repression during neurogenesis raises the possibility of a conserved role in the context of neuronal reprogramming (Zahr et al., 2018; Zhang et al., 2017). However, several other possible mechanisms of how Pum2 regulates protein expression have been reported, including RNA stability and transport (Goldstrohm et al., 2007; Hotz and Nelson, 2017; Martinez et al., 2019). These diverse functionalities leave room for a wider spectrum of potential post-transcriptional regulatory mechanisms to come into play during cell fate conversion. Furthermore, my data suggest that it is worthwhile to further investigate also the molecular mechanisms underlying the contribution of Stau2 to reprogramming. Indeed, Stau2, although less pronounced than Pum2, showed an impact on successful fate conversion and a distinct protein expression pattern along reprogramming. While Stau2 has primarily been recognised as a critical regulator of RNA localisation in both mature neurons and embryonic neurogenesis, there is also evidence that Stau2 is involved in the stabilisation of target mRNAs (Heraud-Farlow et al., 2013; Kiebler et al., 1999; Kusek et al., 2012; Vessey et al., 2012). It would be interesting to ascertain whether Stau2 has a conserved role in RNA localisation during reprogramming or whether it is engaged in additional mechanisms as well. This knowledge will also allow us to determine whether the different contributions of Pum2 and Stau2 to successful cell fate conversion reflect their

distinct roles in the process, as previously hypothesised based on my research findings. In my opinion, it will be essential to elucidate the set of mRNA targets regulated by Stau2 during reprogramming. Again, the best approach would be to start by validating candidate targets derived by cross-referencing the datasets of genes commonly regulated by Neurog2 and Ascl1 during reprogramming and Stau2 targets during mouse embryonic corticogenesis (Chowdhury et al., 2021; Masserdotti et al., 2015). Here, a subset of 13 genes, which are commonly regulated by Neurog2 and Ascl1, were also targets of Stau2 during corticogenesis. Interestingly, similar to Pum2, some of these genes encode transcription factors/co-factors that are primarily associated with the early stages of neurogenesis, *e.g.* Hes5, Hes6 and Trnp1 (Gratton et al., 2003; Hatakeyama et al., 2004; Vaid and Huttner, 2020). In contrast, others encode cytoplasmic/membrane factors that are involved in later developmental processes such as axon guidance, synapse formation and plasticity, *e.g.* Sema5a, Cadm3 and Snca (Biederer et al., 2002; Cheng et al., 2011; Kantor et al., 2004; Niederkofler et al., 2010). Notably, similar to the Pum2 candidate target *Prox1*, *Hes6* has also been reported to contribute critically to neuronal conversion efficiency during Neurog2-induced reprogramming (Masserdotti et al., 2015). In addition to elucidating Pum2 and Stau2 relevant targets during neuronal reprogramming, it is equally important to investigate whether these two RBPs share a common set of targets in this context. For example, the cross-reference analysis mentioned above revealed two potential targets, Slit1 and Dscaml1 that are shared by Pum2 and Stau2. In mature neurons, a significant overlap between their respective targets has been reported, further supporting the hypothesis of a functional interaction between them (Schieweck et al., 2021b). This observation raises the intriguing possibility of a potential functional interaction based on the common regulation of a conserved set of targets in the context of reprogramming. This is consistent with the substantial Pum2-Stau2 colocalisation in induced neurons reported in my thesis. Furthermore, special emphasis should be also put on potential interactors of Pum2 and Stau2. RBPs form RNPs that are highly heterogeneous not only in mRNAs but also in protein composition. The highly dynamic and complex interplay between different RBPs is thought to be crucial for the regulation of neuronal homeostasis and development (Schieweck et al., 2021a). For example, FMRP and DDX1 are potential interactors that are certainly worth validating. Indeed, FMRP is a post-transcriptional regulator with important roles in neurogenesis that has been reported to interact with Pum2 during hippocampal neurogenesis (Guo et al., 2011; Luo et al., 2010; Saffary and Xie, 2011; Zhang et al., 2017). FMRP was also found associated with Stau2-RNP in mature neurons (Fritzsche et al., 2013).

On the other hand, DDX1 has been reported as a critical component of the Stau2 and Pum2-containing RNA complex in RGCs during cortical development (Vessey et al., 2012). It is now commonly accepted that several cell types other than astrocytes can efficiently be converted into neurons (Masserdotti et al., 2016). As we move forward, it is important to focus future research efforts on investigating the role of RBPs, such as Pum2 and Stau2, in cell lineage conversions other than the mentioned astrocyte-to-neuron paradigm. For example, investigating the role of Pum2 and Stau2 in fibroblasts-to-neuron reprogramming, would be a valid starting point to elucidate whether these RBPs exert similar or different contributions in different reprogramming contexts. This knowledge would also broaden the network of regulatory factors involved in neuronal reprogramming from different cell sources. Furthermore, in the field of neuronal reprogramming, the transition from *in vitro* to *in vivo* applications is an essential step towards the ultimate goal of using direct reprogramming of local non-neuronal cells as a therapeutic strategy to restore lost neurons in the brain (Barker et al., 2018). Given the promising results observed *in vitro* regarding the involvement of RBPs in astrocyte-to-neuron reprogramming, it is of utmost importance to direct future studies to validate their role in reprogramming *in vivo* as well, using the appropriate mouse models. This transition would not only confirm the significance of post-transcriptional control mechanisms in reprogramming, but would also raise the exciting prospect of Pum2 (and possibly Stau2) as potential targets for enhancing effective cell fate conversion, a development with huge implications for therapeutic application.

REFERENCES

Barker, R.A., M. Gotz, and M. Parmar. 2018. New approaches for brain repair-from rescue to reprogramming. *Nature*. 557:329-334.

Bartel, D.P. 2004. MicroRNAs: genomics, biogenesis, mechanism, and function. *Cell*. 116:281-297.

Bauer, K.E., I. Segura, I. Gaspar, V. Scheuss, C. Illig, G. Ammer, S. Hutten, E. Basyuk, S.M. Fernandez-Moya, J. Ehses, E. Bertrand, and M.A. Kiebler. 2019. Live cell imaging reveals 3'-UTR dependent mRNA sorting to synapses. *Nat Commun*. 10:3178.

Berninger, B., M.R. Costa, U. Koch, T. Schroeder, B. Sutor, B. Grothe, and M. Gotz. 2007. Functional properties of neurons derived from in vitro reprogrammed postnatal astroglia. *J Neurosci*. 27:8654-8664.

Bertrand, N., D.S. Castro, and F. Guillemot. 2002. Proneural genes and the specification of neural cell types. *Nat Rev Neurosci*. 3:517-530.

Biederer, T., Y. Sara, M. Mozhayeva, D. Atasoy, X. Liu, E.T. Kavalali, and T.C. Sudhof. 2002. SynCAM, a synaptic adhesion molecule that drives synapse assembly. *Science*. 297:1525-1531.

Bocchi, R., G. Masserdotti, and M. Gotz. 2022. Direct neuronal reprogramming: Fast forward from new concepts toward therapeutic approaches. *Neuron*. 110:366-393.

Boczonadi, V., J.S. Muller, A. Pyle, J. Munkley, T. Dor, J. Quartararo, I. Ferrero, V. Karcagi, M. Giunta, T. Polvikoski, D. Birchall, A. Princzinger, Y. Cinnamon, S. Lutzkendorf, H. Piko, M. Reza, L. Florez, M. Santibanez-Koref, H. Griffin, M. Schuelke, O. Elpeleg, L. Kalaydjieva, H. Lochmuller, D.J. Elliott, P.F. Chinnery, S. Edvardson, and R. Horvath. 2014. EXOSC8 mutations alter mRNA metabolism and cause hypomyelination with spinal muscular atrophy and cerebellar hypoplasia. *Nat Commun*. 5:4287.

Breschi, A., M. Munoz-Aguirre, V. Wucher, C.A. Davis, D. Garrido-Martin, S. Djebali, J. Gillis, D.D. Pervouchine, A. Vlasova, A. Dobin, C. Zaleski, J. Drenkow, C. Danyko, A. Scavelli, F. Reverter, M.P. Snyder, T.R. Gingeras, and R. Guigo. 2020. A limited set of transcriptional programs define major cell types. *Genome Res*. 30:1047-1059.

Broadus, J., S. Fuerstenberg, and C.Q. Doe. 1998. Staufen-dependent localization of prospero mRNA contributes to neuroblast daughter-cell fate. *Nature*. 391:792-795.

Buffo, A., M.R. Vosko, D. Erturk, G.F. Hamann, M. Jucker, D. Rowitch, and M. Gotz. 2005. Expression pattern of the transcription factor Olig2 in response to brain injuries: implications for neuronal repair. *Proc Natl Acad Sci U S A*. 102:18183-18188.

Buxbaum, A.R., G. Haimovich, and R.H. Singer. 2015. In the right place at the right time: visualizing and understanding mRNA localization. *Nat Rev Mol Cell Biol*. 16:95-109.

Buxbaum, A.R., B. Wu, and R.H. Singer. 2014. Single beta-actin mRNA detection in neurons reveals a mechanism for regulating its translatability. *Science*. 343:419-422.

Cao, Q., K. Padmanabhan, and J.D. Richter. 2010. Pumilio 2 controls translation by competing with eIF4E for 7-methyl guanosine cap recognition. *RNA*. 16:221-227.

Chanda, S., C.E. Ang, J. Davila, C. Pak, M. Mall, Q.Y. Lee, H. Ahlenius, S.W. Jung, T.C. Sudhof, and M. Wernig. 2014. Generation of induced neuronal cells by the single reprogramming factor ASCL1. *Stem Cell Reports*. 3:282-296.

Chen, E., M.R. Sharma, X. Shi, R.K. Agrawal, and S. Joseph. 2014. Fragile X mental retardation protein regulates translation by binding directly to the ribosome. *Mol Cell*. 54:407-417.

Chen, J., L. Huang, Y. Yang, W. Xu, Q. Qin, R. Qin, X. Liang, X. Lai, X. Huang, M. Xie, and L. Chen. 2023. Somatic Cell Reprogramming for Nervous System Diseases: Techniques, Mechanisms, Potential Applications, and Challenges. *Brain Sci*. 13:524.

Chen, Y.C., N.X. Ma, Z.F. Pei, Z. Wu, F.H. Do-Monte, S. Keefe, E. Yellin, M.S. Chen, J.C. Yin, G. Lee, A. Minier-Toribio, Y. Hu, Y.T. Bai, K. Lee, G.J. Quirk, and G. Chen. 2020. A NeuroD1 AAV-Based Gene Therapy for Functional Brain Repair after Ischemic Injury through In Vivo Astrocyte-to-Neuron Conversion. *Mol Ther*. 28:217-234.

Cheng, F., G. Vivacqua, and S. Yu. 2011. The role of alpha-synuclein in neurotransmission and synaptic plasticity. *J Chem Neuroanat*. 42:242-248.

Cheng, L.C., E. Pastrana, M. Tavazoie, and F. Doetsch. 2009. miR-124 regulates adult neurogenesis in the subventricular zone stem cell niche. *Nat Neurosci*. 12:399-408.

Chia, W., W.G. Somers, and H. Wang. 2008. Drosophila neuroblast asymmetric divisions: cell cycle regulators, asymmetric protein localization, and tumorigenesis. *J Cell Biol*. 180:267-272.

Chouchane, M., A.R. Melo de Farias, D.M.S. Moura, M.M. Hilscher, T. Schroeder, R.N. Leao, and M.R. Costa. 2017. Lineage Reprogramming of Astroglial Cells from Different Origins into Distinct Neuronal Subtypes. *Stem Cell Reports*. 9:162-176.

Chowdhury, R., Y. Wang, M. Campbell, S.K. Goderie, F. Doyle, S.A. Tenenbaum, G. Kusek, T.R. Kiehl, S.A. Ansari, N.C. Boles, and S. Temple. 2021. STAU2 binds a complex RNA cargo that changes temporally with production of diverse intermediate progenitor cells during mouse corticogenesis. *Development*. 148:dev199376.

Chuang, W., A. Sharma, P. Shukla, G. Li, M. Mall, K. Rajarajan, O.J. Abilez, R. Hamaguchi, J.C. Wu, M. Wernig, and S.M. Wu. 2017. Partial Reprogramming of Pluripotent Stem Cell-Derived Cardiomyocytes into Neurons. *Sci Rep*. 7:44840.

Dahm, R., and M. Kiebler. 2005. Cell biology: silenced RNA on the move. *Nature*. 438:432-435.

De Conti, L., M. Baralle, and E. Buratti. 2017. Neurodegeneration and RNA-binding proteins. *Wiley Interdiscip Rev RNA*. 8:wrna.1394.

De Pietri Tonelli, D., J.N. Pulvers, C. Haffner, E.P. Murchison, G.J. Hannon, and W.B. Huttner. 2008. miRNAs are essential for survival and differentiation of newborn neurons but not for expansion of neural progenitors during early neurogenesis in the mouse embryonic neocortex. *Development*. 135:3911-3921.

di Penta, A., V. Mercaldo, F. Florenzano, S. Munck, M.T. Ciotti, F. Zalfa, D. Mercanti, M. Molinari, C. Bagni, and T. Achsel. 2009. Dendritic LSm1/CBP80-mRNPs mark the early steps of transport commitment and translational control. *J Cell Biol*. 184:423-435.

Dong, H., M. Zhu, L. Meng, Y. Ding, D. Yang, S. Zhang, W. Qiang, D.W. Fisher, and E.Y. Xu. 2018. Pumilio2 regulates synaptic plasticity via translational repression of synaptic receptors in mice. *Oncotarget*. 9:32134-32148.

Doyle, M., and M.A. Kiebler. 2011. Mechanisms of dendritic mRNA transport and its role in synaptic tagging. *EMBO J*. 30:3540-3552.

Dreyfuss, G., V.N. Kim, and N. Kataoka. 2002. Messenger-RNA-binding proteins and the messages they carry. *Nat Rev Mol Cell Biol*. 3:195-205.

Driscoll, H.E., N.I. Muraro, M. He, and R.A. Baines. 2013. Pumilio-2 regulates translation of Nav1.6 to mediate homeostasis of membrane excitability. *J Neurosci*. 33:9644-9654.

Dubnau, J., A.S. Chiang, L. Grady, J. Barditch, S. Gossweiler, J. McNeil, P. Smith, F. Buldoc, R. Scott, U. Certa, C. Broger, and T. Tully. 2003. The staufen/pumilio pathway is involved in Drosophila long-term memory. *Curr Biol*. 13:286-296.

Duchaine, T.F., I. Hemraj, L. Furic, A. Deitinghoff, M.A. Kiebler, and L. DesGroseillers. 2002. Staufen2 isoforms localize to the somatodendritic domain of neurons and interact with different organelles. *J Cell Sci*. 115:3285-3295.

Elvira, G., S. Wasiak, V. Blandford, X.K. Tong, A. Serrano, X. Fan, M. del Rayo Sanchez-Carbente, F. Servant, A.W. Bell, D. Boismenu, J.C. Lacaille, P.S. McPherson, L. DesGroseillers, and W.S. Sossin. 2006. Characterization of an RNA granule from developing brain. *Mol Cell Proteomics*. 5:635-651.

Fernandez-Moya, S.M., J. Ehses, K.E. Bauer, R. Schieweck, A.M. Chakrabarti, F.C.Y. Lee, C. Illig, N.M. Luscombe, M. Harner, J. Ule, and M.A. Kiebler. 2021. RGS4 RNA Secondary Structure Mediates Staufen2 RNP Assembly in Neurons. *Int J Mol Sci*. 22:13021.

Fode, C., Q. Ma, S. Casarosa, S.L. Ang, D.J. Anderson, and F. Guillemot. 2000. A role for neural determination genes in specifying the dorsoventral identity of telencephalic neurons. *Genes Dev*. 14:67-80.

Friend, K., Z.T. Campbell, A. Cooke, P. Kroll-Conner, M.P. Wickens, and J. Kimble. 2012. A conserved PUF-Ago-eEF1A complex attenuates translation elongation. *Nat Struct Mol Biol*. 19:176-183.

Fritzsche, R., D. Karra, K.L. Bennett, F.Y. Ang, J.E. Heraud-Farlow, M. Tolino, M. Doyle, K.E. Bauer, S. Thomas, M. Planyavsky, E. Arn, A. Bakosova, K. Jungwirth, A. Hormann, Z. Palfi, J. Sandholzer, M. Schwarz, P. Macchi, J. Colinge, G. Superti-Furga, and M.A. Kiebler. 2013. Interactome of two diverse RNA granules links mRNA localization to translational repression in neurons. *Cell Rep*. 5:1749-1762.

Fuerst, P.G., F. Bruce, M. Tian, W. Wei, J. Elstrott, M.B. Feller, L. Erskine, J.H. Singer, and R.W. Burgess. 2009. DSCAM and DSCAML1 function in self-avoidance in multiple cell types in the developing mouse retina. *Neuron*. 64:484-497.

Furic, L., M. Maher-Laporte, and L. DesGroseillers. 2008. A genome-wide approach identifies distinct but overlapping subsets of cellular mRNAs associated with Staufen1- and Staufen2-containing ribonucleoprotein complexes. *RNA*. 14:324-335.

Gao, Z., K. Ure, J.L. Ables, D.C. Lagace, K.A. Nave, S. Goebbels, A.J. Eisch, and J. Hsieh. 2009. Neurod1 is essential for the survival and maturation of adult-born neurons. *Nat Neurosci*. 12:1090-1092.

Gascon, S., E. Murenu, G. Masserdotti, F. Ortega, G.L. Russo, D. Petrik, A. Deshpande, C. Heinrich, M. Karow, S.P. Robertson, T. Schroeder, J. Beckers, M. Irmler, C. Berndt, J.P. Angeli, M. Conrad, B. Berninger, and M. Gotz. 2016. Identification and Successful Negotiation of a Metabolic Checkpoint in Direct Neuronal Reprogramming. *Cell Stem Cell*. 18:396-409.

Goetze, B., B. Grunewald, S. Baldassa, and M. Kiebler. 2004. Chemically controlled formation of a DNA/calcium phosphate coprecipitate: application for transfection of mature hippocampal neurons. *J Neurobiol*. 60:517-525.

Goetze, B., B. Grunewald, M.A. Kiebler, and P. Macchi. 2003. Coupling the iron-responsive element to GFP--an inducible system to study translation in a single living cell. *Sci STKE*. 2003:PL12.

Goetze, B., F. Tuebing, Y. Xie, M.M. Dorostkar, S. Thomas, U. Pehl, S. Boehm, P. Macchi, and M.A. Kiebler. 2006. The brain-specific double-stranded RNA-binding protein Staufen2 is required for dendritic spine morphogenesis. *J Cell Biol*. 172:221-231.

Gohlke, J.M., O. Armant, F.M. Parham, M.V. Smith, C. Zimmer, D.S. Castro, L. Nguyen, J.S. Parker, G. Gradwohl, C.J. Portier, and F. Guillemot. 2008. Characterization of the proneural gene regulatory network during mouse telencephalon development. *BMC Biol*. 6:15.

Goldstrohm, A.C., T.M.T. Hall, and K.M. McKenney. 2018. Post-transcriptional Regulatory Functions of Mammalian Pumilio Proteins. *Trends Genet*. 34:972-990.

Goldstrohm, A.C., D.J. Seay, B.A. Hook, and M. Wickens. 2007. PUF protein-mediated deadenylation is catalyzed by Ccr4p. *J Biol Chem*. 282:109-114.

Gonda, Y., T. Namba, and C. Hanashima. 2020. Beyond Axon Guidance: Roles of Slit-Robo Signaling in Neocortical Formation. *Front Cell Dev Biol*. 8:607415.

Gotz, M., and W.B. Huttner. 2005. The cell biology of neurogenesis. *Nat Rev Mol Cell Biol*. 6:777-788.

Grande, A., K. Sumiyoshi, A. Lopez-Juarez, J. Howard, B. Sakthivel, B. Aronow, K. Campbell, and M. Nakafuku. 2013. Environmental impact on direct neuronal reprogramming in vivo in the adult brain. *Nat Commun*. 4:2373.

Gratton, M.O., E. Torban, S.B. Jasmin, F.M. Theriault, M.S. German, and S. Stifani. 2003. Hes6 promotes cortical neurogenesis and inhibits Hes1 transcription repression activity by multiple mechanisms. *Mol Cell Biol*. 23:6922-6935.

Gumy, L.F., E.A. Katrukha, L.C. Kapitein, and C.C. Hoogenraad. 2014. New insights into mRNA trafficking in axons. *Dev Neurobiol*. 74:233-244.

Guo, W., A.M. Allan, R. Zong, L. Zhang, E.B. Johnson, E.G. Schaller, A.C. Murthy, S.L. Goggin, A.J. Eisch, B.A. Oostra, D.L. Nelson, P. Jin, and X. Zhao. 2011. Ablation of Fmrp in adult neural stem cells disrupts hippocampus-dependent learning. *Nat Med*. 17:559-565.

Guo, Z., L. Zhang, Z. Wu, Y. Chen, F. Wang, and G. Chen. 2014. In vivo direct reprogramming of reactive glial cells into functional neurons after brain injury and in an Alzheimer's disease model. *Cell Stem Cell*. 14:188-202.

Hatakeyama, J., Y. Bessho, K. Katoh, S. Ookawara, M. Fujioka, F. Guillemot, and R. Kageyama. 2004. Hes genes regulate size, shape and histogenesis of the nervous system by control of the timing of neural stem cell differentiation. *Development*. 131:5539-5550.

Hebert, J.M., and G. Fishell. 2008. The genetics of early telencephalon patterning: some assembly required. *Nat Rev Neurosci*. 9:678-685.

Heinrich, C., M. Bergami, S. Gascon, A. Lepier, F. Vigano, L. Dimou, B. Sutor, B. Berninger, and M. Gotz. 2014. Sox2-mediated conversion of NG2 glia into induced neurons in the injured adult cerebral cortex. *Stem Cell Reports*. 3:1000-1014.

Heinrich, C., R. Blum, S. Gascon, G. Masserdotti, P. Tripathi, R. Sanchez, S. Tiedt, T. Schroeder, M. Gotz, and B. Berninger. 2010. Directing astroglia from the cerebral cortex into subtype specific functional neurons. *PLoS Biol*. 8:e1000373.

Heinrich, C., S. Gascon, G. Masserdotti, A. Lepier, R. Sanchez, T. Simon-Ebert, T. Schroeder, M. Gotz, and B. Berninger. 2011. Generation of subtype-specific neurons from postnatal astroglia of the mouse cerebral cortex. *Nat Protoc*. 6:214-228.

Heins, N., P. Malatesta, F. Cecconi, M. Nakafuku, K.L. Tucker, M.A. Hack, P. Chapouton, Y.A. Barde, and M. Gotz. 2002. Glial cells generate neurons: the role of the transcription factor Pax6. *Nat Neurosci*. 5:308-315.

Hentze, M.W., A. Castello, T. Schwarzl, and T. Preiss. 2018. A brave new world of RNA-binding proteins. *Nat Rev Mol Cell Biol*. 19:327-341.

Heraud-Farlow, J.E., and M.A. Kiebler. 2014. The multifunctional Staufen proteins: conserved roles from neurogenesis to synaptic plasticity. *Trends Neurosci*. 37:470-479.

Heraud-Farlow, J.E., T. Sharangdhar, X. Li, P. Pfeifer, S. Tauber, D. Orozco, A. Hormann, S. Thomas, A. Bakosova, A.R. Farlow, D. Edbauer, H.D. Lipshitz, Q.D. Morris, M. Bilban, M. Doyle, and M.A. Kiebler. 2013. Staufen2 regulates neuronal target RNAs. *Cell Rep*. 5:1511-1518.

Hevner, R.F., R.A. Daza, J.L. Rubenstein, H. Stunnenberg, J.F. Olavarria, and C. Englund. 2003. Beyond laminar fate: toward a molecular classification of cortical projection/pyramidal neurons. *Dev Neurosci*. 25:139-151.

Hevner, R.F., R.D. Hodge, R.A. Daza, and C. Englund. 2006. Transcription factors in glutamatergic neurogenesis: conserved programs in neocortex, cerebellum, and adult hippocampus. *Neurosci Res*. 55:223-233.

Holt, C.E., and E.M. Schuman. 2013. The central dogma decentralized: new perspectives on RNA function and local translation in neurons. *Neuron*. 80:648-657.

Hotz, M., and W.J. Nelson. 2017. Pumilio-dependent localization of mRNAs at the cell front coordinates multiple pathways required for chemotaxis. *Nat Commun*. 8:1366.

Hu, X., S. Qin, X. Huang, Y. Yuan, Z. Tan, Y. Gu, X. Cheng, D. Wang, X.F. Lian, C. He, and Z. Su. 2019. Region-Restrict Astrocytes Exhibit Heterogeneous Susceptibility to Neuronal Reprogramming. *Stem Cell Reports*. 12:290-304.

Huilgol, D., J.M. Levine, W. Galbavy, B.S. Wang, M. He, S.M. Suryanarayana, and Z.J. Huang. 2023. Direct and indirect neurogenesis generate a mosaic of distinct glutamatergic projection neuron types in cerebral cortex. *Neuron*. 111:2557-2569 e2554.

Imayoshi, I., and R. Kageyama. 2014. bHLH factors in self-renewal, multipotency, and fate choice of neural progenitor cells. *Neuron*. 82:9-23.

Kantor, D.B., O. Chivatakarn, K.L. Peer, S.F. Oster, M. Inatani, M.J. Hansen, J.G. Flanagan, Y. Yamaguchi, D.W. Sretavan, R.J. Giger, and A.L. Kolodkin. 2004. Semaphorin 5A is a bifunctional axon guidance cue regulated by heparan and chondroitin sulfate proteoglycans. *Neuron*. 44:961-975.

Kase, Y., T. Shimazaki, and H. Okano. 2020. Current understanding of adult neurogenesis in the mammalian brain: how does adult neurogenesis decrease with age? *Inflamm Regen*. 40:10.

Kempf, J., K. Knelles, B.A. Hersbach, D. Petrik, T. Riedemann, V. Bednarova, A. Janjic, T. Simon-Ebert, W. Enard, P. Smialowski, M. Gotz, and G. Masserdotti. 2021. Heterogeneity of neurons reprogrammed from spinal cord astrocytes by the proneural factors Ascl1 and Neurogenin2. *Cell Rep*. 36:109571.

Kiebler, M.A., and G.J. Bassell. 2006. Neuronal RNA granules: movers and makers. *Neuron*. 51:685-690.

Kiebler, M.A., I. Hemraj, P. Verkade, M. Kohrmann, P. Fortes, R.M. Marion, J. Ortin, and C.G. Dotti. 1999. The mammalian staufen protein localizes to the somatodendritic domain of cultured hippocampal neurons: implications for its involvement in mRNA transport. *J Neurosci*. 19:288-297.

Kim, K.M., H. Cho, K. Choi, J. Kim, B.W. Kim, Y.G. Ko, S.K. Jang, and Y.K. Kim. 2009. A new MIF4G domain-containing protein, CTIF, directs nuclear cap-binding protein CBP80/20-dependent translation. *Genes Dev*. 23:2033-2045.

Kohrmann, M., M. Luo, C. Kaether, L. DesGroseillers, C.G. Dotti, and M.A. Kiebler. 1999. Microtubule-dependent recruitment of Staufen-green fluorescent protein into large RNA-containing granules and subsequent dendritic transport in living hippocampal neurons. *Mol Biol Cell*. 10:2945-2953.

Kusek, G., M. Campbell, F. Doyle, S.A. Tenenbaum, M. Kiebler, and S. Temple. 2012. Asymmetric segregation of the double-stranded RNA binding protein Staufen2 during mammalian neural stem cell divisions promotes lineage progression. *Cell Stem Cell*. 11:505-516.

Lang, M.F., and Y. Shi. 2012. Dynamic Roles of microRNAs in Neurogenesis. *Front Neurosci*. 6:71.

Lee, Q.Y., M. Mall, S. Chanda, B. Zhou, K.S. Sharma, K. Schaukowitch, J.M. Adrian-Segarra, S.D. Grieder, M.S. Kareta, O.L. Wapinski, C.E. Ang, R. Li, T.C. Sudhof, H.Y. Chang, and M. Wernig. 2020. Pro-neuronal activity of Myod1 due to promiscuous binding to neuronal genes. *Nat Cell Biol*. 22:401-411.

Lee, S.W., Y.M. Oh, Y.L. Lu, W.K. Kim, and A.S. Yoo. 2018. MicroRNAs Overcome Cell Fate Barrier by Reducing EZH2-Controlled REST Stability during Neuronal Conversion of Human Adult Fibroblasts. *Dev Cell*. 46:73-84 e77.

Li, P., X. Yang, M. Wasser, Y. Cai, and W. Chia. 1997. Inscuteable and Staufen mediate asymmetric localization and segregation of prospero RNA during Drosophila neuroblast cell divisions. *Cell*. 90:437-447.

Liang, X.G., C. Tan, C.K. Wang, R.R. Tao, Y.J. Huang, K.F. Ma, K. Fukunaga, M.Z. Huang, and F. Han. 2018. Myt1l induced direct reprogramming of pericytes into cholinergic neurons. *CNS Neurosci Ther*. 24:801-809.

Liu, M.H., W. Li, J.J. Zheng, Y.G. Xu, Q. He, and G. Chen. 2020. Differential neuronal reprogramming induced by NeuroD1 from astrocytes in grey matter versus white matter. *Neural Regen Res*. 15:342-351.

Lu, D.C., T. Niu, and W.A. Alaynick. 2015. Molecular and cellular development of spinal cord locomotor circuitry. *Front Mol Neurosci*. 8:25.

Luo, Y., G. Shan, W. Guo, R.D. Smrt, E.B. Johnson, X. Li, R.L. Pfeiffer, K.E. Szulwach, R. Duan, B.Z. Barkho, W. Li, C. Liu, P. Jin, and X. Zhao. 2010. Fragile x mental retardation protein regulates proliferation and differentiation of adult neural stem/progenitor cells. *PLoS Genet*. 6:e1000898.

Macchi, P., A.M. Brownawell, B. Grunewald, L. DesGroseillers, I.G. Macara, and M.A. Kiebler. 2004. The brain-specific double-stranded RNA-binding protein Staufen2:

nucleolar accumulation and isoform-specific exportin-5-dependent export. *J Biol Chem*. 279:31440-31444.

Maeda, N. 2015. Proteoglycans and neuronal migration in the cerebral cortex during development and disease. *Front Neurosci*. 9:98.

Maher-Laporte, M., and L. DesGroseillers. 2010. Genome wide identification of Staufen2-bound mRNAs in embryonic rat brains. *BMB Rep*. 43:344-348.

Makeyev, E.V., J. Zhang, M.A. Carrasco, and T. Maniatis. 2007. The MicroRNA miR-124 promotes neuronal differentiation by triggering brain-specific alternative pre-mRNA splicing. *Mol Cell*. 27:435-448.

Mall, M., M.S. Kareta, S. Chanda, H. Ahlenius, N. Perotti, B. Zhou, S.D. Grieder, X. Ge, S. Drake, C. Euong Ang, B.M. Walker, T. Vierbuchen, D.R. Fuentes, P. Brennecke, K.R. Nitta, A. Jolma, L.M. Steinmetz, J. Taipale, T.C. Sudhof, and M. Wernig. 2017. Myt1l safeguards neuronal identity by actively repressing many non-neuronal fates. *Nature*. 544:245-249.

Marro, S., Z.P. Pang, N. Yang, M.C. Tsai, K. Qu, H.Y. Chang, T.C. Sudhof, and M. Wernig. 2011. Direct lineage conversion of terminally differentiated hepatocytes to functional neurons. *Cell Stem Cell*. 9:374-382.

Martinez, J.C., L.K. Randolph, D.M. Iascone, H.F. Pernice, F. Polleux, and U. Hengst. 2019. Pum2 Shapes the Transcriptome in Developing Axons through Retention of Target mRNAs in the Cell Body. *Neuron*. 104:931-946 e935.

Masserdotti, G., S. Gascon, and M. Gotz. 2016. Direct neuronal reprogramming: learning from and for development. *Development*. 143:2494-2510.

Masserdotti, G., S. Gillotin, B. Sutor, D. Drechsel, M. Irmler, H.F. Jorgensen, S. Sass, F.J. Theis, J. Beckers, B. Berninger, F. Guillemot, and M. Gotz. 2015. Transcriptional Mechanisms of Proneural Factors and REST in Regulating Neuronal Reprogramming of Astrocytes. *Cell Stem Cell*. 17:74-88.

Mattugini, N., R. Bocchi, V. Scheuss, G.L. Russo, O. Torper, C.L. Lao, and M. Gotz. 2019. Inducing Different Neuronal Subtypes from Astrocytes in the Injured Mouse Cerebral Cortex. *Neuron*. 103:1086-1095 e1085.

McKay, N.D., B. Robinson, R. Brodie, and N. Rooke-Allen. 1983. Glucose transport and metabolism in cultured human skin fibroblasts. *Biochim Biophys Acta*. 762:198-204.

Mee, C.J., E.C. Pym, K.G. Moffat, and R.A. Baines. 2004. Regulation of neuronal excitability through pumilio-dependent control of a sodium channel gene. *J Neurosci*. 24:8695-8703.

Menon, K.P., S. Andrews, M. Murthy, E.R. Gavis, and K. Zinn. 2009. The translational repressors Nanos and Pumilio have divergent effects on presynaptic terminal growth and postsynaptic glutamate receptor subunit composition. *J Neurosci*. 29:5558-5572.

Menon, K.P., S. Sanyal, Y. Habara, R. Sanchez, R.P. Wharton, M. Ramaswami, and K. Zinn. 2004. The translational repressor Pumilio regulates presynaptic morphology and controls postsynaptic accumulation of translation factor eIF-4E. *Neuron*. 44:663-676.

Min, H., R.C. Chan, and D.L. Black. 1995. The generally expressed hnRNP F is involved in a neural-specific pre-mRNA splicing event. *Genes Dev*. 9:2659-2671.

Misra, K., H. Luo, S. Li, M. Matise, and M. Xiang. 2014. Asymmetric activation of Dll4-Notch signaling by Foxn4 and proneural factors activates BMP/TGFbeta signaling to specify V2b interneurons in the spinal cord. *Development*. 141:187-198.

Mofatteh, M., and S.L. Bullock. 2017. SnapShot: Subcellular mRNA Localization. *Cell*. 169:178-178 e171.

Monshausen, M., U. Putz, M. Rehbein, M. Schweizer, L. DesGroseillers, D. Kuhl, D. Richter, and S. Kindler. 2001. Two rat brain staufen isoforms differentially bind RNA. *J Neurochem*. 76:155-165.

Moore, F.L., J. Jaruzelska, M.S. Fox, J. Urano, M.T. Firpo, P.J. Turek, D.M. Dorfman, and R.A. Pera. 2003. Human Pumilio-2 is expressed in embryonic stem cells and germ cells and interacts with DAZ (Deleted in AZoospermia) and DAZ-like proteins. *Proc Natl Acad Sci U S A*. 100:538-543.

Morris, S.A. 2016. Direct lineage reprogramming via pioneer factors; a detour through developmental gene regulatory networks. *Development*. 143:2696-2705.

Nagy, A., and K. Nagy. 2010. The mysteries of induced pluripotency: where will they lead? *Nat Methods*. 7:22-24.

Nakahata, S., T. Kotani, K. Mita, T. Kawasaki, Y. Katsu, Y. Nagahama, and M. Yamashita. 2003. Involvement of Xenopus Pumilio in the translational regulation that is specific to cyclin B1 mRNA during oocyte maturation. *Mech Dev*. 120:865-880.

Niederkofler, V., T. Baeriswyl, R. Ott, and E.T. Stoeckli. 2010. Nectin-like molecules/SynCAMs are required for post-crossing commissural axon guidance. *Development*. 137:427-435.

Noctor, S.C., V. Martinez-Cerdeno, L. Ivic, and A.R. Kriegstein. 2004. Cortical neurons arise in symmetric and asymmetric division zones and migrate through specific phases. *Nat Neurosci*. 7:136-144.

Pang, Z.P., N. Yang, T. Vierbuchen, A. Ostermeier, D.R. Fuentes, T.Q. Yang, A. Citri, V. Sebastiano, S. Marro, T.C. Sudhof, and M. Wernig. 2011. Induction of human neuronal cells by defined transcription factors. *Nature*. 476:220-223.

Parisi, M., and H. Lin. 2000. Translational repression: a duet of Nanos and Pumilio. *Curr Biol*. 10:R81-83.

Park, H.Y., H. Lim, Y.J. Yoon, A. Follenzi, C. Nwokafor, M. Lopez-Jones, X. Meng, and R.H. Singer. 2014. Visualization of dynamics of single endogenous mRNA labeled in live mouse. *Science*. 343:422-424.

Parra, A.S., and C.A. Johnston. 2022. Emerging Roles of RNA-Binding Proteins in Neurodevelopment. *J Dev Biol*. 10:23.

Pascale, E., C. Caiazza, M. Paladino, S. Parisi, F. Passaro, and M. Caiazzo. 2022. MicroRNA Roles in Cell Reprogramming Mechanisms. *Cells*. 11:940.

Pataskar, A., J. Jung, P. Smialowski, F. Noack, F. Calegari, T. Straub, and V.K. Tiwari. 2016. NeuroD1 reprograms chromatin and transcription factor landscapes to induce the neuronal program. *EMBO J*. 35:24-45.

Pereira, M., M. Birtele, S. Shrigley, J.A. Benitez, E. Hedlund, M. Parmar, and D.R. Ottosson. 2017. Direct Reprogramming of Resident NG2 Glia into Neurons with Properties of Fast-Spiking Parvalbumin-Containing Interneurons. *Stem Cell Reports*. 9:742-751.

Pilaz, L.J., and D.L. Silver. 2015. Post-transcriptional regulation in corticogenesis: how RNA-binding proteins help build the brain. *Wiley Interdiscip Rev RNA*. 6:501-515.

Rakic, P. 1972. Mode of cell migration to the superficial layers of fetal monkey neocortex. *J Comp Neurol*. 145:61-83.

Ramon-Cueto, A., and J. Avila. 1998. Olfactory ensheathing glia: properties and function. *Brain Res Bull*. 46:175-187.

Regev, A., S.A. Teichmann, E.S. Lander, I. Amit, C. Benoist, E. Birney, B. Bodenmiller, P. Campbell, P. Carninci, M. Clatworthy, H. Clevers, B. Deplancke, I. Dunham, J. Eberwine, R. Eils, W. Enard, A. Farmer, L. Fugger, B. Gottgens, N. Hacohen, M. Haniffa, M. Hemberg, S. Kim, P. Klenerman, A. Kriegstein, E. Lein, S. Linnarsson, E. Lundberg, J. Lundeberg, P. Majumder, J.C. Marioni, M. Merad, M. Mhlanga, M. Nawijn, M. Netea, G. Nolan, D. Pe'er, A. Phillipakis, C.P. Ponting, S. Quake, W. Reik, O. Rozenblatt-Rosen, J. Sanes, R. Satija, T.N. Schumacher, A. Shalek, E. Shapiro, P. Sharma, J.W. Shin, O. Stegle, M. Stratton, M.J.T. Stubbington, F.J. Theis, M. Uhlen, A. van Oudenaarden, A. Wagner, F. Watt, J. Weissman, B. Wold, R. Xavier, N. Yosef, and P. Human Cell Atlas Meeting. 2017. The Human Cell Atlas. *Elife*. 6:e27041.

Rivetti di Val Cervo, P., R.A. Romanov, G. Spigolon, D. Masini, E. Martin-Montanez, E.M. Toledo, G. La Manno, M. Feyder, C. Pifl, Y.H. Ng, S.P. Sanchez, S. Linnarsson, M. Wernig, T. Harkany, G. Fisone, and E. Arenas. 2017. Induction of functional dopamine neurons from human astrocytes in vitro and mouse astrocytes in a Parkinson's disease model. *Nat Biotechnol*. 35:444-452.

Sachse, S.M., S. Lievens, L.F. Ribeiro, D. Dascenco, D. Masschaele, K. Horre, A. Misbaer, N. Vanderroost, A.S. De Smet, E. Salta, M.L. Erfurth, Y. Kise, S. Nebel, W. Van Delm, S. Plaisance, J. Tavernier, B. De Strooper, J. De Wit, and D. Schmucker. 2019. Nuclear import of the DSCAM-cytoplasmic domain drives signaling capable of inhibiting synapse formation. *EMBO J*. 38:e99669.

Saffary, R., and Z. Xie. 2011. FMRP regulates the transition from radial glial cells to intermediate progenitor cells during neocortical development. *J Neurosci*. 31:1427-1439.

Samavarchi-Tehrani, P., A. Golipour, L. David, H.K. Sung, T.A. Beyer, A. Datti, K. Woltjen, A. Nagy, and J.L. Wrana. 2010. Functional genomics reveals a BMP-driven mesenchymal-to-epithelial transition in the initiation of somatic cell reprogramming. *Cell Stem Cell*. 7:64-77.

Sartor, F., J. Anderson, C. McCaig, Z. Miedzybrodzka, and B. Muller. 2015. Mutation of genes controlling mRNA metabolism and protein synthesis predisposes to neurodevelopmental disorders. *Biochem Soc Trans*. 43:1259-1265.

Schieweck, R., J. Ninkovic, and M.A. Kiebler. 2021a. RNA-binding proteins balance brain function in health and disease. *Physiol Rev*. 101:1309-1370.

Schieweck, R., T. Riedemann, I. Forne, M. Harner, K.E. Bauer, D. Rieger, F.Y. Ang, S. Hutten, A.F. Demleitner, B. Popper, S. Derdak, B. Sutor, M. Bilban, A. Imhof, and M.A. Kiebler. 2021b. Pumilio2 and Staufen2 selectively balance the synaptic proteome. *Cell Rep*. 35:109279.

Schieweck, R., E.C. Schoneweiss, M. Harner, D. Rieger, C. Illig, B. Sacca, B. Popper, and M.A. Kiebler. 2021c. Pumilio2 Promotes Growth of Mature Neurons. *Int J Mol Sci*. 22.

Schuurmans, C., and F. Guillemot. 2002. Molecular mechanisms underlying cell fate specification in the developing telencephalon. *Curr Opin Neurobiol*. 12:26-34.

Schwartz, N.B., and M.S. Domowicz. 2018. Proteoglycans in brain development and pathogenesis. *FEBS Lett*. 592:3791-3805.

Schweers, B.A., K.J. Walters, and M. Stern. 2002. The Drosophila melanogaster translational repressor pumilio regulates neuronal excitability. *Genetics*. 161:1177-1185.

Sessa, A., C.A. Mao, A.K. Hadjantonakis, W.H. Klein, and V. Broccoli. 2008. Tbr2 directs conversion of radial glia into basal precursors and guides neuronal amplification by indirect neurogenesis in the developing neocortex. *Neuron*. 60:56-69.

Sharangdhar, T., Y. Sugimoto, J. Heraud-Farlow, S.M. Fernandez-Moya, J. Ehses, I. Ruiz de Los Mozos, J. Ule, and M.A. Kiebler. 2017. A retained intron in the 3'-UTR of Calm3 mRNA mediates its Staufen2- and activity-dependent localization to neuronal dendrites. *EMBO Rep*. 18:1762-1774.

Shin, J., C. Gu, E. Park, and S. Park. 2007. Identification of phosphotyrosine binding domain-containing proteins as novel downstream targets of the EphA8 signaling function. *Mol Cell Biol*. 27:8113-8126.

Southall, T.D., and A.H. Brand. 2009. Neural stem cell transcriptional networks highlight genes essential for nervous system development. *EMBO J*. 28:3799-3807.

Spassov, D.S., and R. Jurecic. 2002. Cloning and comparative sequence analysis of PUM1 and PUM2 genes, human members of the Pumilio family of RNA-binding proteins. *Gene*. 299:195-204.

Spellman, R., and C.W. Smith. 2006. Novel modes of splicing repression by PTB. *Trends Biochem Sci*. 31:73-76.

St Johnston, D., D. Beuchle, and C. Nusslein-Volhard. 1991. Staufen, a gene required to localize maternal RNAs in the Drosophila egg. *Cell*. 66:51-63.

Stoykova, A., D. Treichel, M. Hallonet, and P. Gruss. 2000. Pax6 modulates the dorsoventral patterning of the mammalian telencephalon. *J Neurosci*. 20:8042-8050.

Sun, X., Z. Tan, X. Huang, X. Cheng, Y. Yuan, S. Qin, D. Wang, X. Hu, Y. Gu, W.J. Qian, Z. Wang, C. He, and Z. Su. 2019. Direct neuronal reprogramming of olfactory ensheathing cells for CNS repair. *Cell Death Dis*. 10:646.

Tan, X., and S.H. Shi. 2013. Neocortical neurogenesis and neuronal migration. *Wiley Interdiscip Rev Dev Biol*. 2:443-459.

Tang, S.J., D. Meulemans, L. Vazquez, N. Colaco, and E. Schuman. 2001. A role for a rat homolog of staufen in the transport of RNA to neuronal dendrites. *Neuron*. 32:463-475.

Treutlein, B., Q.Y. Lee, J.G. Camp, M. Mall, W. Koh, S.A. Shariati, S. Sim, N.F. Neff, J.M. Skotheim, M. Wernig, and S.R. Quake. 2016. Dissecting direct reprogramming from fibroblast to neuron using single-cell RNA-seq. *Nature*. 534:391-395.

Tsacopoulos, M., and P.J. Magistretti. 1996. Metabolic coupling between glia and neurons. *J Neurosci*. 16:877-885.

Vaid, S., and W.B. Huttner. 2020. Transcriptional Regulators and Human-Specific/Primate-Specific Genes in Neocortical Neurogenesis. *Int J Mol Sci*. 21:4614.

Van Etten, J., T.L. Schagat, J. Hrit, C.A. Weidmann, J. Brumbaugh, J.J. Coon, and A.C. Goldstrohm. 2012. Human Pumilio proteins recruit multiple deadenylases to efficiently repress messenger RNAs. *J Biol Chem*. 287:36370-36383.

Vasan, L., E. Park, L.A. David, T. Fleming, and C. Schuurmans. 2021. Direct Neuronal Reprogramming: Bridging the Gap Between Basic Science and Clinical Application. *Front Cell Dev Biol*. 9:681087.

Vessey, J.P., G. Amadei, S.E. Burns, M.A. Kiebler, D.R. Kaplan, and F.D. Miller. 2012. An asymmetrically localized Staufen2-dependent RNA complex regulates maintenance of mammalian neural stem cells. *Cell Stem Cell*. 11:517-528.

Vessey, J.P., L. Schoderboeck, E. Gingl, E. Luzi, J. Riefler, F. Di Leva, D. Karra, S. Thomas, M.A. Kiebler, and P. Macchi. 2010. Mammalian Pumilio 2 regulates dendrite morphogenesis and synaptic function. *Proc Natl Acad Sci U S A*. 107:3222-3227.

Vessey, J.P., A. Vaccani, Y. Xie, R. Dahm, D. Karra, M.A. Kiebler, and P. Macchi. 2006. Dendritic localization of the translational repressor Pumilio 2 and its contribution to dendritic stress granules. *J Neurosci*. 26:6496-6508.

Vierbuchen, T., A. Ostermeier, Z.P. Pang, Y. Kokubu, T.C. Sudhof, and M. Wernig. 2010. Direct conversion of fibroblasts to functional neurons by defined factors. *Nature*. 463:1035-1041.

Wan, J., M. Yourshaw, H. Mamsa, S. Rudnik-Schoneborn, M.P. Menezes, J.E. Hong, D.W. Leong, J. Senderek, M.S. Salman, D. Chitayat, P. Seeman, A. von Moers, L. Graul-Neumann, A.J. Kornberg, M. Castro-Gago, M.J. Sobrido, M. Sanefuji, P.B. Shieh, N. Salamon, R.C. Kim, H.V. Vinters, Z. Chen, K. Zerres, M.M. Ryan, S.F. Nelson, and J.C. Jen. 2012. Mutations in the RNA exosome component gene EXOSC3 cause pontocerebellar hypoplasia and spinal motor neuron degeneration. *Nat Genet*. 44:704-708.

Wan, Y., and Y. Ding. 2023. Strategies and mechanisms of neuronal reprogramming. *Brain Res Bull*. 199:110661.

Wang, L.L., C. Serrano, X. Zhong, S. Ma, Y. Zou, and C.L. Zhang. 2021a. Revisiting astrocyte to neuron conversion with lineage tracing in vivo. *Cell*. 184:5465-5481 e5416.

Wang, M., L. Oge, M.D. Perez-Garcia, L. Hamama, and S. Sakr. 2018. The PUF Protein Family: Overview on PUF RNA Targets, Biological Functions, and Post Transcriptional Regulation. *Int J Mol Sci*. 19:410.

Wang, X., Z. Pei, A. Hossain, Y. Bai, and G. Chen. 2021b. Transcription factor-based gene therapy to treat glioblastoma through direct neuronal conversion. *Cancer Biol Med*. 18:860-874.

Wapinski, O.L., T. Vierbuchen, K. Qu, Q.Y. Lee, S. Chanda, D.R. Fuentes, P.G. Giresi, Y.H. Ng, S. Marro, N.F. Neff, D. Drechsel, B. Martynoga, D.S. Castro, A.E. Webb, T.C. Sudhof, A. Brunet, F. Guillemot, H.Y. Chang, and M. Wernig. 2013. Hierarchical mechanisms for direct reprogramming of fibroblasts to neurons. *Cell*. 155:621-635.

Wayman, G.A., Y.S. Lee, H. Tokumitsu, A.J. Silva, and T.R. Soderling. 2008. Calmodulin-kinases: modulators of neuronal development and plasticity. *Neuron*. 59:914-931.

White, E.K., T. Moore-Jarrett, and H.E. Ruley. 2001. PUM2, a novel murine puf protein, and its consensus RNA-binding site. *RNA*. 7:1855-1866.

Wickens, M., D.S. Bernstein, J. Kimble, and R. Parker. 2002. A PUF family portrait: 3'UTR regulation as a way of life. *Trends Genet*. 18:150-157.

Wreden, C., A.C. Verrotti, J.A. Schisa, M.E. Lieberfarb, and S. Strickland. 1997. Nanos and pumilio establish embryonic polarity in Drosophila by promoting posterior deadenylation of hunchback mRNA. *Development*. 124:3015-3023.

Wu, Z., M. Parry, X.Y. Hou, M.H. Liu, H. Wang, R. Cain, Z.F. Pei, Y.C. Chen, Z.Y. Guo, S. Abhijeet, and G. Chen. 2020. Gene therapy conversion of striatal astrocytes into GABAergic neurons in mouse models of Huntington's disease. *Nat Commun*. 11:1105.

Xiang, Z., L. Xu, M. Liu, Q. Wang, W. Li, W. Lei, and G. Chen. 2021. Lineage tracing of direct astrocyte-to-neuron conversion in the mouse cortex. *Neural Regen Res*. 16:750-756.

Xue, Y., K. Ouyang, J. Huang, Y. Zhou, H. Ouyang, H. Li, G. Wang, Q. Wu, C. Wei, Y. Bi, L. Jiang, Z. Cai, H. Sun, K. Zhang, Y. Zhang, J. Chen, and X.D. Fu. 2013. Direct conversion of fibroblasts to neurons by reprogramming PTB-regulated microRNA circuits. *Cell*. 152:82-96.

Xue, Y., H. Qian, J. Hu, B. Zhou, Y. Zhou, X. Hu, A. Karakhanyan, Z. Pang, and X.D. Fu. 2016. Sequential regulatory loops as key gatekeepers for neuronal reprogramming in human cells. *Nat Neurosci*. 19:807-815.

Yang, G., C.A. Smibert, D.R. Kaplan, and F.D. Miller. 2014. An eIF4E1/4E-T complex determines the genesis of neurons from precursors by translationally repressing a proneurogenic transcription program. *Neuron*. 84:723-739.

Yang, Y., J. Jiao, R. Gao, H. Yao, X.F. Sun, and S. Gao. 2013. Direct conversion of adipocyte progenitors into functional neurons. *Cell Reprogram*. 15:484-489.

Ye, B., C. Petritsch, I.E. Clark, E.R. Gavis, L.Y. Jan, and Y.N. Jan. 2004. Nanos and Pumilio are essential for dendrite morphogenesis in Drosophila peripheral neurons. *Curr Biol*. 14:314-321.

Yoo, A.S., A.X. Sun, L. Li, A. Shcheglovitov, T. Portmann, Y. Li, C. Lee-Messer, R.E. Dolmetsch, R.W. Tsien, and G.R. Crabtree. 2011. MicroRNA-mediated conversion of human fibroblasts to neurons. *Nature*. 476:228-231.

Zahr, S.K., G. Yang, H. Kazan, M.J. Borrett, S.A. Yuzwa, A. Voronova, D.R. Kaplan, and F.D. Miller. 2018. A Translational Repression Complex in Developing Mammalian Neural Stem Cells that Regulates Neuronal Specification. *Neuron*. 97:520-537 e526.

Zhang, L., Z. Lei, Z. Guo, Z. Pei, Y. Chen, F. Zhang, A. Cai, G. Mok, G. Lee, V. Swaminathan, F. Wang, Y. Bai, and G. Chen. 2020. Development of Neuroregenerative Gene Therapy to Reverse Glial Scar Tissue Back to Neuron-Enriched Tissue. *Front Cell Neurosci*. 14:594170.

Zhang, L., J.C. Yin, H. Yeh, N.X. Ma, G. Lee, X.A. Chen, Y. Wang, L. Lin, L. Chen, P. Jin, G.Y. Wu, and G. Chen. 2015. Small Molecules Efficiently Reprogram Human Astroglial Cells into Functional Neurons. *Cell Stem Cell*. 17:735-747.

Zhang, M., D. Chen, J. Xia, W. Han, X. Cui, N. Neuenkirchen, G. Hermes, N. Sestan, and H. Lin. 2017. Post-transcriptional regulation of mouse neurogenesis by Pumilio proteins. *Genes Dev*. 31:1354-1369.

AFFIDAVIT

Eidesstattliche Versicherung/Affidavit

Hiermit versichere ich an Eides statt, dass ich die vorliegende Dissertation “The role of RNA-binding proteins in astrocyte-to-neuron reprogramming” selbstständig angefertigt habe, mich außer der angegebenen keiner weiteren Hilfsmittel bedient und alle Erkenntnisse, die aus dem Schrifttum ganz oder annähernd übernommen sind, als solche kenntlich gemacht und nach ihrer Herkunft unter Bezeichnung der Fundstelle einzeln nachgewiesen habe.

I hereby confirm that the dissertation “The role of RNA-binding proteins in astrocyte-to-neuron reprogramming” is the result of my own work and that I have only used sources or materials listed and specified in the dissertation.

Munich, 16.10.2023 Giuliana Ciccopiedi

Signature

LIST OF CONTRIBUTIONS

For this doctoral thesis, I contributed to the experimental design and performed all experiments, data collection, analysis and interpretation of results, unless explicitly stated otherwise in the text.

Prof. Dr. Michael A. Kiebler (LMU Munich) and Prof. Dr. Jovica Ninkovic (LMU Munich) conceived and supervised the project.

Prof. Dr. Jovica Ninkovic, Dr. Giacomo Masserdotti (LMU Munich) and Dr. Florence Bareyre (LMU Munich) contributed to the experimental design and the data interpretation.

Prof. Dr. Jovica Ninkovic and Sabine Thomas performed pilot experiments of neuronal reprogramming in Pum2 and Stau2-depleted conditions, which I have subsequently reproduced in Fig.11 of this thesis.

Prof. Dr. Magdalena Götz (LMU Munich, Helmholtz Munich) provided us with the C57Bl6/J mouse line, cell culture material, virus preparation and laboratory infrastructure for training and initial experiments. She also provided HEK 293GPG cells for retrovirus production. Furthermore, she provided continuous scientific feedback at the regular Reprogramming Club meetings throughout the entire time period of this project.

Tatiana Simon-Ebert (Götz laboratory) provided training for astrocyte cell culture.

Paulina Chlebik (Götz laboratory) provided training for retrovirus production.

Ilaria Brentari and Renate Dombi (Kiebler laboratory) cloned the Pum2 and Stau2 knockdown constructs: pFu3a-H1-shNTC-pCAG-tagRFP; pFu3a-H1-shPum2-pCAG-tagRFP; pFu3a-H1-shStau2-pCAG-tagRFP.

Dr. Karl E. Bauer assisted me in the analysis of the colocalisation experiments (Fig.7, 10).

Dr. Karl E. Bauer, Ulrike Kring and Sabine Thomas prepared the embryonic hippocampal neurons for staining experiments (Fig.6).

Munich,16.10.2023 Signature Prof. Dr. Michael A. Kiebler

Signature Giuliana Ciccopiedi

ACKNOWLEDGEMENTS

Here I would like to sincerely thank all the people who have accompanied me on this journey and have enabled me to conclude this first step in my research career. First of all, I would like to thank my supervisor Prof. Dr. Michael Kiebler for giving me the opportunity to work in his laboratory. I greatly appreciated his guidance, continuous encouragement and scientific support throughout my PhD. The experience in his laboratory was a great opportunity to grow not only professionally but also personally. I would like to express my sincere gratitude to Prof. Dr. Jovica Ninkovic, who has been instrumental in carrying out this research project. I would like to thank him for teaching and guiding me with his expertise and insightful ideas throughout these years of my PhD. A very special thanks goes to Dr. Giacomo Masserdotti, for his constant availability to provide me with brilliant comments and suggestions that have greatly impacted my project. I would also like to thank Prof. Dr. Magdalena Götz for her continuous scientific feedback and extremely valuable advice on the project during the Reprogramming Club meetings.

A special thanks also goes to the Graduate School of Systemic Neurosciences (GSN), which provided me with the ideal opportunity to learn new skills through high quality courses and to broaden my scientific horizons in a very international network. I am also very grateful for the financial support they provided to enable me to successfully complete the PhD programme. I have also greatly appreciated the constant support received by all the GSN coordinators, whom I would like to thank for their immense work. I would like to thank Dr. Florence Bareyre, who was part of my TAC and provided me with valuable suggestions for the project. I would like to give special credit to all the member of the laboratory of Prof. Dr. Magdalena Götz, from whom I had the privilege to learn and exchange ideas for the successful completion of the project. In particular, I would like to thank Tatiana Simon-Ebert and Paulina Chiblek for their excellent teaching and constant technical support.

I would like to thank all the members of the Kiebler lab. Throughout the years of my PhD, every single person in the lab has provided me with extreme support, mentoring, encouragement, and the best atmosphere in the lab. My PhD journey would not have been the same without you. First of all, I would like to thank Sabine Thomas for managing the lab and supervising my project, and for her constant availability over the years. Thanks to Dr. Stefanie Ohlig, who supervised me during the first part of my PhD. Special thanks to Dr. Karl Bauer, who was a great mentor and guided me with patience and valuable advice during the last part of my journey. His scientific feedback and support were essential to the successful

completion of this dissertation. I would like to thank my great colleague Kenneth Klau, who shared his motivation with me on all the good and less good days. I would also like to thank Dr. Rico Schieweck for the continuous and insightful scientific discussions, which were a great inspiration for my project. I thank Renate Dombi for her constant and great technical support and for always being encouraging, supportive and kind to me. Many thanks to Ulrike Kring for the great technical support in cell culture tasks. I also want to warmly thank Dr. Max Harner, Daniela Rieger, Lejla Krenic-Balic and Rachel Choo for their efficient contributions, interest and support. Special thanks to Korbinian Dischinger for his help in handling administrative tasks related to my PhD over the past months. Many thanks to Dr. Barbara Nitz for her help in designing the icons for the figures of the dissertation. Special thanks also to Andrea Wilytsch, Ralf Bigiel and Serpil Yildirim for their great help taking over all of the non-scientific work.

Thanks to all the members of the Cell Biology Department for being part of this amazing journey.